(1)

WAPD-TM-1349
DOE RESEARCH AND
DEVELOPMENT REPORT

FORCES IN BOLTED JOINTS : ANALYSIS METHODS AND TEST RESULTS UTILIZED FOR NUCLEAR-CORE APPLICATIONS

(LWBR Development Program)

MARCH 1981

CONTRACT DE-AC11-76PN00014

BETTIS ATOMIC POWER LABORATORY
WEST MIFFLIN, PENNSYLVANIA

Operated for the U. S. Department of Energy by
WESTINGHOUSE ELECTRIC CORPORATION

DISCLAIMER

FORCES IN BOLTED JOINTS:

ANALYSIS METHODS AND TEST RESULTS UTILIZED FOR NUCLEAR-CORE APPLICATIONS

(LWBR Development Program)

P.J. Crescimanno
K.L. Keller

Contract No. DE-AC11-76PN00014

March 1981

Printed in the United States of America
Available from
National Technical Information Service
U.S. Department of Commerce
5285 Port Royal Road
Springfield, VA 22161

NOTE

This document is an interim memorandum prepared primarily for internal reference and does not represent a final expression of the opinion of Westinghouse. When this memorandum is distributed externally, it is with the express understanding that Westinghouse makes no representation as to completeness, accuracy, or useability of information contained therein.

BETTIS ATOMIC POWER LABORATORY **WEST MIFFLIN, PENNSYLVANIA 15122**

Operated for the Department of Energy
by WESTINGHOUSE ELECTRIC CORPORATION

FOREWORD

The Shippingport Atomic Power Station located in Shippingport, Pennsylvania was the first large-scale, central-station nuclear power plant in the United States and the first plant of such size in the world operated solely to produce electric power. This program was started in 1953 to confirm the practical application of nuclear power for large-scale electric power generation. It has provided much of the technology being used for design and operation of the commercial, central-station nuclear power plants now in use.

Subsequent to development and successful operation of the Pressurized Water Reactor in the Atomic Energy Commission (now Department of Energy, DOE) owned reactor plant at the Shippingport Atomic Power Station, the Atomic Energy Commission in 1965 undertook a research and development program to design and build a Light Water Breeder Reactor core for operation in the Shippingport Station.

The objective of the Light Water Breeder Reactor (LWBR) program has been to develop a technology that would significantly improve the utilization of the nation's nuclear fuel resources employing the well-established water reactor technology. To achieve this objective, work has been directed toward analysis, design, component tests, and fabrication of a water-cooled, thorium oxide fuel cycle breeder reactor for installation and operation at the Shippingport Station. The LWBR core started operation in the Shippingport Station in the Fall of 1977 and is expected to be operated for about 4 to 5 years or more. At the end of this period, the core will be removed and the spent fuel shipped to the Naval Reactors Expended Core Facility for a detailed examination to verify core performance including an evaluation of breeding characteristics.

In 1976, with fabrication of the Shippingport LWBR core nearing completion, the Energy Research and Development Administration, now DOE, established the Advanced Water Breeder Applications (AWBA) program to develop and disseminate technical information which would assist U.S. industry in evaluating the LWBR concept for commercial-scale applications. The program is exploring some of the problems that would be faced by industry in adapting technology confirmed in the LWBR program. Information being developed includes concepts for commercial-scale prebreeder cores which would produce uranium-233 for light water breeder cores while producing electric power, improvements for breeder cores based on the technology developed to fabricate and operate the Shippingport LWBR core, and other information and technology to aid in evaluating commercial-scale application of the LWBR concept.

All three development programs (Pressurized Water Reactor, Light Water Breeder Reactor, and Advanced Water Breeder Applications) are under the technical direction of the Office of the Deputy Assistant Secretary for Naval Reactors of DOE. They have the goal of developing practical improvements in the utilization of nuclear fuel resources for generation of electrical energy using water-cooled nuclear reactors.

Technical information developed under the Shippingport, LWBR, and AWBA programs has been and will continue to be published in technical memoranda, one of which is this present report.

INTENTIONALLY BLANK

TABLE OF CONTENTS

		Page No.
I.	INTRODUCTION AND SCOPE	1
II.	ANALYSIS OF PRELOAD IN BOLTED JOINTS	3
	A. Calculation of Internal Forces in a Bolted Joint	3
	1. Relation of Mismatch to Internal Forces	3
	2. Effect of Thermal Expansion	8
	3. Effect of Stress Relaxation	10
	4. Importance of Bolted Joint Preload and Some Practical Design Guidelines	13
	B. Two Methods for Attaining Initial Preload in LWBR Core Assemblies	15
	1. Preload by Control of Applied Torque	16
	2. Preload by Control of Bolt Head Rotation	17
	3. Torque vs. Head Rotation: Some Relative Merits	22
III.	PRELOAD TESTS AND TEST RESULTS	24
	A. Multiple Tightening Tests	24
	B. Preload Tests	25
	1. Preload by Torque Control	25
	2. Preload by Control of Bolt Head Rotation	27
	C. Special Tests	29
	1. Preload Determined by Joint Separation Force	29
	2. Joint Bearing Load Test	30
	3. Measurement of Residual Torque	32
	D. Conclusions	34
IV.	APPENDICES	
	Appendix A: Design Stresses in Bolted Joints	69
	Appendix B: Example of a Bolted Joint Preload Analysis	75
	Appendix C: Consideration of Axial and Bending Flexibilities in a Coaxial Joint	85
	Appendix D: An Engineering Analysis of Time Independent Plastic Deformation on Bolt and Joint Forces	111
	Appendix E: Assessing Material Stress Relaxation When Total Strains Do Not Remain Constant	117
	REFERENCES	143
	ACKNOWLEDGEMENTS	143

LIST OF TABLES

Table		Page
1	Test Summary of Torque-Preload Assembly Coefficients and Friction Coefficients	54
B.1	Stiffness Calculation Work Sheet (Illustrative Example)	81
B.2	Bolt Load Calculation Sheet (Illustrative Example)	83
C.1	Loads and Stresses at 70°F (Illustrative Example)	108
C.2	Loads and Stresses at 600°F (Illustrative Example)	109
E.1	Useful Formulas For Specific Fractional Relaxation Factors	132
E.2	Calculated Results For Example Problem	139
E.3	Calculated Bolt and Joint Displacements for Example Problem	141

LIST OF FIGURES

Figure		Page
1	Mechanical Idealization of Bolted Joint to a System of Springs	35
2	Bolted Joint Internal Forces as a Function of Working Load	36
3	Effect of Preload Level on Alternating Bolt Force	37
4	Multiple Tightening Test Typical Data Trend	38
5	Variation in the Joint Assembly Coefficient vs the Number of Times the Joint is Tightened (for several LWBR joints)	39
6	Bolted Joints in LWBR Blanket Assembly	40
7	Bolted Joints in the LWBR Movable Fuel Assembly	41
8	Bolted Joints in LWBR Reflector Assembly	42
9	REM-208 Test Set-up: Blanket Top Base Plate Bolt	43
10	Torque-Preloaded Test, Typical Single Specimen Data: Blanket Top Base Plate Joint	44
11	Torque-Preloaded Test, "Uncorrected" Pooled Data: Blanket Top Base Plate Joint	45

LIST OF FIGURES (cont'd)

Figure		Page
12	Torque-Preloaded Test, Pooled Data for Blanket Top Base Plate Joint	46
13	Torque-Preloaded Test, Pooled Data for Blanket Bottom Base Plate Joint	47
14	Torque-Preloaded Test, Pooled Data for Blanket Guide Tube Extension Joint	48
15	Torque-Preload Test, Pooled Data for Blanket Shear Key Joint	49
16	Torque-Preload Test, Pooled Data for Movable Fuel Top Base Plate Joint	50
17	Torque-Preload Test, Pooled Data for Movable Fuel Grid Joint	51
18	Torque-Preload Test, Pooled Data for Reflector Seal Block Joint	52
19	Torque-Preloaded Test, Pooled Data for Reflector Stub Tube Joint	53
20	Universal Tightening Fixture with Typical Joint Test Assembly, SCC Test Joints	55
21	Actual Test Assembly, SCC Test	56
	Test Set-up for Tightening Bolted Joints; SCC Test	57
23	Typical Experimental Data for Blanket Top Base Plate Joint	58
24	Preload-Head Rotation Test, Pooled Data for Blanket Top Base Plate Joint	59
25	Preload-Head Rotation Test, Pooled Data for Blanket Bottom Base Plate Joint	60
26	Preload-Head Rotation Test, Pooled Data for Blanket Guide Tube Extension Joint	61
27	Preload-Head Rotation Test, Pooled Data for Reflector Seal Block Joint	62
28	Test Assembly for Joint Separation Test	63
29	Blanket Grid to Post Joint Separation Test Data	64

LIST OF FIGURES (cont'd)

Figure		Page
30	Bearing Load Test Assembly - Support Post Joint	65
31	Bearing Test Data - Support Post Joint	66
32	Plastic Deformation of Test Specimen Due to Bearing Loads	67
33	Strains on the Surface of a Bolt Shank	68
B.1	Guide Tube Extension Joint	69
C.1	Generalization of a Coaxial Joint with Axial and Bending Flexibilities	101
C.2	Surfaces Defining Axial Bolt Force as a Function of External Forces F_2 and F_3	102
C.3	Bolted Joint Separation Zones	103
C.4	Idealization of Blanket Grid Joint	104
C.5	Relation Between Hinge Angle and Flexural Rotation of Bolted Joint Elements	105
C.6	Pivot Point Detail	106
C.7	Useful Relations for Determining Elastic Flexibilities (or Stiffnesses)	107
D.1	Effect of Plastic Deformation on Elastic "Mismatch" - A Physical Illustration	115
D.2	Effect of Plastic Deformation on Elastic "Mismatch" - A Graphic Illustration	116
E.1	Specific Relaxation Graphs for Some Cases of Interest	133
E.2	Mismatches and Displacements (Total and Elastic Residual)	134
E.3	Influence of ψ and ζ On Specific Relaxation Factor	135
E.4	Influence of ψ and ζ On Fractional Load Remaining	136
E.5	Effect of Variations In Relaxation Rates Between Bolt and Joint In a Simple Two-Region Connection	137
E.6	Example Problem for Assessment of Relaxation Factor When Total Displacements Are Not Constant	138
--	Model Work Sheet for Stiffness Calculations	144
--	Model Work Sheet for Calculated Preloads and Stresses	145

LIST OF SYMBOLS

A = curve fitting constant for relaxation factor

A_c = minimum cross-sectional area of bolt

A_i = cross-sectional area of region "i"

A_{sh} = cross-sectional area of bolt shank (must be consistent with J_{sh})

B = curve fitting constant for relaxation factor

B_b = design bearing area

B_{sb} = design shear area in bolt thread

B_{sn} = design shear area in nut thread

C = bolted joint assembly coefficient

C_b, C_{j1}, C_{j2} = elastic redistribution parameter for external loading

D_c = diameter (or effective diameter) of minimum cross-sectional area of bolt

D_h = effective diameter for head frictional torque

D_i = bolt hole diameter in the contacting joint region

D_o = bolt head diameter

D_m = major diameter of bolt thread

D_p = pitch diameter of bolt thread

D_r = minimum root diameter of bolt thread

E, E_i = Young's elastic modulus (for material in region "i" when subscripted)

F_i = axial force supported by region "i"

F_o = elastic preload

$\mathcal{F}$ = fast neutron fluence

G = shear modulus of elasticity

H_i = elastic bending stiffness of region "i"

i = representation for a region label (e.g., "b" for bolt, "j" for joint) or a dummy index in a summation expression

I_e = design engagement length of bolt thread

LIST OF SYMBOLS (cont'd)

I_i = rectangular moment of inertia for region "i"

J_{sh} = polar moment of inertia for minimum shank cross section of bolt (must be consistent with A_{sh})

K_i = elastic linear stiffness of region "i"

L_i = design length of region "i"

L_{sh} = clamped length of bolt shank

L_e = equivalent length of bolt shank (consistent with A_{sh})

M_o = elastic premoment

M_i = bending moment supported by region "i"

m = function parameter

M = preload force per degree of head rotation (see Equations (36) and (37))

N = number of clamped regions in joint

n = number of screw threads per inch, function parameter

Q_b = shear force acting across bolt shank

q_1, q_2 = hinge arm lengths

P, P', P_o = elastic preload

R_i = (standard) relaxation factor of region "i"

r_1, r_2 = bolt-to-joint axial stiffness ratios

$S(r)$ = stress intensity at radius "r" in bolt cross section

S = average (area weighted mean value) stress intensity in bolt cross section

s = connector foot spacer clearance, Laplace transform differentiation operator

α_i = linear thermal expansion per degree temperature change in region "i"

T_a = applied tightening torque to bolt head

T_h = resisting torque under bolt head during tightening

T_h' = resisting torque under bolt head after tightening

LIST OF SYMBOLS (cont'd)

T_t = resisting torque in bolt threads during tightening

T'_t = resisting torque in bolt threads after tightening

T_r = residual torque in bolt shank

U_b = minimum pitch diameter of bolt

U_n = maximum pitch diameter of nut

V_b = minimum major diameter of bolt

V_n = maximum minor diameter of nut

W = externally applied working force to bolted joint

W^-_{sep}, W^+_{sep} = values of working force causing separation between bolted joint members

w = dummy variable for integration

x_i = linear displacement of node "i" relative to a fixed reference

y,z = relaxation exposure level

$\bar{\alpha}_i$ = linear coefficient of thermal expansion for region "i", mean value

α = one half of screw thread profile angle

$\alpha_n = \tan^{-1} [\tan \alpha \cos \lambda]$

Δ, Δ_ℓ = system linear mismatch (Equations (3) and (C3))

Δ_r = system angular mismatch (Equation (C3))

δ_i = linear displacement of one end of region "i" relative to the other end (e.g., region elongation)

δ_e, δ' = elastic linear displacement

δ_t, δ = total linear displacement

δ_p = linear displacement caused by plastic deformation

δ_{pl} = depth of plastic indentation (Figure C.6)

θ_{th} = screw thread rotation angle (degrees)

θ_{sh} = bolt shank twist angle (degrees)

θ_h = bolt head rotation angle (degrees)

LIST OF SYMBOLS (cont'd)

θ_i = rotational displacement of node "i" relative to a fixed reference (see Figure C.1)

ϕ_i = angular rotation of one end of region "i" relative to the other end (caused by bending)

ϕ_c = hinge opening angle

η = ratio of residual-to-applied torque (Equation (34))

λ = screw thread helix angle

λ_i = the portion of the initial elastic elongation (or contraction) of region "i" that is "lost" because of relaxation effects

μ = coefficient of friction

υ = Poisson's ratio

ρ_1, ρ_2 = bolt to joint rotational stiffness ratios

ρ_i = specific relaxation factor for region i, also equal to (δ_p/δ_t)

σ_B = maximum bending tensile stress in bolt

σ_b = average bearing stress

σ_M = membrane tensile stress in bolt

τ_M = membrane shear stress in bolt

τ_t = average shear stress in screw threads

ζ = fractional stress relaxation factor (also $\delta_e(z)/\delta_t(0)$, $\delta'(z)/\delta(0)$, e^{-Az})

ψ = fractional total displacement factor (also $\delta_t(z)/\delta_t(0)$, $\delta(z)/\delta(0)$)

Analytical methods and test data employed in the core design of bolted joints for the LWBR core are presented. The effects of external working loads, thermal expansion, and material stress relaxation are considered in the formulation developed to analyze joint performance. Extensions of these methods are also provided for bolted joints having both axial and bending flexibilities, and for the effect of plastic deformation on internal forces developed in a bolted joint. Design applications are illustrated by examples.

FORCES IN BOLTED JOINTS: ANALYSIS METHODS AND TEST RESULTS UTILIZED FOR NUCLEAR CORE APPLICATION

(LWBR Development Program)

P.J. Crescimanno
K.L. Keller

I. INTRODUCTION AND SCOPE

This report presents the analytic methods and experimental data that were used to compute the forces and stresses developed in the core bolted joints for the Light Water Breeder Reactor (LWBR). The primary mode of structural fastening within the LWBR core is the bolted joint. These bolted connections, which were designed to remain tight over the operating life of the core, had to satisfy a series of constraints not normally encountered in general structural applications. For example, material and size of both bolt and joint had to be controlled to minimize the effects they could have on nuclear breeding (from parasitic neutron capture), corrosion, and joint temperature. Also, as a direct consequence of their nuclear application, these bolted joints had to be sufficiently preloaded to offset the effects of radiation enhanced material relaxation without allowing critical stress limits to be exceeded (even for very low probability accidental modes of high loading). In addition, the following usual requirements also had to be satisfied: no slippage or impacting between the joint members due to external loading, acceptable fatigue usage from cyclic loads, partial (or complete) compensation of thermal expansion effects when dissimilar materials are used in the bolted joint, and the use of simple methods of joint tightening (e.g., by torque wrench) during assembly of components. Trying to satisfy all these requirements simultaneously resulted in designs where the magnitude of bolt assembly preloads (elastic clamping forces produced in

tightened bolts) were confined to narrow acceptance bands. To determine the widest permissible range of preloads, and to achieve this range with a high level of confidence, the following procedures were developed:

1. Analytical methods that simplified the process of combining all pertinent factors affecting bolt preload (supported experimentally by tightening tests of selected LWBR bolted joints).
2. Preload control methods for joints tightened to either a torque limit or a rotation limit.
3. Tightening techniques that minimized the effect of friction or preload variation.

Because of the universal nature of bolted joints as a means of structural fastening, and the attention given to bolted joint design constraints of common interest to all nuclear reactors, it was concluded that the bolted joint technology developed for LWBR could add to the developing body of knowledge applicable to the nuclear industry. This report presents some of this technology in the form of test results and analytic relations useful to the design evaluation of bolted joints. References are provided for results not derived from first principles. In derived expressions the steps to obtain the final formulas are outlined in sufficient detail so that modifications can be easily made for different assumptions. Specifically, the topics presented are:

(a) Calculation of internal forces in a bolted joint, including effects of working load, thermal expansion, and stress relaxation,
(b) Effect of preload and composite system flexibility on cyclic bolt loading,
(c) Two tightening methods used by LWBR to control preload,
(d) Design stresses to be computed in joint analyses,
(e) Tests and test results to determine bolt preload levels and stable levels of bearing stress,
(f) Illustrative examples of calculations for a conventional bolted joint and an eccentric "rocking" joint, and
(g) Extension of the basic elastic analysis to account for the occurrence of time independent plastic deformation in the joint under load.

II. ANALYSIS OF PRELOAD IN BOLTED JOINTS

A. Calculation of Internal Forces in a Bolted Joint

1. Relation of Mismatch to Internal Forces

In the development of a mechanical design, calculations are required frequently to assess the effects produced by factors that alter the constrained elastic displacements in a bolted joint. With a "mismatch" (or joint interference) concept, simplified mathematical relations can be derived which may be used to perform these assessments. The joint elastic mismatch, as employed here, is the net difference in free lengths between the members of the loaded joint if they were imagined to be in a disengaged state (no loosening of the bolt by rotation is implied, however). This concept is illustrated in Figure 1, which shows a physical picture of a bolted joint (Figure 1a) that has been mechanically idealized into a system of loaded springs (Figure 1b) which is disengaged in the sense that all forces acting on this system are removed (Figure 1c). In this final illustration the difference in the free length between the bolt and joint members is defined as the joint elastic mismatch and is labelled in Figure 1c by the symbol Δ. Note that if there is no mismatch in the joint there can be no joint preload: the bolt and joint member free lengths must imply interference before internally generated constraining forces can develop in the assembled connection. Further, it should be noted that Δ is a "signed" quantity. Figure 1c illustrates the case when $\Delta > 0$, which indicates the presence of a preload in the assembled joint. However, if $\Delta < 0$, that is if the free length of the bolt exceeds the free length of the joint members in series, a loose joint (no preload) occurs. These observations are useful since the joint mismatch could be severely changed, even completely eliminated, by such phenomena as thermal expansion (or contraction), material relaxation, and even plastic deformation. The advantage of the mismatch concept is that it provides an image for the attribute of mutual constraint whose modification by a variety of phenomena can be easily visualized.

Figure 1(b) portrays the equivalent spring system of the bolted joint under load, which attains this loaded configuration upon displacement from the initial free state shown in Figure 1(c). Let the displacements of nodes A, B, C, and D be X_1, X_2, X_3, and X_0 respectively: the positive sense for displacement being indicated by the arrows shown in the figure. As illustrated in Figure 1(b), node D remains fixed and nodes B and C come together in the loaded joint. From

examination of Figures 1(b) and 1(c) it is seen that $x_0 = 0$, x_1 and x_2 will be negative displacements, and x_3 will be a positive displacement. Using these displacements, the extensions (or compression) of the individual regions are perceived to be,

$$\left.\begin{aligned} \delta_b &= x_3 - x_0 \\ \delta_{j1} &= x_1 - x_0 \\ \delta_{j2} &= x_2 - x_1 \end{aligned}\right\} \quad (1)$$

Thus it is observed that δ_b is the extension of the bolt required in Figure (1), whereas δ_{j1} and δ_{j2} represent the compression of the two joint regions (because the terminating nodes move toward each other in going from the free state to the loaded state). Using the symbols K_b, K_{j1}, and K_{j2} for the elastic stiffnesses of the bolt and joint members respectively, the following relationships apply in the bolted joint.

a. Stiffness Relations

$$\left.\begin{aligned} F_b &= K_b \delta_b \quad , \delta_b > 0 \\ F_{j1} &= K_{j1} \delta_{j1} \, , \delta_{j1} \leq 0 \\ F_{j2} &= K_{j2} \delta_{j2} \, , \delta_{j2} \leq 0 \end{aligned}\right\} \quad (2)$$

The local displacement inequalities in Equation (2), which apply specifically to the basic bolted joint model illustrated in Figure 1, reflect the assumption that the joint members j1 and j2 cannot support tensile forces (non-cohesive joint surfaces are assumed) and that the tensile loading exists only in the bolt.

Examination of Figures 1(c) and 1(b) reveals that if the bolt develops an elongation, δ_b, the assembled joint members must develop a corresponding compressive displacement, $\delta_{j1} + \delta_{j2}$, in order to be in contact with the bolt. Thus we observe that following conditions on displacements must exist.

b. Compatibility of Displacements

$$\delta_{j1} + \delta_{j2} = -(\Delta - \delta_b)$$

or

$$\delta_b - \delta_{j1} - \delta_{j2} = \Delta \quad . \quad (3)$$

By consideration of the system of node displacements, the static equilibrium of forces at nodes A and B, Figure 1(b), requires,

$$\sum F_B = -K_b (x_3 - x_0) - K_{j2} (x_2 - x_1) = 0$$

$$\sum F_A = W - K_{j1} (x_1 - x_0) + K_{j2} (x_2 - x_1) = 0$$

which, in terms of the member displacements defined in Equation (1) may be restated as follows:

c. Static Equilibrium of Forces

$$\left.\begin{aligned} K_b \delta_b + K_{j2} \delta_{j2} &= 0 \\ K_{j1} \delta_{j1} - K_{j2} \delta_{j2} &= W \end{aligned}\right\} \quad (4)$$

It is convenient and useful (as will be seen in Appendix C) to express Equations (3) and (4) in matrix form. Thus,

$$\begin{bmatrix} 1 & -1 & -1 \\ K_b & 0 & K_{j2} \\ 0 & K_{j1} & -K_{j2} \end{bmatrix} \cdot \begin{bmatrix} \delta_b \\ \delta_{j1} \\ \delta_{j2} \end{bmatrix} = \begin{bmatrix} \Delta \\ 0 \\ W \end{bmatrix} . \quad (5)$$

Solving Equation (5)* for the individual member displacements yields,

$$\delta_b = \frac{\frac{1}{K_b} \Delta + \frac{1}{K_b K_{j1}} W}{\left[\frac{1}{K_b} + \frac{1}{K_{j1}} + \frac{1}{K_{j2}}\right]} , \quad (6)$$

$$\delta_{j1} = \frac{-\frac{1}{K_{j1}} \Delta + \frac{1}{K_{j1}} \left[\frac{1}{K_b} + \frac{1}{K_{j2}}\right] W}{\left[\frac{1}{K_b} + \frac{1}{K_{j1}} + \frac{1}{K_{j2}}\right]} , \quad (7)$$

*Note: The determinant of the coefficient matrix in Equation (5) is

$$-K_b K_{j1} - K_b K_{j2} - K_{j1} K_{j2}$$

which may also be expressed,

$$-K_b K_{j1} K_{j2} \left[\frac{1}{K_b} + \frac{1}{K_{j1}} + \frac{1}{K_{j2}}\right] .$$

and

$$\delta_{j2} = \frac{-\frac{1}{K_{j2}}\Delta - \frac{1}{K_{j1}K_{j2}}W}{\left[\frac{1}{K_b} + \frac{1}{K_{j1}} + \frac{1}{K_{j2}}\right]} \quad . \tag{8}$$

Using these displacement relations and Equation (2), the member forces can be expressed by

$$F_b = \frac{\Delta + \frac{1}{K_{j1}}W}{\left[\frac{1}{K_b} + \frac{1}{K_{j1}} + \frac{1}{K_{j2}}\right]} \quad , \tag{9}$$

$$F_{j1} = \frac{-\Delta + \left(\frac{1}{K_b} + \frac{1}{K_{j2}}\right)W}{\left[\frac{1}{K_b} + \frac{1}{K_{j1}} + \frac{1}{K_{j2}}\right]} \quad , \tag{10}$$

and

$$F_{j2} = \frac{-\Delta - \frac{1}{K_{j1}}W}{\left[\frac{1}{K_b} + \frac{1}{K_{j1}} + \frac{1}{K_{j2}}\right]} \quad . \tag{11}$$

If no working force is acting on the joint, the only load present is the bolt preload. This force is defined by the following useful equality.

$$P = \frac{\Lambda}{\left[\frac{1}{K_b} + \frac{1}{K_{j1}} + \frac{1}{K_{j2}}\right]} \quad . \tag{12}$$

A simplification of Equations (9) to (11) is possible if the following definitions for bolt-to-joint stiffness ratios are adopted:

$$r_1 = \frac{K_b}{K_{j1}} \text{ and } r_2 = \frac{K_b}{K_{j2}} \quad . \tag{13}$$

Equations (9) and (11) may then be written

$$F_b = P + \frac{r_1}{(1 + r_1 + r_2)}W, \; F_{j1} = -P + \frac{(1 + r_2)}{(1 + r_1 + r_2)}W, \text{ and } F_{j2} = -F_b \quad .$$

These equalities are valid only up to the point of joint separation. The condition for incipient separation within the joint portrayed in Figure 1 occurs when

either $F_b \longrightarrow 0$ or $F_{j1} \longrightarrow 0$ under the action of the imposed working force, W. Therefore the two separation working forces may be defined as follows:

$$W_{sep}^{-} = -\frac{(1 + r_1 + r_2)}{r_1} P, \; F_b = 0 \tag{14}$$

and

$$W_{sep}^{+} = \frac{(1 + r_1 + r_2)}{(1 + r_2)} P, \; F_{j1} = 0 \quad . \tag{15}$$

When joint separation occurs, the joint members being loaded support the working force in its entirety. Consequently, the bolted joint relations for internal forces applicable to full range of working loads can be written as,

$$F_b = \begin{cases} 0 \;, & W \leq -\dfrac{(1 + r_1 + r_2)}{r_1} P \\ P + \dfrac{r_1}{(1 + r_1 + r_2)} W, & -\dfrac{(1 + r_1 + r_2)}{r_1} P < W < \dfrac{(1 + r_1 + r_2)}{(1 + r_2)} P \\ W \;, & \dfrac{(1 + r_1 + r_2)}{(1 + r_2)} P \leq W \end{cases} \tag{16}$$

and

$$F_{j1} = \begin{cases} W \;, & W \leq -\dfrac{(1 + r_1 + r_2)}{r_1} P \\ -P \dfrac{(1 + r_2)}{(1 + r_1 + r_2)} W, & -\dfrac{(1 + r_1 + r_2)}{r_1} P < W < \dfrac{(1 + r_1 + r_2)}{(1 + r_2)} P \\ 0 \;, & \dfrac{(1 + r_1 r_2)}{(1 + r_2)} P \leq W \end{cases} \tag{17}$$

where

$$F_{j2} = -F_b \quad . \tag{18}$$

Graphs of F_b and F_{j1} as functions of W appear in Figure 2. In this derivation it should be noted that the elastic stiffnesses were assumed to remain unchanged throughout the range of variation for W. Although this is generally a

satisfactory assumption, this condition may not be satisfied in certain bolted joints depending upon the nature of the materials present, the seating of the clamped surfaces, or the geometric shape of the clamped region.

The most common simplification of Equations (16) and (17) applies to the case when the working load acts directly under the bolt head. In this situation regions j1 and j2 are considered to form the composite region j1'. Region j2' may be considered infinitesimally thin (e.g., having zero flexible length) so that $K_{j2'} = \infty$. Thus, the flexibility relations for the "primed" regions become,

$$\frac{1}{K_{j1'}} = \frac{1}{K_{j1}} + \frac{1}{K_{j2}} \quad \text{and} \quad \frac{1}{K_{j2'}} = 0$$

With this modification, Equations (9) and (10) reduce to,

$$F_b = P + \frac{\frac{1}{K_{j1'}}}{\left[\frac{1}{K_b} + \frac{1}{K_{j1'}}\right]} W \tag{19}$$

and

$$F_{j1'} = -P + \frac{\frac{1}{K_b}}{\left[\frac{1}{K_b} + \frac{1}{K_{j1'}}\right]} W \quad . \tag{20}$$

Naturally, these equations are only applicable when W is below the separation load (e.g., $W < (1 + \frac{K_b}{K_{j1'}})\ P$).

A useful result obtained from the preceding derivations is the relation presented in Equation (12), which accounts for the effect of changes in mismatch (constrained elastic displacement) and elastic stiffness on a significant parameter, namely the bolt preload. This equation is easily generalized for N joint regions in Equation (21), which follows:

$$P = \frac{\Delta}{\left[\frac{1}{K_b} + \sum_{i=1}^{N} \frac{1}{K_{ji}}\right]} \quad . \tag{21}$$

2. Effect of Thermal Expansion

Thermal expansion effects on preload are introduced directly with the mismatch concept. To demonstrate, consider a bolted joint which was tightened

to attain an assembly preload, P_1, at room temperature. Compute the stiffnesses* of the bolt and joint at room temperature and, for example, at the elevated temperature of interest. Using the variation of Young's elastic modulus with temperature, form the sum of reciprocal stiffnesses at the assembly temperature,

$$\left[\frac{1}{K_b} + \sum_{i=1}^{N} \frac{1}{K_{ji}}\right]_1 ,$$

and at the elevated temperature,

$$\left[\frac{1}{K_b} + \sum_{i=1}^{N} \frac{1}{K_{ji}}\right]_2 .$$

From Equation (21) the initial assembly mismatch is obtained, namely

$$\Delta_1 = \left[\frac{1}{K_b} + \sum_{i=1}^{N} \frac{1}{K_{ji}}\right]_1 P_1 .$$

Referring to Figure 1(c) it is seen that an expansion of the bolt <u>decreases</u> the mismatch, whereas an expansion of the joint members tends to <u>increase</u> the mismatch. Thus if the linear expansion per degree temperature change is given by

$$\mathscr{S}_b = \bar{\alpha}_b L_b \tag{22}$$

for the bolt, and by

$$\mathscr{S}_j = \sum_{i=1}^{N} \bar{\alpha}_{ji} L_{ji} \tag{23}$$

for the joint members, the net expansion of the bolt relative to the joint per degree change in temperature is given by $\mathscr{S}_b - \mathscr{S}_j$, where $\bar{\alpha}_i$ is the mean coefficient of thermal expansion for region "i" over the entire temperature range from

*Stiffness may be computed on the basis of regions stressed uniformly over their length, e.g., $K_i = A_i E_i / L_i$, or with appropriate axial variations in stress as in References (a) and (b). Stiffness calculations for a typical bolted joint are illustrated in Appendix B.

t_1 to t_2, and "L_i" is the corresponding region clamped length. Over the full temperature range the net expansion must therefore be $(\mathscr{l}_b - \mathscr{l}_j)\ (t_2 - t_1)$. Accordingly, the mismatch at temperature t_2 becomes

$$\Delta_2 = \Delta_1 - (\mathscr{l}_b - \mathscr{l}_j)\ (t_2 - t_1) \quad . \tag{24}$$

Since Equation (24) represents the new mismatch at the elevated temperature t_2, new preload is computed via Equation (21), namely

$$P_2 = \frac{\Delta_2}{\left[\frac{1}{K_b} + \sum_{i=1}^{N} \frac{1}{K_{ji}}\right]_2} \quad .$$

Provided this preload does not imply the occurrence of plastic deformation in the joint (otherwise Δ_2 would have to be modified for plasticity effects), the correct preload resulting from the temperature change shall have been computed.

3. Effect of Stress Relaxation

Stress relaxation is a form of material creep whereby a fraction of the initial elastic strain in a body is converted into non-recoverable plastic strain while the total strain in the body remains unchanged. The fraction of the elastic strain that is lost in this process is called a "relaxation factor." For a material whose elastic strain is directly proportional to its stress, the loss in elastic strain is accompanied by a proportional loss in stress level. Employing the symbols δ, for the original elastic displacement; R, for relaxation factor; and λ, for lost elastic displacement; stress relaxation in a bolted joint would be characterized by lost elastic displacements equal to $\lambda = R\delta$ in general, or as given by Equation (25) for the joint illustrated in Figure 1.

$$\lambda_b = R_b\ \delta_b,\ \lambda_{j1} = R_{j1}\ \delta_{j1},\ \text{and}\ \lambda_{j2} = R_{j2}\ \delta_{j2} \quad . \tag{25}$$

If the final displacements are denoted by a primed superscript, the resulting elastic displacements for bolt and joint members are,

$$\delta'_b = (1 - R_b)\ \delta_b,\ \delta'_{j1} = (1 - R_{j1})\ \delta_{j1},\ \text{and}\ \delta'_{j2} = (1 - R_{j2})\ \delta_{j2} \quad . \tag{26}$$

Using Equation (3) the resulting mismatch after relaxation must be

$$\Delta' = \delta'_b - \delta'_{j1} - \delta'_{j2}$$

which, upon substitution of Equation (26), becomes,

$$\Delta' = (1 - R_b)\,\delta_b - (1 - R_{j1})\,\delta_{j1} - (1 - R_{j2})\,\delta_{j2} \quad .$$

If the external load W remains constant over the period of relaxation, then by substitution of the expressions in Equations (6), (7), and (8) for the initial displacements the relaxed mismatch becomes,

$$\Delta' = \frac{\left[\frac{(1 - R_b)}{K_b} + \frac{(1 - R_{j1})}{K_{j1}} + \frac{(1 - R_{j2})}{K_2}\right]}{\left[\frac{1}{K_b} + \frac{1}{K_{j1}} + \frac{1}{K_{j2}}\right]}\,\Delta$$

$$+ \frac{\left[\frac{(1 - R_b)}{K_b}\frac{1}{K_{j1}} - \frac{(1 - R_{j1})}{K_{j1}}\left(\frac{1}{K_b} + \frac{1}{K_{j2}}\right) + \frac{(1 - R_{j2})}{K_{j2}}\frac{1}{K_{j1}}\right]}{\left[\frac{1}{K_b} + \frac{1}{K_{j1}} + \frac{1}{K_{j2}}\right]}\,W \quad .$$

If no external load was present during the relaxation process, then the relaxed mismatch equation simplifies to,

$$\Delta' = \frac{\left[\frac{(1 - R_b)}{K_b} + \frac{(1 - R_{j1})}{K_{j1}} + \frac{(1 - R_{j2})}{K_{j2}}\right]}{\left[\frac{1}{K_b} + \frac{1}{K_{j1}} + \frac{1}{K_{j2}}\right]}\,\Delta, \text{ for } W = 0$$

Since, from Equation (12), the relaxed preload must be

$$P' = \frac{\Delta'}{\left[\frac{1}{K_b} + \frac{1}{K_{j1}} + \frac{1}{K_{j2}}\right]} \quad ,$$

the relaxed preload relative to the initial preload takes a form similar to that for the relaxed and initial mismatches, namely

$$P' = \frac{\left[\frac{(1 - R_b)}{K_b} + \frac{(1 - R_{j1})}{K_{j1}} + \frac{(1 - R_{j2})}{K_{j2}}\right]}{\left[\frac{1}{K_b} + \frac{1}{K_{j1}} + \frac{1}{K_{j2}}\right]}\,P \quad .$$

These results are generalized, via Equation (21), for N joint regions as follows:

$$\Delta' = \frac{\left[\frac{(1 - R_b)}{K_b} + \sum_{i=1}^{N} \frac{(1 - R_{j1})}{K_{ji}}\right]}{\left[\frac{1}{K_b} + \sum_{i=1}^{N} \frac{1}{K_{ji}}\right]} \Delta \qquad (27)$$

and

$$P' = \frac{\left[\frac{(1 - R_b)}{K_b} + \sum_{i=1}^{N} \frac{(1 - R_{ji})}{K_{ji}}\right]}{\left[\frac{1}{K_b} + \sum_{i=1}^{N} \frac{1}{K_{ji}}\right]} P \quad . \qquad (28)$$

The reduced mismatch in Equation (27) could result in a relocation of some of the joint interfaces in the bolted joint. If this occurs, a change in total strain may be implied during the relaxation process for some joint members, which is not strictly consistent with the tests that were used to obtain the relaxation factors. Material relaxation tests are usually run at constant total strain, whereas the total strain of the individual joint components cannot be constant if each component develops a different level of relaxation over the same time period. However, this does not introduce large errors provided that calculated changes of total strain in the most prominent elastic members (usually the bolt itself) are small compared to the original total strains.* It is noted that no change in total strain will occur for any bolted joint member if all relaxation factors are the same, therefore the condition of small changes in total strain will usually be satisfied if relaxation factors among the different members are not "too dissimilar." Also, if one member approaches complete relaxation ($R \rightarrow 1.0$) Equations (27) and (28) could lead to unrealistic predictions. To use these equations in this case, it is best to divide the relaxation history into a number of segments where relaxation effects from segment-to-segment are computed successively, and where the "reasonably small" total strain

*For a uniformly strained region, i, this amounts to a comparison of the quantity $[(1-R_i)P - P']/K_iL_i$ to P/K_iL_i.

change within each segment is simultaneously satisfied for the rapidly relaxing member. The terms "too dissimilar" and "reasonably small" are deliberately left undefined because they are based on judgments considering the member stiffnesses and the design function of the joint.

When the total strain cannot be considered (even approximately) constant during the relaxation period, it may not be appropriate to use the previously defined "standard" relaxation factor, R. A modification of this factor, defined and derived in Appendix E as a "specific" relaxation factor, is used in place of the standard factor and Equations (27) and (28) are altered slightly. The term "specific" is used here because this factor is computed for a specific variation of the total strain (with time or exposure level) during the relaxation period. This variation is typically slow and continuous, and is caused by processes independent of the relaxation process itself (as in the case of stress free volumetric growth caused either by thermal expansion or material swelling, or from gradual changes in external loading).

4. Importance of Bolted Joint Preload and Some Practical Design Guidelines

If a bolted connection joining two structures is either loose or insufficiently tightened, the following structurally undesirable and self-worsening developments may occur:

a. Relative motion between the joint members and bolt, permitted by looseness in the joint, could result in surface wear and increased stressed from impact loads;
b. Axial and transverse alignment of the joined structures, relative to each other, could be disturbed; and
c. Any hydraulic seal provided by the connection could be degraded because of leakage in the joint.

A lightly loaded or poorly proportioned joint could also be responsible for the fatigue failure of a bolt in a joint subjected to cyclic loading. The consequence of these conditions on bolt fatigue life is more subtle than the previously listed occurrences and requires some discussion. In presenting the elastic response of a preloaded joint to an externally applied working load, it will be recalled that the incremental change in bolt load was less than the corresponding incremental change in the working load if joint separation did not take place (see Figure 2). When the working load exceeds the upper separation

load in Figure 2, the bolt itself supports the working load and any changes in the working load directly affects the bolt load on a one-for-one basis. Since the fatigue strength of the bolt will depend upon its alternating stress intensity and the number of load cycles to be sustained, and since design changes cannot affect the number of load cycles, it is obvious that design modifications will be directed towards reducing the alternating stress intensity or to making the stress intensity acceptable through a change in bolt material. Assuming no change in bolt material or dimensions, a decrease in range of the alternating bolt forces is needed to reduce the alternating stress intensity. A simple way to achieve this objective is to merely increase the bolted joint preload level. This is illustrated in Figure 3, which shows the characteristic graph of bolt load vs. working load applicable to a typical joint for two states of preload. If it is supposed that the same alternating working force acts for each of the preload states portrayed, the graphic construction of the cyclic bolt force in Figure 3 shows that the range of variation in the bolt load can be altered by changing the level of preload. However, it should be observed that once a sufficiently high preload is attained so that joint separation cannot occur during a cylce, continued increases in preload cause no further reduction in amplitude of the alternating component of the bolt force. In this case the range of variation of the bolt force for the given working load variation is completely determined by the slope of the characteristic response curve for the bolted joint. As shown in Figure 2 (and Section II.A.1) this slope is a function of the bolted joint stiffnesses, which can be changed only if the stiffnesses are changed. As an example, for the system illustrated in Figure 1 (and whose response is graphed in Figure 2) a reduction in the bolt response slope may be attained by either reducing K_b and K_{j2} or increasing K_{j1}.

In designs optimized to satisfy a multiplicity of constraints it is seldom that a redesign can be achieved by altering only one feature (preload, dimensions, material, etc.): more typically two or more features must be simultaneously changed to optimize the redesign to the original constraints. This results in a considerable complication to the overall design process. To minimize unnecessary complications, the following general design guidelines are offered for consideration:

a. Keep bolt and joint shapes and arrangements simple. This is an advantage for component fabrication as well as for computational analysis.

b. Develop the greatest elastic mismatch in the tightened joint that is consistent with stress, size, and material constraints. This provides compensation for relaxation and local plasticity effects that may be difficult to quantify. If significant elastic mismatch is provided by joint members as well as the bolt, a greater degree of freedom will be present in making adjustments during possible future design optimizations.

c. Avoid joint separation under static loading and joint "chattering" (intermittent separation) during dynamic loading through suitable choices of preload and member stiffnesses. In very high frequency applications the bolt and joint acoustic response should be designed to avoid the extra fatigue cycles caused by natural frequency excitation by the high frequency external loading.

d. Do not assign a small axial length to cross sections developing the highest average strains, otherwise small, unanticipated increases in mismatch could result in relatively large increases in local strain if that region begins to deform plastically, with failure being the consequence. This is a common problem when bolts contain short undercut (minimum cross section) regions.

B. Two Methods for Attaining Initial Preload in LWBR Core Assemblies

Initial preloads have been obtained in bolted joints using the following commonly applied methods of joint tightening: (a) assembly of joint with an elastically stretched bolt (external tensioner produces mismatch which, upon release of external bolt load, causes a joint preload without the presence of residual torque); (b) assembly of joint with a thermally extended bolt, due to temperature difference between bolt and joint or due to differential thermal expansion when bolted joint is not at room temperature (mismatch produced by material thermal contraction results in joint preload without residual torque when bolted joint attains room temperature); (c) assembly of joint tightened to a specific level of torsional resistance (torque is produced by head and thread friction on the loaded bolt); and (d) assembly of joint tightened to a specific head rotation angle (angle is measured from a lightly clamped starting condition). In the assembly of LWBR core components only the torque and head

rotation methods of tightening were used, consequently analyses for preload developed by only torque and head rotation methods are presented in the discussion that follows.

1. Preload by Control of Applied Torque

A common way to limit bolt preloads to prescribed levels is to tighten a bolt to a specific torque. To achieve this preload control it is necessary to know the coefficients of sliding friction between moving surfaces in the threaded region of the bolt and under the bolt head or nut. If these frictional coefficients are well known, the relation between the applied torque, T_a, and bolt preload, P, may be computed using the following equation (or other equivalent forms of this equation as derived in machine design textbooks such as Reference (c)):

$$T_a = \frac{1}{2}\left[\mu D_h + \left[\frac{\cos \alpha_n \sin \lambda + \mu \cos \lambda}{\cos \alpha_n \cos \lambda - \mu \sin \lambda}\right] D_p\right] P \quad , \tag{29}$$

where

T_a = applied torque, lb-in

P = bolt preload, lb

μ = coefficient of sliding friction (assumed same for head and thread)

D_o = head diam. (between flats on nut), in.

D_i = hole diam. under head, in.

D_h = effective diam. for head friction torque, in. For the case of a uniform coefficient of friction over a circular annular area with uniform contact pressure, one may use

$$D_h = \frac{2}{3}\left[\frac{D_o^3 - D_i^3}{D_o^2 - D_i^2}\right]$$

n = number of threads per inch

α = 1/2 thread profile angle (30° for standard threads)

D_p = bolt thread pitch diam

λ = helix angle = $\tan^{-1}\left[\frac{1}{n \pi D_p}\right]$

$\alpha_n = \tan^{-1}[\tan \alpha \cos \lambda]$

Frequently, the coefficients of friction are not well known, and the relationship between preload and torque must be experimentally determined. In this case it has been found convenient to fit data to the equation,

$$T_a = C\, D_m\, P \tag{30}$$

where T_a and P are as previously defined, and where

D_m = bolt thread major diam.

C = assembly coefficient.

By comparison of Equations (29) and (30) it is clear that the assembly coefficient may be expressed,

$$C = \frac{1}{2}\left[\mu\,\frac{D_h}{D_m} + \left[\frac{\cos\,\alpha_n\,\sin\,\lambda + \mu\,\cos}{\cos\,\alpha_n\,\cos\,\lambda - \mu\,\sin}\right]\frac{D_p}{D_m}\right] . \tag{31}$$

Experimental data fitted to Equation (30) allows determination of assembly coefficients for a particular design application, and also allows coefficients of friction to be computed and related to applicable combinations of sliding surfaces.

In many practical situations $\mu < 0.3$, $\lambda < 5°$, and $\alpha = 30°$, so that

$$\frac{\cos\,\alpha_n\,\sin\,\lambda + \mu\,\cos\,\lambda}{\cos\,\alpha_n\,\cos\,\lambda - \mu\,\sin\,\lambda} \approx \tan\,\lambda + \frac{\mu}{\cos\,\alpha_n} .$$

Since

$$\tan\,\lambda = \frac{1}{n\,\pi\,D_p} ,$$

Equation (31) may be simplified to the following useful approximation,

$$C \approx \left[\frac{1}{2\,n\,\pi\,D_m}\right] + \left[\frac{D_h}{2\,D_m} + \frac{D_p}{1.732\,D_m}\right]\mu ,$$

which shows the prominent effect that the coefficient of friction can have on the assembly torque when tightening to a given preload.

2. Preload by Control of Bolt Head Rotation

If the joint being bolted is rigid, rotation from an initially "tight" condition will result in an elongation of the bolt from strictly geometric considerations due to turning of the screw threads. Further rotation of the screw

thread would be required to attain the same bolt elongation if the joint were flexible. It should be noted that the rotation in the threaded region must be somewhat less than the rotation of the bolt head because of the twist in the shank (between head and first engaged thread). Therefore the determination of preload by head rotation, which is primarily controlled by thread geometry, must also include corrections for the torsional stiffness of the bolt and the axial stiffnesses of both the bolt and joint. Assuming only coaxial loading (no bending) of the bolted joint, each of the preceding concerns is considered separately and then combined into a final result in the derivation that follows.

a. Mismatch Caused by Thread Rotation

If the joint is rigid, the mismatch (Section II.A.1) must be,

$$\Delta = \frac{1}{n}\left[\frac{\theta_{th}}{360}\right] \tag{32}$$

where

θ_{th} = thread rotation angle, degrees
n = number of threads per inch.

In this case $\Delta = \delta_b$. However if the joint is flexible, it would develop some compressive displacement and $\Delta = \delta_b - \delta_j$, (see Equation (3) and Figure 1).

b. Bolt Preload

Due to the presence of a mismatch, Δ, if K_b is the bolt stiffness, and K_j is the overall joint stiffness (e.g., $\frac{1}{K_j} = \sum_{i=1}^{N} \frac{1}{K_{ji}}$), then the preload must be given by Equation (21), or

$$P = \frac{\Delta}{\left[\frac{1}{K_b} + \frac{1}{K_j}\right]} \quad . \tag{33}$$

c. Twisting of the Bolt Shank

When a torque is applied to a bolt head to tighten a joint, friction on all sliding surfaces, in addition to the frictionless components of the forces acting on the screw helix, combine to produce an opposite and equal resisting

torque. Thus if T_t and T_h are the total resisting torques from the thread and head respectively when an applied torque external to the head is T_a, summing all torques for a system in static equilibrium yields,

$$T_t + T_h + T_a = 0 \quad .$$

In the preceding equality it shall be assumed (for convenience only) that T_a is numerically positive, which thereby implies that the resisting torques T_t and T_h are numerically negative. When the external torque T_a is removed, the final torques at the thread and head respectively become T_t' and T_h'. Thus,

$$T_t' + T_h' = 0 \quad .$$

Defining the residual torque left in the shank to be

$$T_r = T_h' = -T_t' \quad ,$$

the residual torque can be quantified via the two cases that follow:

$$\underline{\text{Case 1}}: \quad |T_t| \leq |T_h|$$

If $|T_t| \leq |T_h|$, then $|T_t| \leq 1/2\ T_a$. Upon removal of T_a the direction of frictional forces under the head will reverse letting T_h' be a positively signed quantity. Since the head can support T_t without slipping we have

$$T_t' = T_t \text{ and } T_h' = -T_t' = |T_t|$$

so that

$$T_r \leq 1/2\ T_a.$$

$$\underline{\text{Case 2}}: \quad |T_t| > |T_h|$$

If $|T_t| > |T_h|$, then $|T_h| < 1/2\ T_a$. Upon removal of T_a the direction of frictional forces under the head will reverse, letting T_h' be a positively signed quantity. However, owing to the fact that $|T_t| > |T_h|$, the head will slip since it can only maintain a torque $T_h' = -T_h = |T_h|$ for the axial load being supported. Assuming the frictional drag forces on the thread are always sufficient to keep the preloaded bolt from backing out, the bolt preload will be maintained even if some of the thread drag forces must change direction. This drops the net torque developed on the screw threads to a magnitude that can be supported by the head, thus

$$T_t' = -T_h'$$

where

$$T_h' = |T_h| < 1/2\ T_a \quad .$$

Consequently,

$$T_r < 1/2\ T_a \quad .$$

From both cases 1 and 2, which encompass the full range of possibilities, it is concluded that the shank residual torque is always less than or equal to, half the applied torque. Stated as an equality this is expressed,

$$T_r = \eta\ T_a \ , \ 0 < \eta \leq 1/2 \quad . \tag{34}$$

In some of the bolt tightening tests described in Section III, shear stresses were measured with strain rosettes. The results of these measurements indicated that an $\eta \approx 1/4$ was typical. Since only a few bolt designs were tested in this way, this value for η may not be generally applicable to other designs. However, it does support the reality of a residual torque and its expected magnitude.

The shank twist angle and residual torque are related as follows:

$$T_r = \frac{G\ J_{sh}}{L_{sh}} \left(\frac{\pi}{180}\ \theta_{sh}\right)$$

where

G - shear modulus

J_{sh} = polar moment of inertia of shank (mean value for bolt over the clamped length of joint)

L_{sh} = shank length (clamped length of joint)

θ_{sh} = total twist angle over shank length, in degrees.

Noting that

$$G = \frac{E}{2\ (1 + \upsilon)}$$

where E is Young's elastic modulus and υ is Poisson's ratio; and that in terms of an equivalent shank length, L_e, and shank cross-sectional area, A_{sh} (consistent with J_{sh}), the bolt stiffness may be expressed by,

$$K_b = \frac{A_{sh}E}{L_e} \quad ;$$

the torque-twist angle relation may be put into the following form,

$$T_r = \frac{\pi}{(1 + \upsilon)} \left[\frac{J_{sh}}{A_{sh}}\right]\left[\frac{L_e}{L_{sh}}\right] K_b \left[\frac{\theta_{sh}}{360}\right] \quad . \tag{35}$$

d. Total Head Rotation

The total head rotation must be the sum of the rotation by the screw thread plus the twist in the shank. In terms of ratios already formed;

$$\frac{\theta_h}{360} = \frac{\theta_{th}}{360} + \frac{\theta_{sh}}{360} \quad .$$

From Equations (32) and (33) the rotation in the threaded region is expressed,

$$\frac{\theta_{th}}{360} = n \left[\frac{1}{K_b} + \frac{1}{K_j}\right] P \quad ,$$

and from Equation (35) the rotation in the shank is expressed,

$$\frac{\theta_{sh}}{360} = \frac{(1 + \upsilon)}{\pi} \left[\frac{A_{sh}}{J_{sh}}\right]\left[\frac{L_{sh}}{L_e}\right] \frac{1}{K_b} T_r \quad .$$

Since from Equations (34) and (30) the residual torque can be expressed,

$$T_r = \eta\, C\, D_m P \quad ,$$

and for a circular shank cross section it can be shown that

$$\frac{A_{sh}}{\pi J_{sh}} = \frac{2}{A_{sh}} \quad ,$$

the equation for shank rotation may be expressed

$$\frac{\theta_{sh}}{360} = \frac{2\ (1 + \upsilon)}{A_{sh}} \left[\frac{L_{sh}}{L_e}\right] \frac{\eta\, C\, D_m}{K_b} P \quad .$$

Adding the derived expressions for the thread and shank rotations, the following result is attained for the total head rotation:

$$\frac{\theta_h}{360} = \left[n \left[\frac{1}{K_b} + \frac{1}{K_j}\right] + \frac{L_{sh}}{L_e} \left[\frac{2\ (1 + \upsilon)\ D_m\ n\ C}{A_{sh}}\right] \frac{1}{K_b} \right] P \quad .$$

From this equation the following expression for preload is attained:

$$P = \frac{1}{360\left[n\left[\frac{1}{K_b}+\frac{1}{K_j}\right]+\frac{L_{sh}}{L_e}\left[\frac{2(1+\upsilon)\,D_m\,n\,C}{A_{sh}}\right]\frac{1}{K_b}\right]}\theta_h \qquad (36)$$

For convenience, a description of the parameters in the preceding equation are listed as follows:

P = bolt preload
K_b = axial bolt stiffness
K_j = axial joint stiffness
D_m = bolt thread major diameter (nominal value)
n = number of threads per inch
C = assembly coefficient
η = T_r/T_a, ratio of residual torque to maximum torque developed during tightening
A_{sh} = circular cross-section area of shank
L_{sh} = length of shank with area A_{sh}
L_e = equivalent shank length (= $A_{sh}\,E/K_b$)
υ = Poisson's ratio
θ_h = head rotation angle (degrees) .

Since parameter values at the following levels,

$$\frac{L_{sh}}{L_e} \approx 1,\ \eta = 1/2,\ \upsilon = 0.3,\ \text{and}\ A_{sh} \approx \frac{\pi}{4} D_m^2$$

are frequently encountered, a useful approximation of Equation (36) is,

$$P = \frac{1}{360\left[\eta\left[\frac{1}{K_b}+\frac{1}{K_j}\right]+1.66\left[\frac{C}{D_m}\right]\frac{1}{K_b}\right]}\theta_h \ .$$

3. Torque vs. Head Rotation: Some Relative Merits

With either the torque or head rotation methods of controlling joint tightening there are advantages and disadvantages. The relative merits of these methods dictate when one method is more appropriate to use than the other in a particular application. For example, the use of torque control depends greatly on the coefficients of sliding friction. Difficulties that arise with this method of tightening are almost exclusively associated with factors that affect

variability in frictional resistance. To overcome this difficulty various practices have been recommended. Some of these involve the obvious control of surface finishes and the combination of metals which may be allowed to slide over each other. Others require the use of lubricants, a hard metallic plating on the threads (e.g., chrome plating), or both. Still other practices recommend tightening only once to avoid the effect of uncontrolled changes in the finish of mating surfaces from scoring, which can arise from successive tightenings. In LWBR the converse was found to be beneficial, since the variability of frictional effects was considerably reduced after three successive tightenings prior to a final tightening (see Figure 4). These bolts were chrome plated, and were lubricated with two coats of Neolube* prior to each tightening. The successive tightenings in this case appear to result in a "wearing-in" of the sliding surfaces. Whatever "prescription" is employed, the use of tightening to a torque limit usually requires attention to factors which reduce the variability of frictional resistance. When frictional coefficients are well known, and are themselves well controlled, the use of a torque limit to control preload is generally preferred.

On the other hand, tightening to an angular limit of head rotation is virtually insensitive to variability in frictional levels. What is critical in this case is the stiffness of the clamped members. In the derivation of bolt preload as a function of head rotation it was assumed that the joint stiffness was constant and was not a function of head rotation angle. If all of the clamped region surfaces are fully seated inside the joint "cones of influence" (compressive regions between the loaded extremeties of the bolt), then the assumption of non-changing joint stiffness is reasonable. However, if a joint member is warped, and all clamped surfaces are not seating flush against one another, the joint stiffness will be influenced by local bending as well as compression. The bending component to stiffness will change as the load increases since bending will be developed over smaller and smaller spans until full seating of the warped surface has occurred. Therefore in order to make practical use of head rotation as a control on preload it is imperative that all joint surfaces be fully seated. To eliminate the effect of small seating

---

*A commercially prepared lubricant consisting of a colloidal graphite suspension in alcohol.

nonuniformities of this type, a small seating torque can be applied prior to tightening by head rotation. If the preload produced by the seating torque is P_o, then Equation (36) is modified as follows,

$$P = P_o + M\,\theta_h \tag{37}$$

where M represents the multiplier of θ_h in Equation (36).

The attainment of preload by head rotation, while generally superior to use of torque control alone, has some notable disadvantages. First, the head rotation angle should be much larger than the potential angular error in making that rotation. Second, universal tools to perform this tightening procedure do not exist as "off the shelf" items: they must be custom made to fit the applicable joint assembly operation. Also, they take more space than a torque wrench, and the protractor segment used to measure angles cannot always be located close to the bolt head. The danger in using extensions to the bolt head is that then the torsional twist of the extension must be accounted for, which is undesirable from a measurement error point of view. In addition, there may be some head counter-rotation (slipping back) when the wrench torque reduces to zero, which must be compensated for in the head rotation under load. Therefore, while head rotation can lead to improved preload control, it could also be a more costly tightening procedure to tool and perform, and may be limited by physical access requirements.

III. PRELOAD TESTS AND TEST RESULTS

A. Multiple Tightening Tests

The tightening of a bolted joint to a specific preload by means of assembly torque control is particularly susceptible to the variability of coefficients of friction at sliding surfaces. On the assumption that the variability of frictional resistance to sliding motion is due to surface irregularities and surface debris produced during the initial tightening, it was considered feasible to pursue a course of action whereby mating surfaces could "wear-in" and stabilize frictional resistance. To test this hypothesis, multiple tightening tests of various bolt designs were conducted. These bolts had chrome-plated threads (except for the grid-to-support post fastener) and were lubricated with two coats of a colloidal graphite lubricant before each tightening. Five joint designs representing nearly the entire range of thread and bolt sizes and bolting materials used in the LWBR core were tested in this fashion to attain a

given maximum bolt load for as many as five distinct tightenings. The results for one such bolt are presented in Figure 4. As this figure shows, the torque-load response becomes more repeatable after the third or fourth tightening. This conclusion is generally supported by the data gathered for the entire population of bolts and joints tested. Figure 5 displays the average joint assembly coefficient of each design tested as a function of the number of times the bolt was tightened. As the figure indicates, the coefficient tends to stabilize for most designs after the second tightening. From these results it was concluded that each core bolt should be tightened a minimum of three times. The sections that follow describe the testing performed to determine the maximum range of preloads to be expected, given that each bolt would be tightened at least three times during assembly of the LWBR core.

B. Preload Tests

1. Preload By Torque Control

Tightening tests were conducted to develop maximum and minimum assembly coefficients for core joints using the multiple tightening technique just discussed. Knowing the maximum assembly coefficient it was then possible to specify the minimum tightening torques to generate initial preloads high enough to prevent joint separation and unacceptable fatigue damage under all operation conditions throughout the core lifetime. The general locations and structural character of some of the LWBR core joints of interest are presented in Figures 6 through 8. The structures illustrated in these figures are core modules, which are arranged in LWBR as 12 sets of movable fuel and stationary blanket modules surrounded by 15 stationary reflector modules. Critical configurations for power generation and reactor control are attained by raising or lowering the movable fuel modules (see Reference (d)).

The initial tests were performed with mini-joint mockups (as in Figure 9) into which was inserted a cylindrical load cell. The cell was clamped coaxially in the test joint and loaded compressively as the bolt was tightened. The applied torque (or measured bolt force) was increased in specified amounts until the maximum load of interest was attained. The bolts were then removed from the text fixture, examined for unusual wear spots, relubricated and retightened at least three times per bolt. As many as twelve pairs of bolts and mating nuts were used in order to provide sufficient data for a good statistical evaluation.

A typical set of tightening results is illustrated in Figure 10. In addition to showing the recorded data, this figure contains a least-squares straight line fit to the data. Two sets of data analyses were performed. The data pertaining to each individual specimen was plotted as well as the pooled data from all specimens of a given bolted joint design. An example of the pooled data analysis appears in Figure 11. In both Figures 10 and 11 the best-fit line through the data has a definite bias away from the origin of the graph. This was surprising since there is no physical basis for this observation. Because of the large body of data originally collected for the movable fuel grid bolt, these data were examined very closely. They were expected to reveal such a bias most distinctly if one existed. In the testing for the joint, four different load cells were used to measure the preloads in twelve different test bolts. three bolts to each load cell. Grouping the torque versus load data according to the load cell used showed that: (1) the within group scatter about the group best fit line was generally smaller than the scatter about the overall best fit line when all the data were pooled; (2) the best fit lines for each group showed a distinct bias away from the origin; and (3) the slopes, hence the joint assembly coefficients, of all the lines were statistically the same with a 95% confidence level. Based on these results and on the physical implausibility of having a torque with no resulting preload or vice versa, it was concluded that each load cell possessed a bias, which introduced a constant error in the indicated preload for each bolt. To remove the bias, the best fit line for each specimen was calculated using the observed data. The apparent load with torque equal zero was then calculated. This "bias load" was then subtracted from each of the observed loads thus forcing the best fit line for that specimen to go through the origin. The adjusted data were then pooled to determine the range of the assembly coefficient for that joint. The results of applying this type of correction to the data for the blanket top base plate bolt appear in Figure 12, which shows that the magnitude of data scatter is roughly proportional to the load (or torque) level, a result which is physically plausible. Figures 13 through 19 are similar data portrayals prepared in the manner just described.

Additional bolt preload measurements were made during bolt tightenings for a separate series of stress corrosion cracking (SCC) tests. The fixtures and tightening techniques used in this test are discussed in some detail in the next

section and will not be repeated here. However the pertinent torques and preloads obtained during fixture assembly have been recorded and are included in Figures 12, 13, 14, and 18.

A summary of the measured assembly coefficients derived from the torque vs preload test data (maximum and minimum of the indicated ranges) is listed in Table 1. To make these results more useful, Table 1 also includes the screw thread size, the interfacing materials and "averaged" coefficients of friction. These friction coefficients were derived from the assembly coefficients using Equation (31) and assume that the same coefficient exists under the bolt head as in the threads.

2. Preload by Control of Bolt Head Rotation

To perform a valid test of bolt preload vs head rotation, the test fixture must possess the same stiffness as the design joint of interest (see Equation (36), Section II.B.2). The same stiffness was achieved by using fixtures built up of discs and cylinders with a combined stiffness equal to the calculated stiffnesses of the design joints. A typical fixture of this type is shown in Figure 20. In addition to satisfying similarity in stiffness, the size and materials of the fixture components were also chosen to insure that interfacing surfaces are prototypical. The upper and lower discs were made so that the fixtures for the various joint designs tested could be assembled in the "universal" tightening fixture shown in Figure 20. Bolt loads were inferred from strain gages mounted both on the bolts themselves and on the outer surface of the clamped joint cylinder. The complete test set-up including the protractor used to measure head rotation is shown in Figures 21 and 22.

In each test run a similar sequence was followed. The pieces were lubricated as described earlier, assembled, and installed into the tightening fixture. An initial seating torque was applied, to seat all of the joint components firmly. The indicated rotation of the bolt head was set to zero. An increment of head rotation was applied and the maximum torque was noted along with the indicated angular rotation at that torque. The torque was relaxed to zero, noting the head springback angle (approximately 3° observed at high loads for most tests). Torques, angles, and strain gage readings were recorded before increasing the load. This procedure was repeated until full rotation was attained, after which the joint was disassembled for examination of rubbing surface wear.

The information gathered in this test is typified by the data obtained for the blanket top base plate joint and is illustrated in Figure 23. The bolt loads indicated in this figure were calculated from the joint cylinder strains only, although axial strain gages were also mounted on the bolt shank. This was done to simplify the data presentation by eliminating redundant results in Figure 23, and also because the most consistent load indications were obtained from the joint cylinder strain gages. This is attributed to the superior bonding of these externally mounted gages, which were Mylar-backed strain gages bonded with a cyanoacrylate adhesive. The strain gages mounted directly on the bolt were of somewhat lower quality. They were paper-backed and bonded with Duco Cement to facilitate removal by an acetone bath without disassembling the fixture after the final tightening.

From the graph of preload vs torque in Figure 23, it is observed that a significant difference in response is indicated between the three bolts loaded in this test. This is apparently caused by the different levels of friction operating in these specimens. The data are bounded by the shaded lines shown on the left side of Figure 23. Using these lines and applying Equation (30), assembly coefficient extremes for this bolted joint were computed. These extremes suggest that assembly coefficients could lie in the range of $0.08 \leq C \leq 0.40$. Expected preloads for top base plate bolts are confined to the region between the shaded lines on the left side of Figure 23. For example, at an applied torque of 1200 lb-in (100 lb-ft) the attained preload may be anywhere from 4000 lbs to 20,000 lbs. However, plotting the same preload data against the head rotation angle developed after a 300 lb-in (25 lb-ft) seating torque, the graphic portrayal on the right side of Figure 23 is obtained. Employing Equation (36), and accounting for the maximum variation of fixture stiffness along with the previously assumed variation of assembly coefficients, it is observed that the predicted range of preloads is consistent with the experimental data and defines a region with a much narrower variation for preload than provided by use of torque level control alone. To illustrate, consider the head rotation angle producing the same peak preload (20,000 lbs) as produced with the 1200 lb-in torque. From Figure 23 this angle is observed to be approximately 57°. Employing head rotation control, the expected preload range for this angle varies from 14,400 lbs to 20,000 lbs under the extreme

conditions indicated. This is a difference of only 5600 lbs, whereas for the comparable set of conditions under torque control the expected preload could range from 4000 lbs to 20,000 lbs, a difference of 16,000 lbs.

As has already been stated, the rotation controlled preload is sensitive to the clamped elastic stiffness of the connection. But once a joint has been firmly seated, the variation of stiffness from joint-to-joint of the same design must be relatively small. Consequently, the additional loading attained by a head rotation after seating will be essentially the same for all such joints. This cannot be said for torque control of preload, which can vary significantly from joint-to-joint of the same design. In fact, the major source of preload variation from head rotation control is caused by the load uncertainties of the initial seating torque. This is also illustrated in Figure 23, where a load variation of 4000 lbs exists just after seating the joint. The 57° head rotation has increased the preload uncertainty only 1600 lbs while the gross load level is increased 15,000 lbs (from 5000 lbs to 20,000 lbs total). This illustrates again the characteristic advantage of head rotation control over torque control in minimizing the variation in preload.

Figures 24 through 27 present the data obtained for preload versus head rotation. The limit lines in these graphs are not the "prediction" limit lines drawn in the right half of Figure 23, instead they merely represent the extremes indicated by the data.

C. Special Tests

1. Preload Determined by Joint Separation Force

A test was designed to examine how various tightening methods would affect the preload developed in the blanket grid to support post bolt. The test apparatus, which is shown in Figure 28, differed from the other methods used to investigate bolt preloads in that the joint separation load was used to calculate the preload. The separation load is defined as the minimum external load which reduces the compressive force between the clamped members to zero and separation is imminent. Using the method illustrated in Table B.1 of Appendix B to calculate the joint stiffness, and applying Equations (13) and (15) it was found that the preload was 99% of the separation load. The advantage of using the separation load as a measure of preload is that the external loads were well known at all times; they were applied by a material test machine whose load

cells were calibrated to within 1% accuracy. The most apparent disadvantage was the time consumed in setting up the assembly in the testing machine. With this method preload was only determined for the fully tightened joint: the variation of preload with applied torque, or with the number of times the torquing sequence is repeated, could not be determined.

To model the bearing surfaces, washers made from the appropriate materials were installed under the head of the bolt. Washer rotation was restrained to insure that relative motion took place at the right interface. Prototypical bolts and nuts were tightened in the fixture following each of the tightening procedures to be investigated. A test run consisted of tightening a new and previously unused bolt, nut and washers as many times as the particular procedure required. After the final tightening for a test specimen, the fixture was mounted onto the threaded machine adapters and then pulled. Dial indicators were mounted on the text fixture to measure the separation of the joint. The specimen was pulled until a separation of 0.005 inch was indicated. The load was recorded at each 0.001-inch increment of separation. From the load versus separation data, a straight line was drawn through the data and extrapolated back to the load at which separation had started. Data are displayed in Figure 29 for bolts tightened by two different procedures. A description of the individual tightening procedures are noted on the figure. As expected the data lie on straight lines with a slope representing the approximate flexibility of the bolt (since the bolt is considerably more flexible than any other component in the connection). Although the data from these tests supported the conclusion that all the tightening methods investigated produced preloads that were approximately equal to the preloads secured with the original reference assembly method, these tests did enable LWBR to choose the tightening technique with the best repeatability.

2. Joint Bearing Load Test

In developing a bolted joint design, a common concern is that the high bearing stress under a bolt head may cause unacceptable loss of preload or failure of the joint components due to localized plastic deformation. Limiting such bearing stresses to the material yield strength is a conservative way of assuring that such failures will not occur. In the course of satisfying space, access, or clearance requirements, situations can arise where bearing stresses exceed the material yield strength (S_y) where the contact area is small. The

simplest correction is to merely increase the contact area. However, an increase in bearing area cannot always be achieved without perturbing one or more critical design dimensions. In these cases a total redesign may be required unless it can be shown that a limit higher than S_y can safely be used. A somewhat higher bearing stress is tolerable in bolted joints, and the ASME recommends a limit of 2.7 S_y for the average bearing stresses under the heads of threaded structural fasteners in paragraph NG 3230, Section III of the 1974 Boiler and Pressure Vessel Code.

A bolted joint is used in the LWBR core (the reflector support post-to-base plate connection) which could develop average bearing stresses beyond the material yield strength under certain operational conditions. Due to the shape of the clamped members in this joint, it was concluded that the relatively close proximity to a free surface on one side of the bolt hole might result in a reduction of bearing stress capability which would make the ASME limit inapplicable. Accordingly, a test was conducted at room temperature to evaluate the bearing performance of this member. This test consisted of a joint mockup as shown in Figures 30(a) and (b) in which a simulated bolt head was pressed against the Zircaloy "foot" with a materials testing machine. Reference measurements (of load and machine ram displacments) were made at a seating load of 50 lbs. The maximum ram load was increased in 2000-lb increments. After each load increment was applied the load was reduced to 50 lbs and measurements for plastic deformation were made. The ram load was increased in this manner until a peak load of 24,000 lbs, three times the maximum expected bolt preload in the LWBR joint, was attained. At the peak test load it was found that although a permanent deformation of 16 mils had developed, it was developed without any evidence of displacement instability, cracking, or shear failure. A graph of load vs permanent deformation measured during this test appears on Figure 32.

It may be observed, in Figure 31, that first indications of measurable plastic deformation occurred at a test load of 6000 lbs. Since the bearing area under the bolt head is 0.156 square inch, this corresponds to an average bearing stress of 38,500 psi which is slightly above the tabulated 0.2% offset yield strength (37,000 psi) of annealed and unirradiated Zircaloy at room temperature. It is also noted that plastic deformation of the joint increases at a uniform, low rate up to a ram load of 16,000 lbs. Beyond this load a marked change in the plastic stiffness of the joint is displayed; at 16,000 lbs the

joint develops approximately a 1-mil plastic set, whereas after a 50% increase in load to 24,000 lbs a plastic set of 16 mils is observed. At 16,000 lbs the average bearing contact stress is 102,600 psi, which is equivalent to 2.77 S_y. Hence it is concluded that the ASME limit remains applicable to this joint design. In addition, these results confirm that the 2.7 S_y limit provides good assurance that plastic deformation will be acceptably small even if the compressed joint area is sufficiently nonsymmetrical. The surface appearance of the regions which underwent plastic deformation (the Inconel 600 locking cup and simulated Zircaloy support post foot) are shown in Figure 32.

3. Measurement of Residual Torque

In Section II.B.2.c of this report it was concluded that the residual-to-applied torque fraction η must be less than or equal to 0.5. The maximum value of η was used in calculating the stress intensity in the various bolt designs for comparison with design stress limits. To determine how conservative the use of this maximum value was, strain measurements were made during bolt preload testing from which actual values for η could be computed. The testing and analysis performed was as follows.

To provide an estimate of the residual-to-applied torque fraction, rectangular strain gage rosettes were fastened to the shank of some of the LWBR bolts tested. Strains indicated by the rosette elements as the bolts were tightened were recorded to calculate the shear strain at the surface of the bolt, which in turn was used to calculate the residual torque. The bolts tested were made from NiCrFe X-750 and had chromium plated threads. In each of the joints the hardened bolt material under the head and the plated threads interfaced with relatively soft NiCrFe 600 or type 304 stainless steel.

The shear strain was calculated from the tensile strains sensed by the three elements of the rectangular strain rosette shown schematically in Figure 33(a). The strain condition is portrayed on the Mohr circle in Figure 33(b). The measured normal strains are designated ε_0, for the circumferential component, ε_{90}, for the axial component, and ε_{45}, for the strain component sensed by the gage element oriented at an angle of 45° between the other two. The angles AOB and BOC are each 90°, twice the angle between adjacent elements. The torsional shear strain is represented by twice the

length of the line AD. It can be proven (left to the reader) that triangles AOD, BOE, and COF are congruent and therefore the length OE is equal to the length AD. Thus,

$$\frac{1}{2}\gamma = \text{Length AD} = \text{Length OE} = \frac{1}{2}(\varepsilon_{90} + \varepsilon_0) - \varepsilon_{45}$$

or

$$\gamma = \varepsilon_{90} - 2\varepsilon_{45} + \varepsilon_0 \quad .$$

To relate the shear strain to the applied torque first recall

$$\tau = \frac{E}{2(1+\upsilon)}\gamma \quad ,$$

where

τ = shear stress
E = Young's elastic modulus
υ = Poisson's ratio
γ = "engineering" shear strain .

From Reference (e), for a solid circular shank,

$$\tau = \frac{2T}{\pi r^3}$$

where

τ is the shear stress measured at the surface
T is the torque,
and r is the radius of the shank.

Putting these results together and solving for T

$$T = \frac{\pi r^3 E}{4(1+\upsilon)}[\varepsilon_{90} - 2\varepsilon_{45} + \varepsilon_0]$$

where the term outside the square brackets is a constant depending on the radius of the bolt shank and its material properties.

Using data from the thirteen specimens of four different joint designs tightened three times each, an average residual torque fraction $\eta = 0.23$ was calculated. Residual torque in seven out of eight of these bolts were found to be less than 33% of the applied torque, and less than 42% of the applied torque

in 95% of the cases. These results indicate that there is substantial conservatism in calculating the stress intensity in the bolt based on a residual torque fraction of 0.50.

D. Conclusions

In addition to providing experimental information to determine the range of preloads attained in the LWBR bolted joints, the following major conclusions were also established by the bolted joint tightening tests:

1. The analytic trends predicted by Equations (30) and (36), relating preload to applied torque and head rotation respectively, were observed in the recorded data. As anticipated from tightening analyses of joints containing relatively long and flexible bolts, a significantly smaller variation in preload was attainable with head rotation control than with torque control. Further, only small increases in preload uncertainty occurred as head rotation increased, whereas a much greater uncertainty in preload resulted from torque controlled tightening, and this uncertainty was directly proportional to the torque level. Therefore, where control of assembly preload was critical, control of bolt head rotation was utilized unless it was not feasible to provide a rotation measuring fixture.
2. LWBR bolts were typically made of high strength steels and nickel alloys, with threads machined to a class 2 fit. The bolt threads were chrome plated to reduce thread scoring and friction. With these bolts it was found that minimum friction levels were attained after three tightenings (bolts were lubricated with a graphite suspension between tightenings). Also for each type of bolt tested, a minimum of preload scatter was evidenced when the entire set was subjected to three successive tightenings. Therefore, it was concluded that more consistent preloads would be attained if all bolted joints were tightened at least three times.
3. During bolted joint testing, residual torque levels were measured and were found to be approximately 25% of the applied torque in more joints examined (although a value as great as 42% of the applied torque was also observed). These measurements support the conclusion drawn in Section II.B.2.c, that the residual torque in a bolt must be less than, or equal to, 50% of the applied tightening torque.

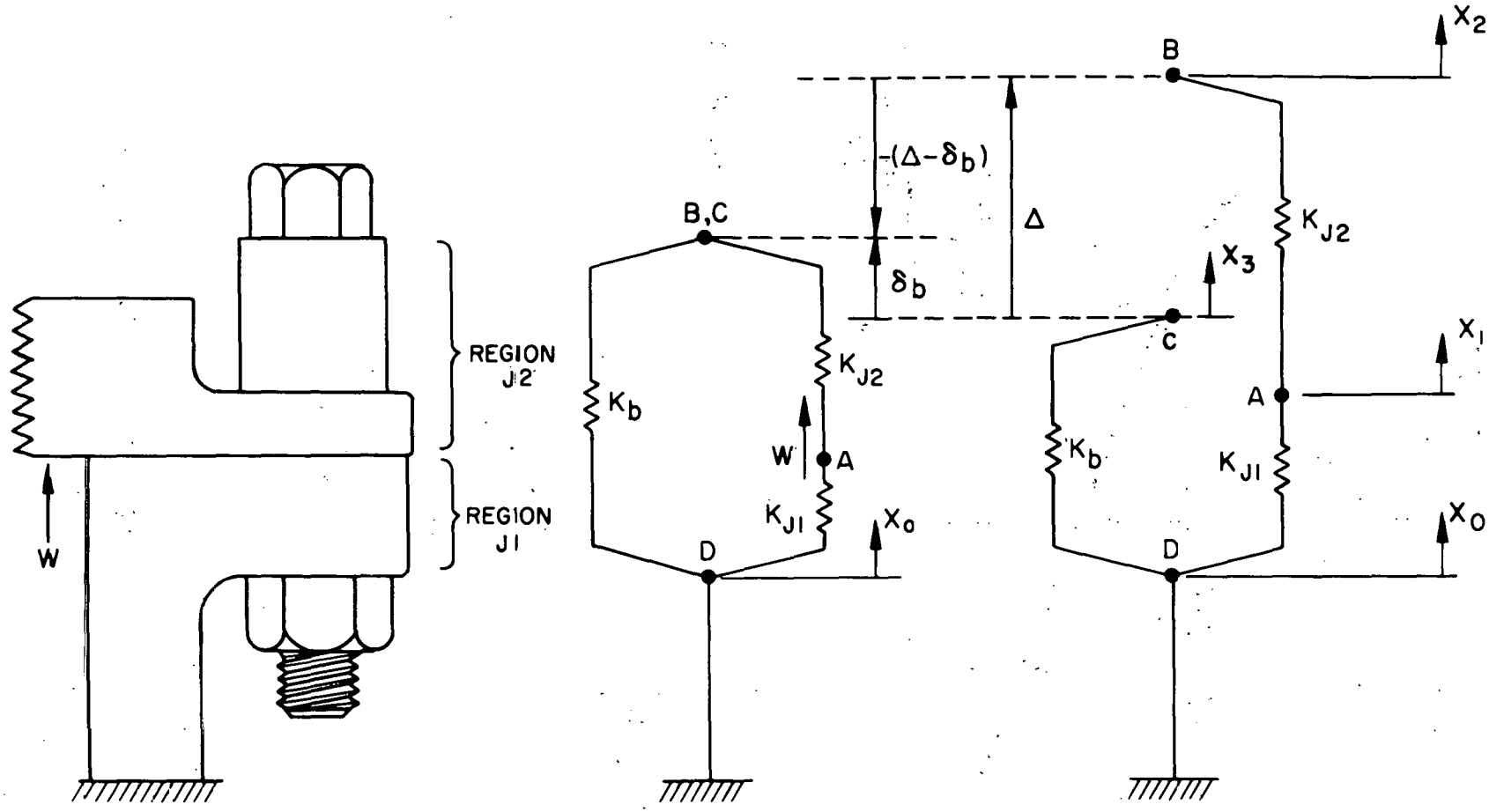

(a) PHYSICAL JOINT (ENGAGED AND LOADED)

(b) ONE DIMENSIONAL MECHANICAL SCHEMATIC OF JOINT (ENGAGED AND LOADED)

(c) ONE DIMENSIONAL MECHANICAL SCHEMATIC OF JOINT (DISENGAGED, UNLOADED)

Figure 1. Mechanical Idealization of Bolted Joint to a System of Springs (One Dimensional - Coaxial Loading Assumed)

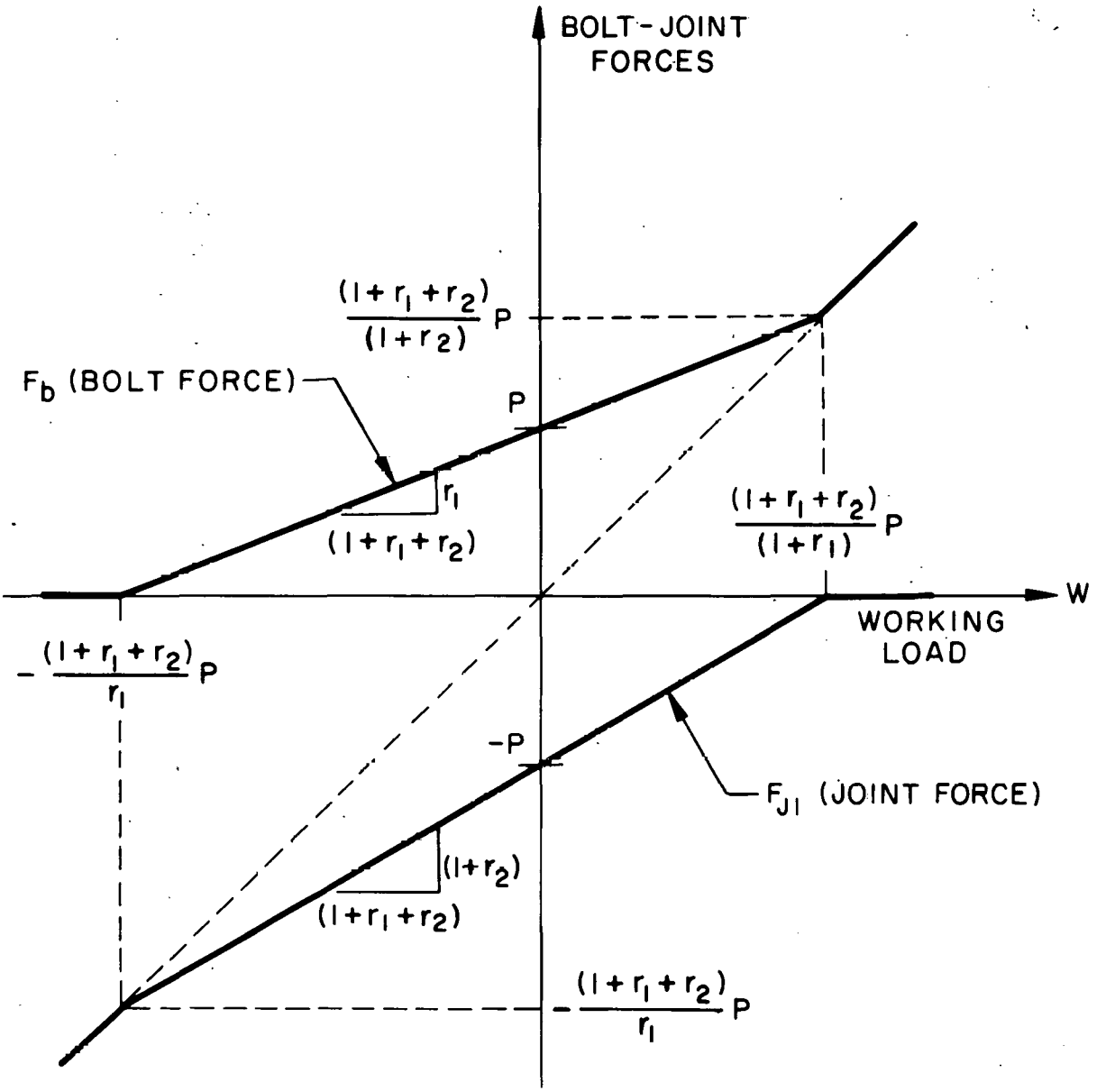

$$r_1 = \frac{K_b}{K_{j1}} \qquad r_2 = \frac{K_b}{K_{j2}}$$

Figure 2. Bolted Joint Internal Forces as a Function of Working Load

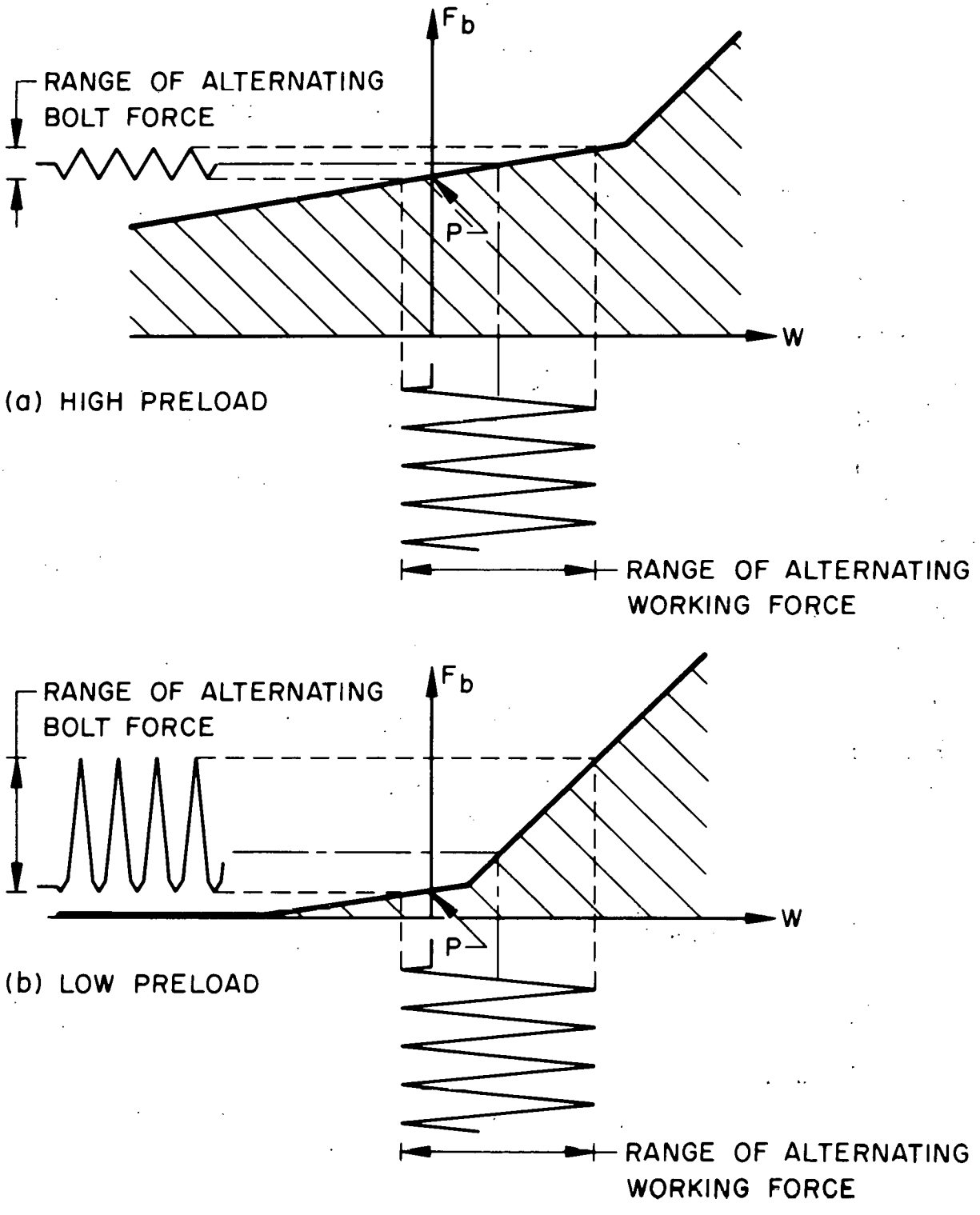

Figure 3. Effect of Preload Level on Alternating Bolt Force

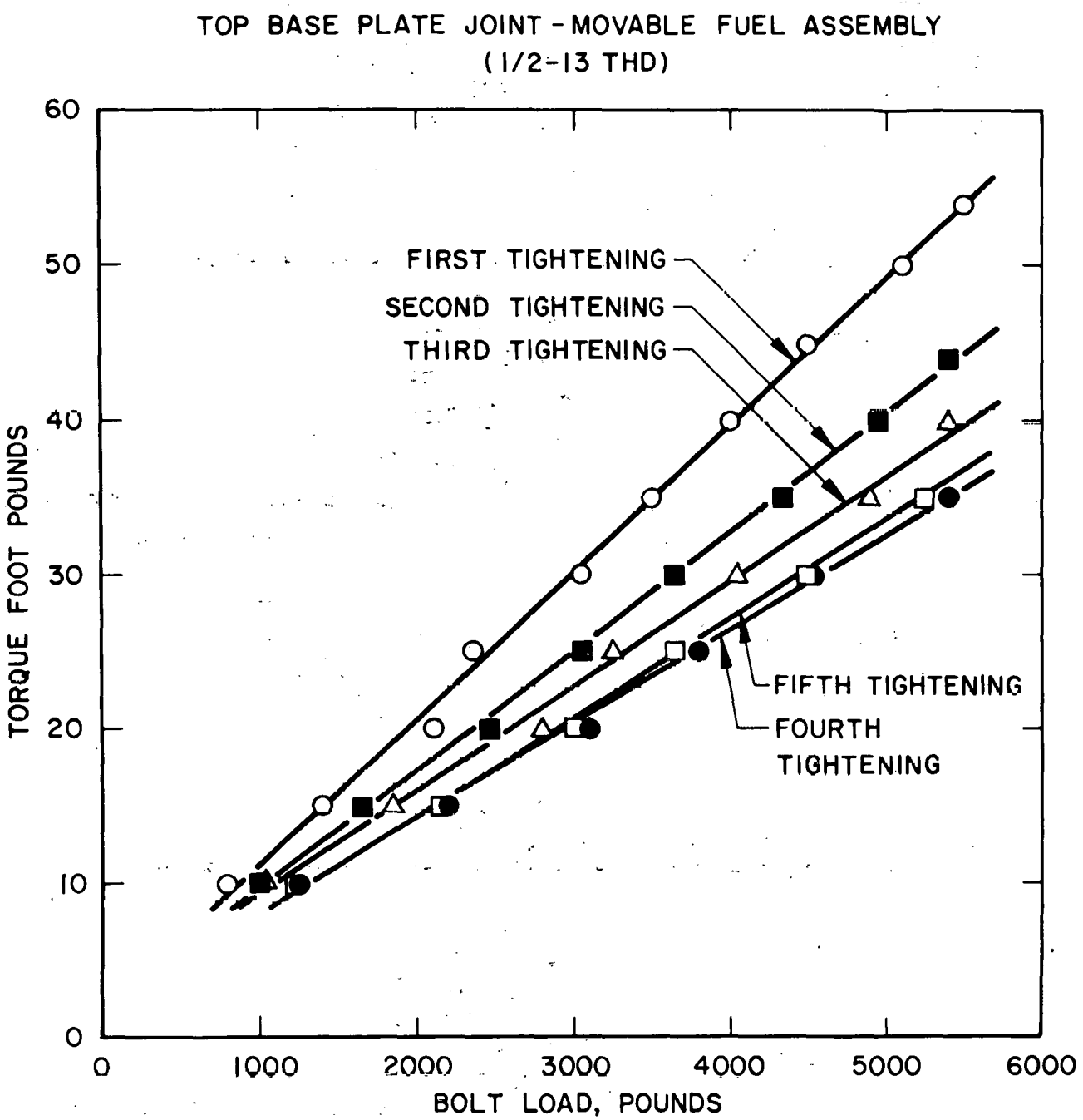

Figure 4. Multiple Tightening Test Typical Data Trend

LEGEND

SYMBOL	TYPE OF BOLT	THREAD SIZE	MATERIAL	Cr PLATED
△	REFLECTOR STUB TUBE	0.4375-14 UNC-2A	TYPE 304 CRES	YES
□	SEED GRID BOLT	0.164 – 32 UNC-2A	AM350	NO
○	SEED TOP BASE PLATE	0.500 – 13 UNC-2A	17-4PH CRES	YES
◇	BLANKET TOP BASE PLATE	0.750 – 10 UNC-2A	NiCrFeX750 COND BH	YES
▽	BLANKET SHEAR KEY BOLT	0.500 – 13 UNC-2A	NiCrFeX750 COND BH	YES

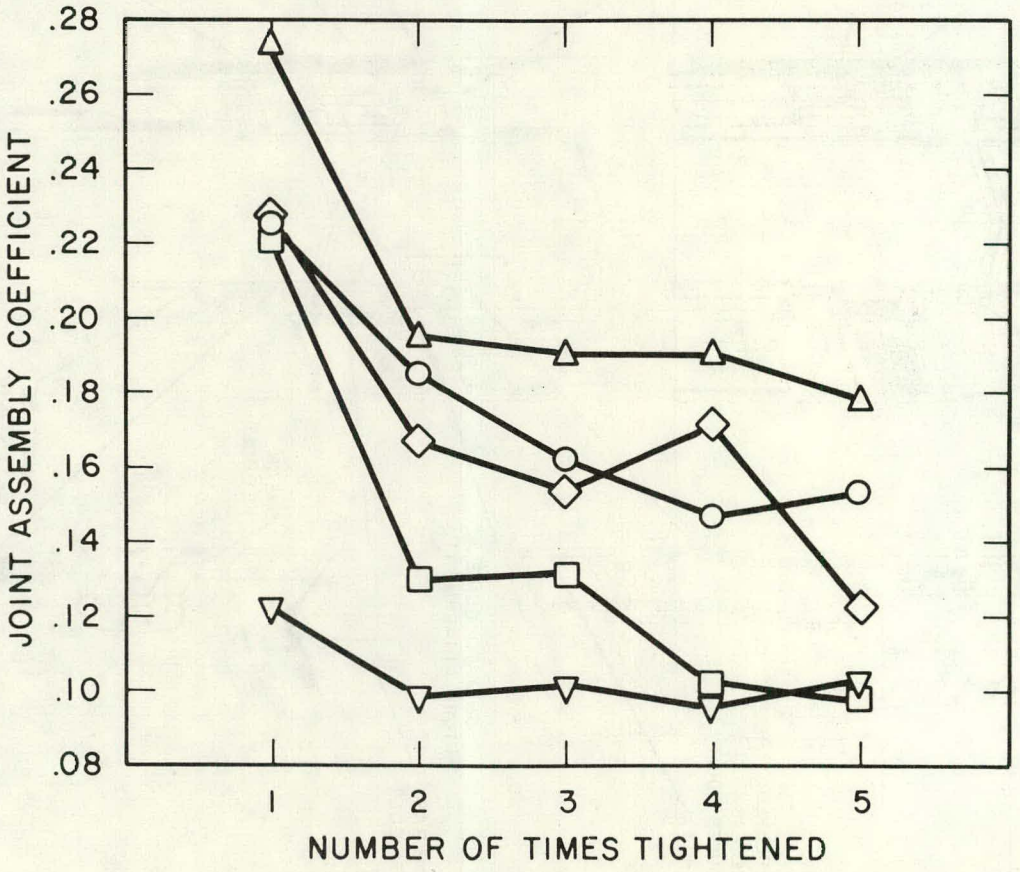

Figure 5. Variation in the Joint Assembly Coefficient versus the Number of Times the Joint is Tightened (for several LWBR joints)

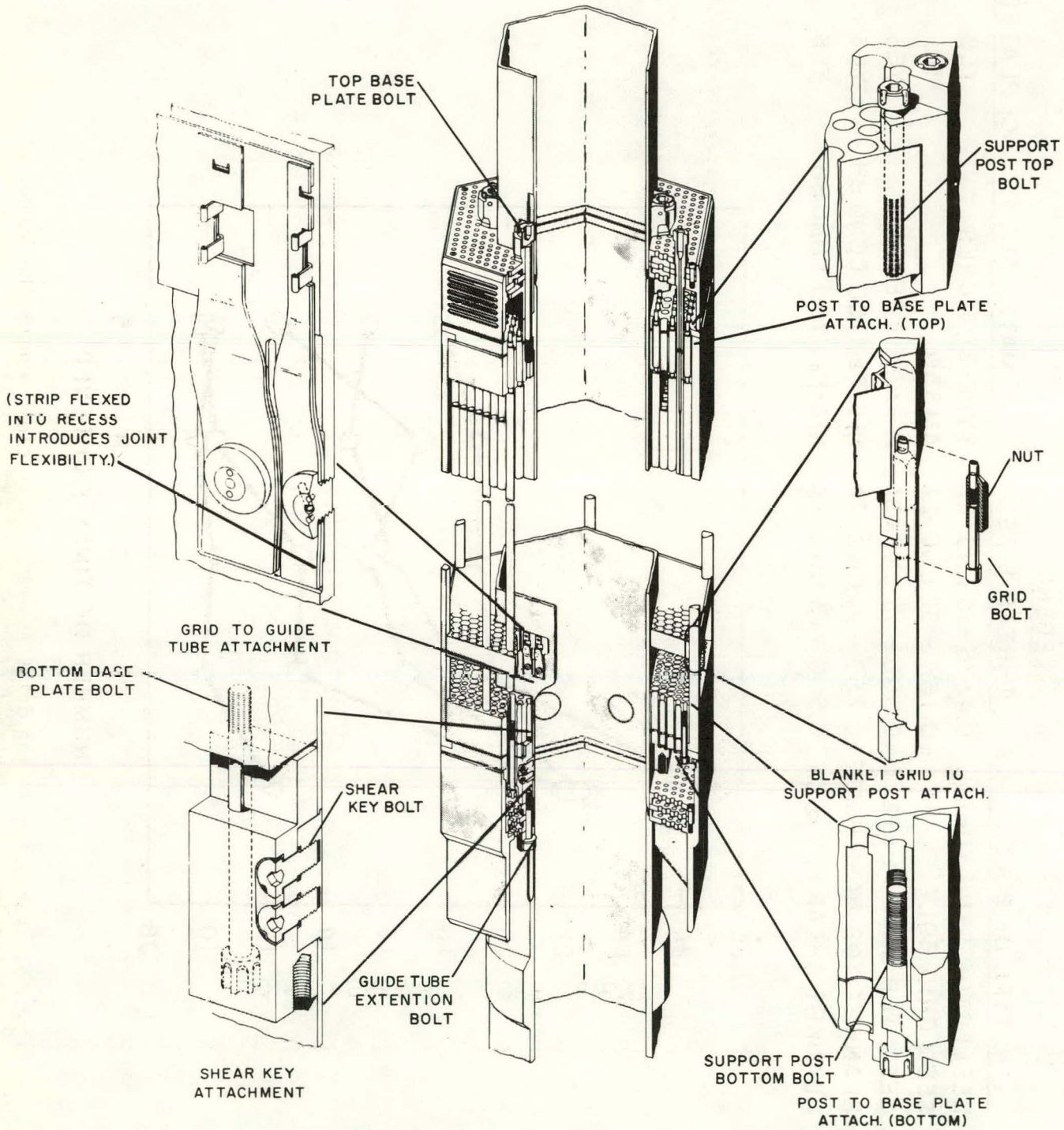

Figure 6. Bolted Joints in LWBR Blanket Assembly

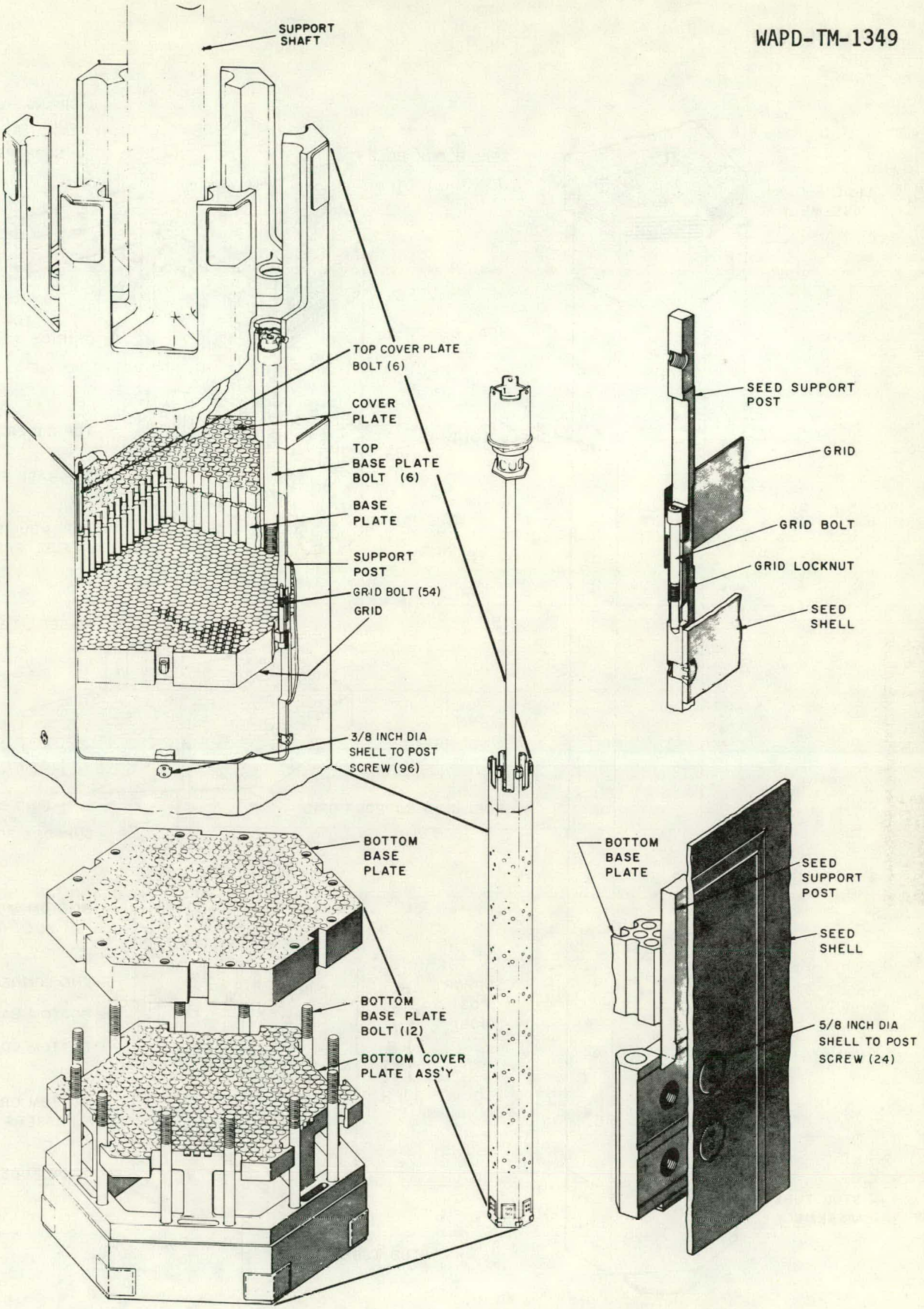

Figure 7. Bolted Joints in the LWBR Movable Fuel Assembly

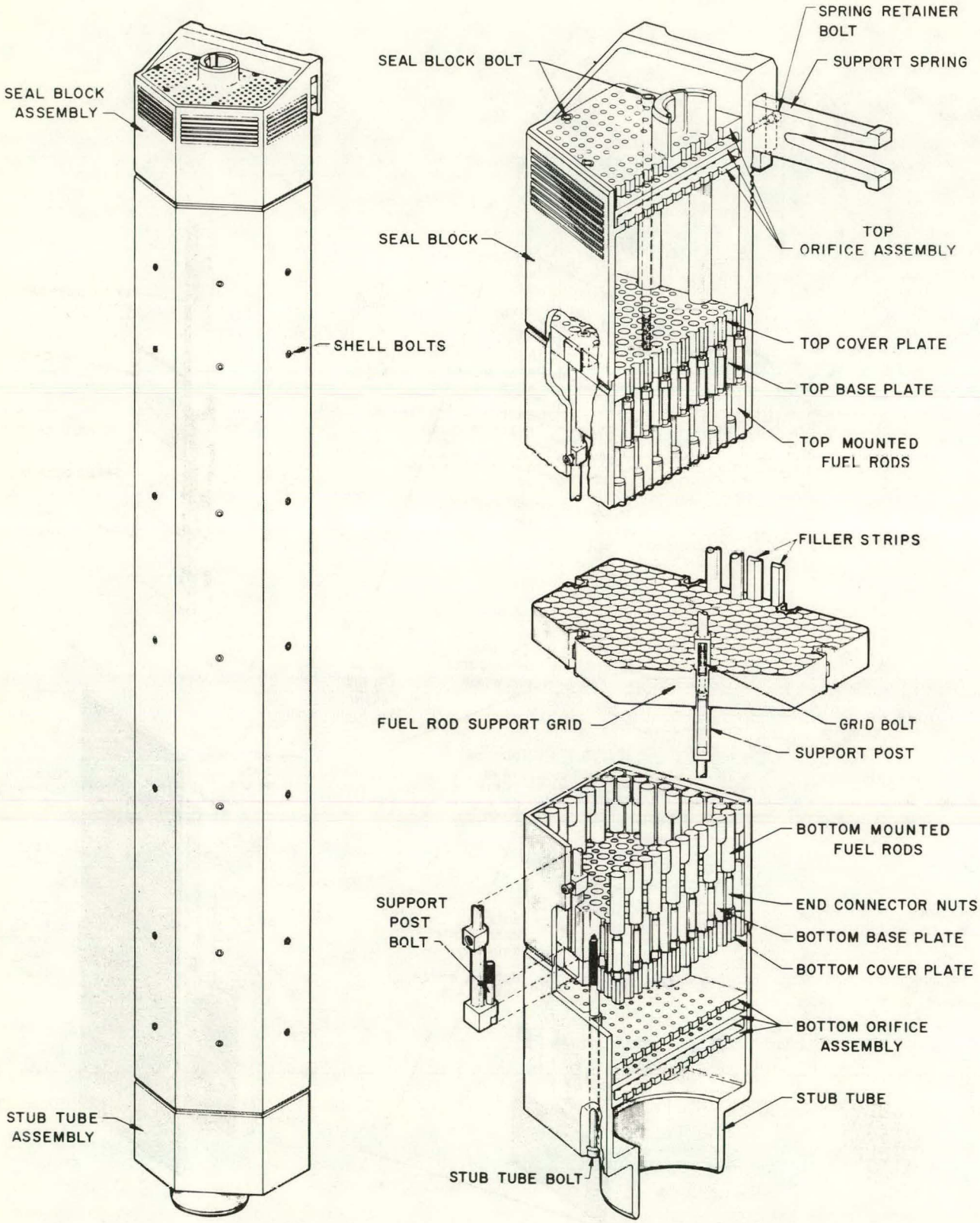

Figure 8. Bolted Joints in LWBR Reflector Assembly

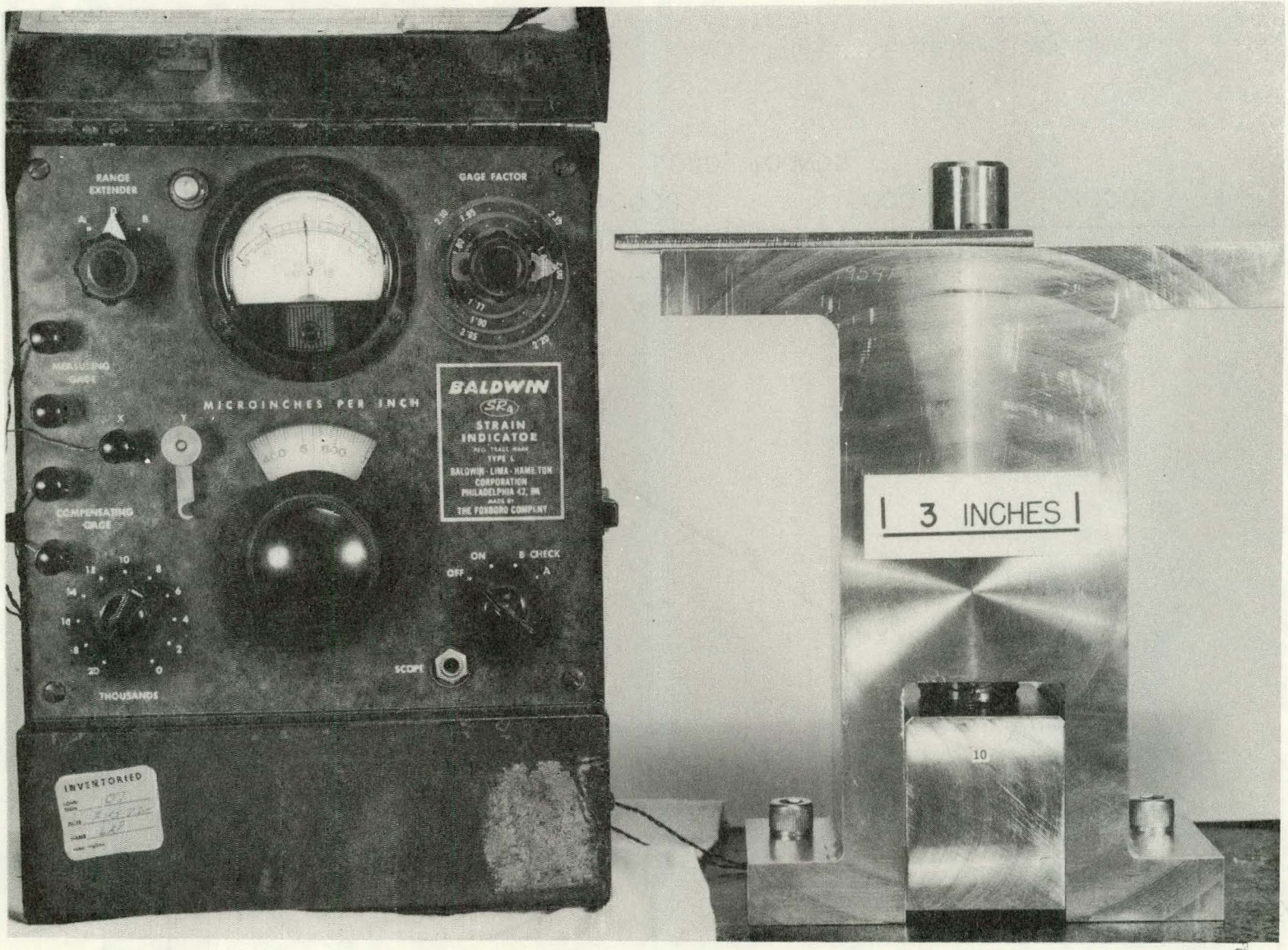

Figure 9. REM-208 Test Set-up: Blanket Top Base Plate Bolt
(Neg. No. 47906-2)

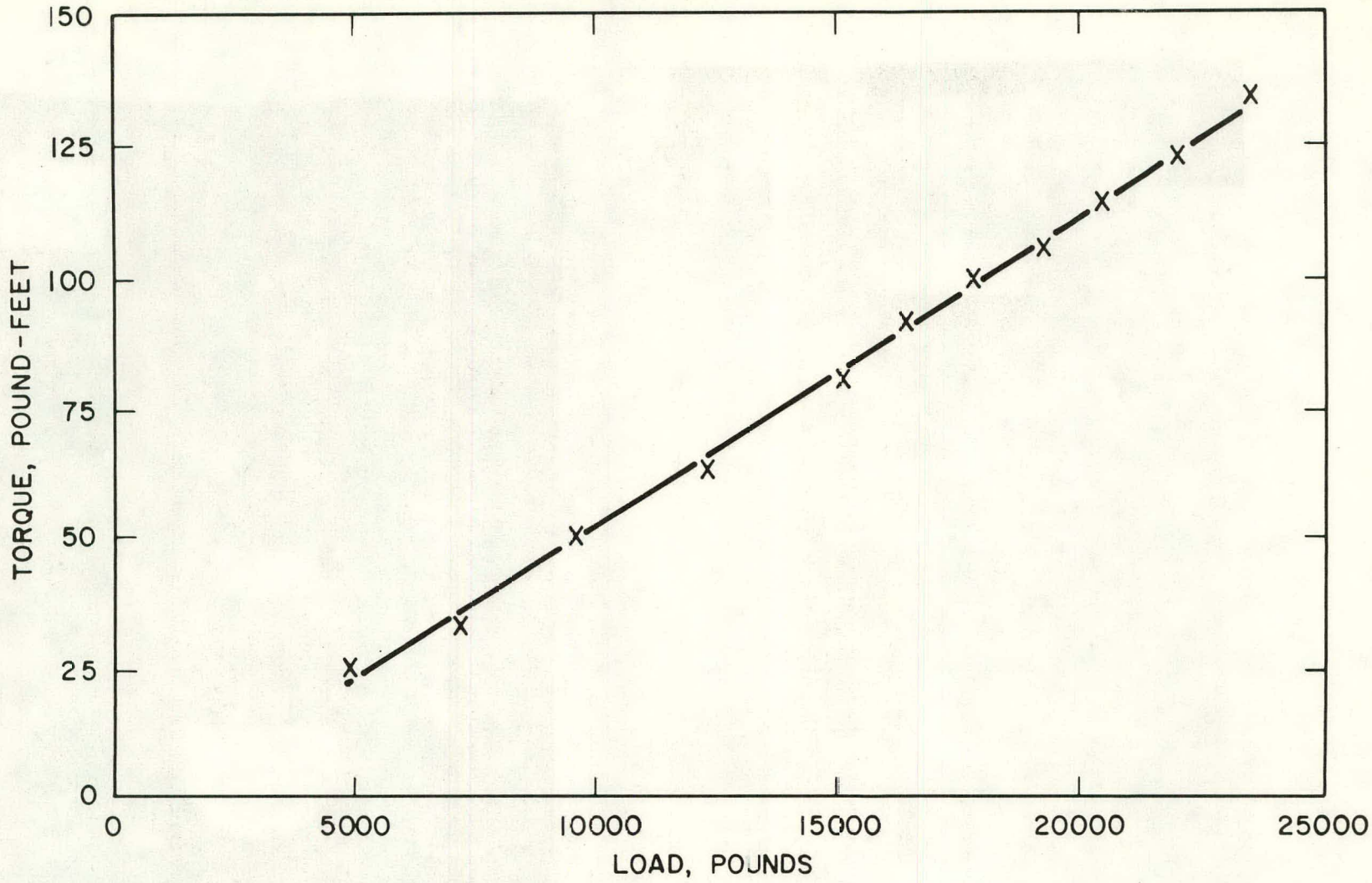

Figure 10. Torque-Preload Test, Typical Single Specimen Data: Blanket Top Base Plate Joint

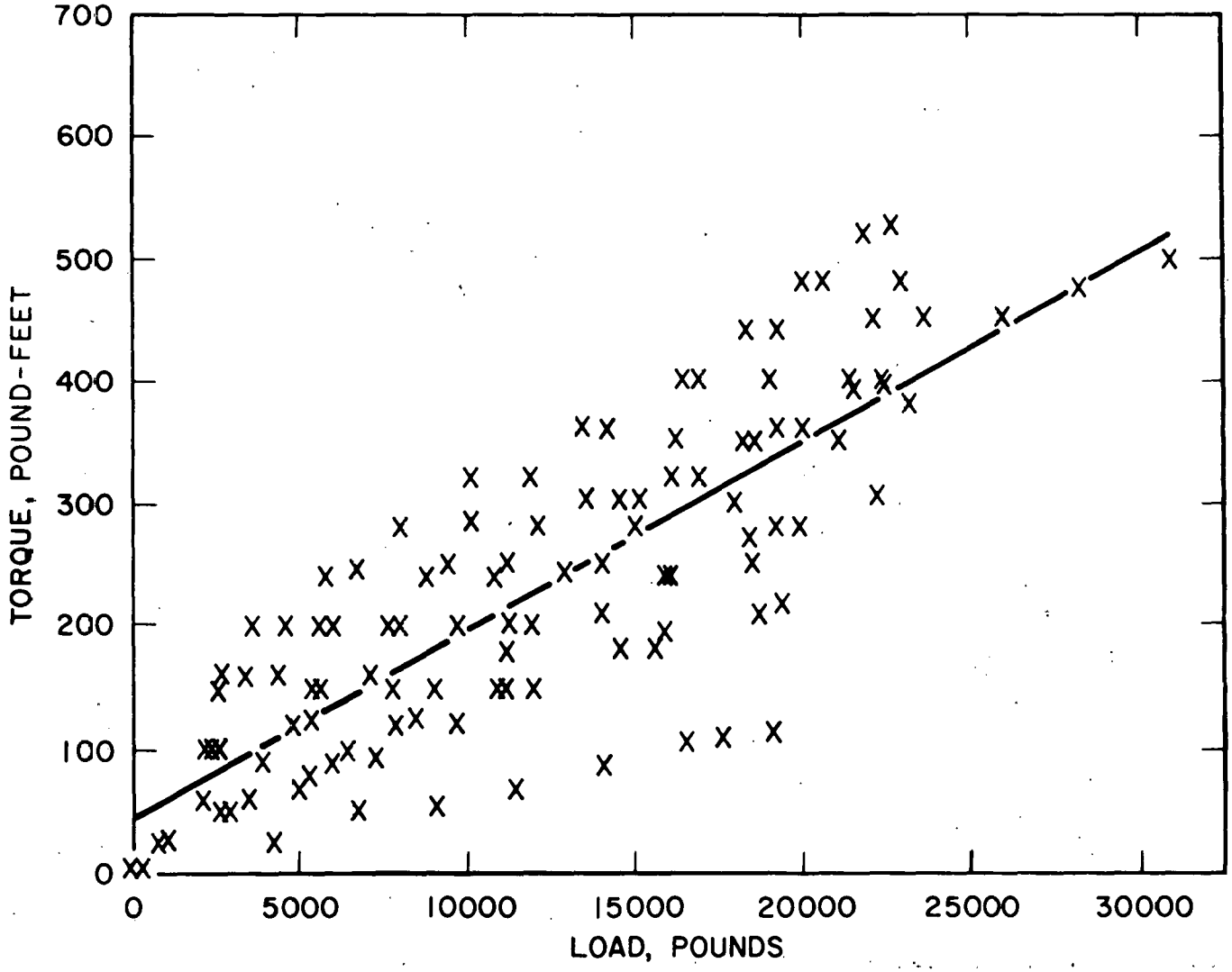

Figure 11. Torque-Preload Test "Uncorrected" Pooled Data: Blanket Top Base Plate Joint

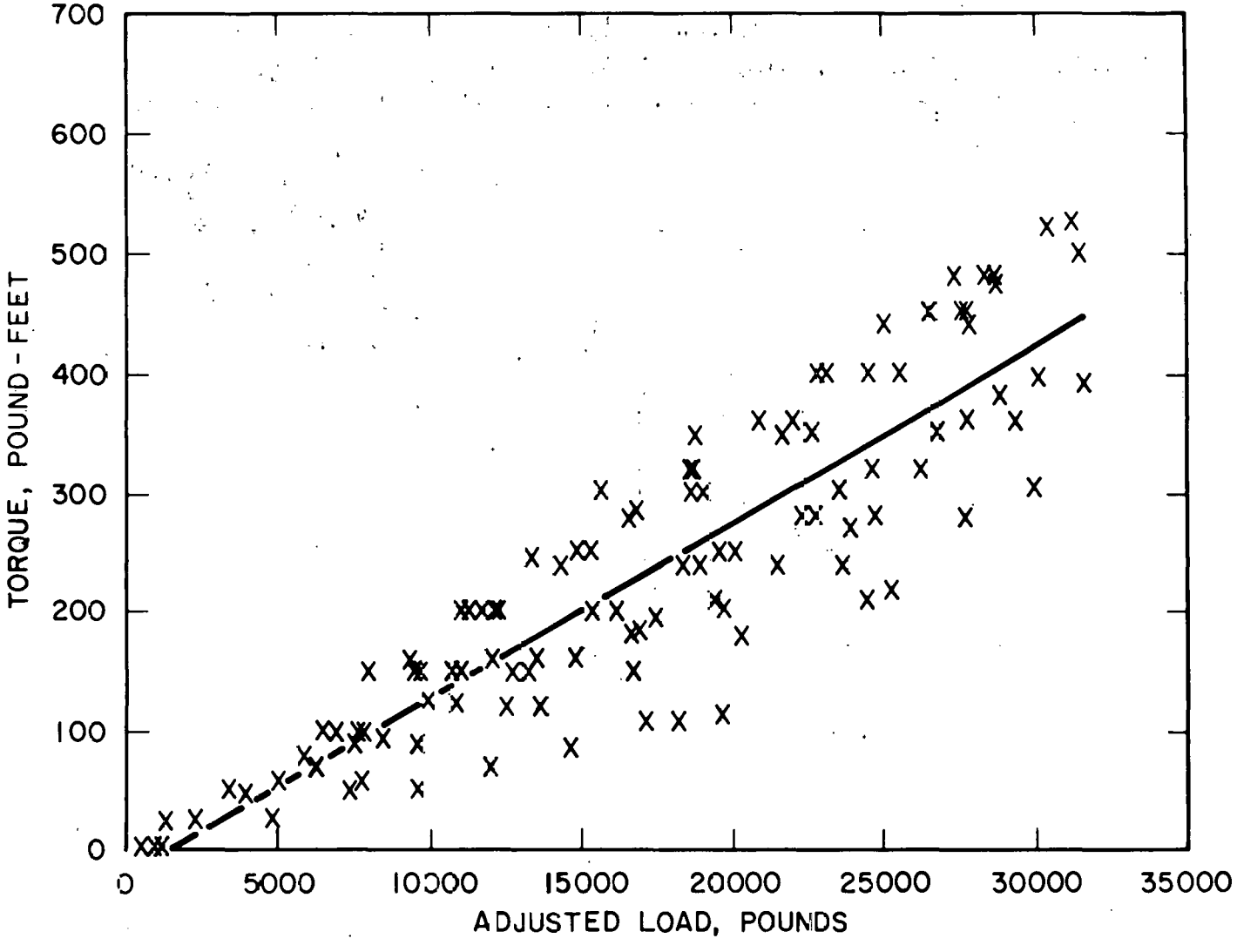

Figure 12. Torque-Preload Test, Pooled Data for Blantet Top Base Plate Joint

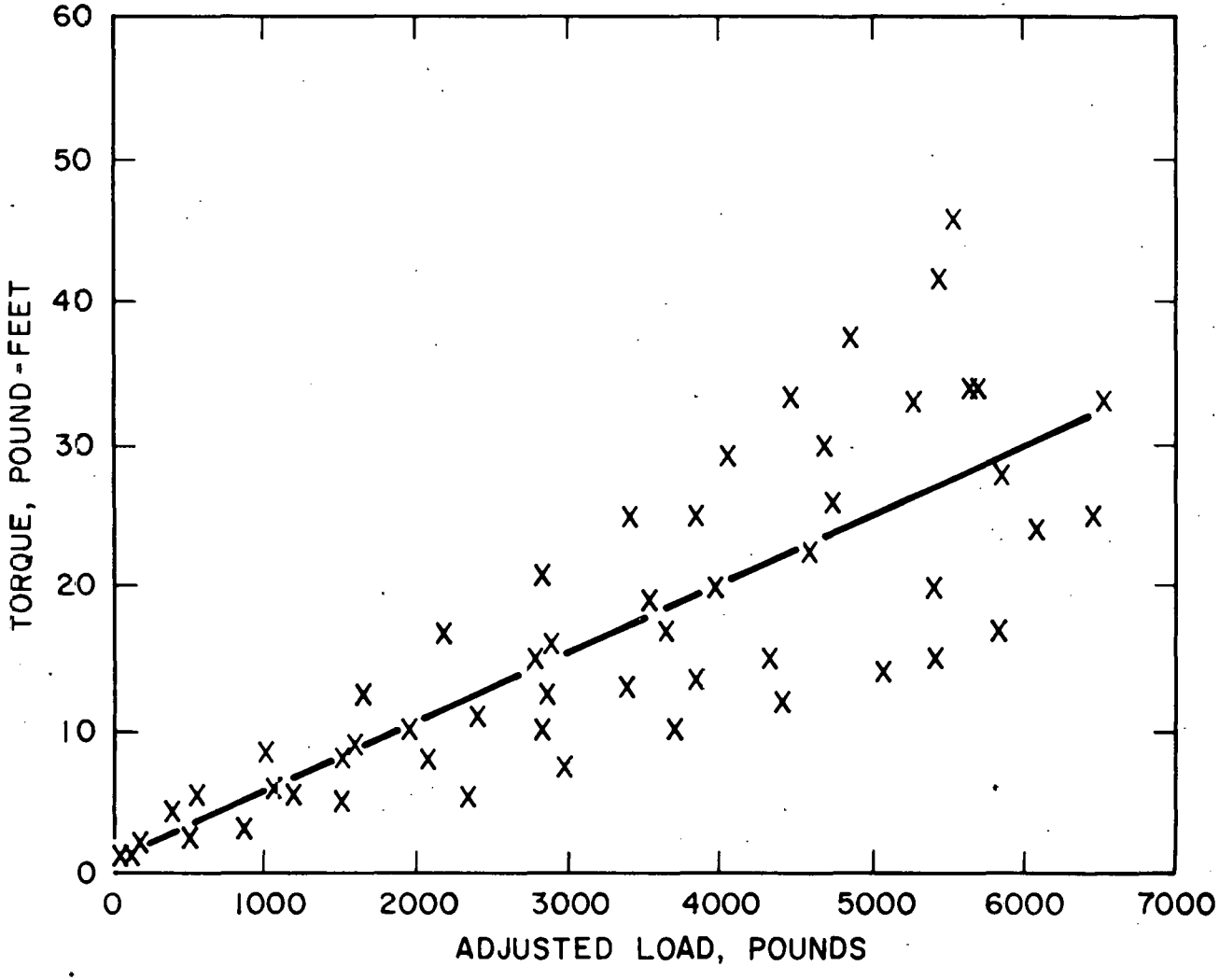

Figure 13. Torque-Preload Test, Pooled Data for Blanket Bottom Base Plate Joint

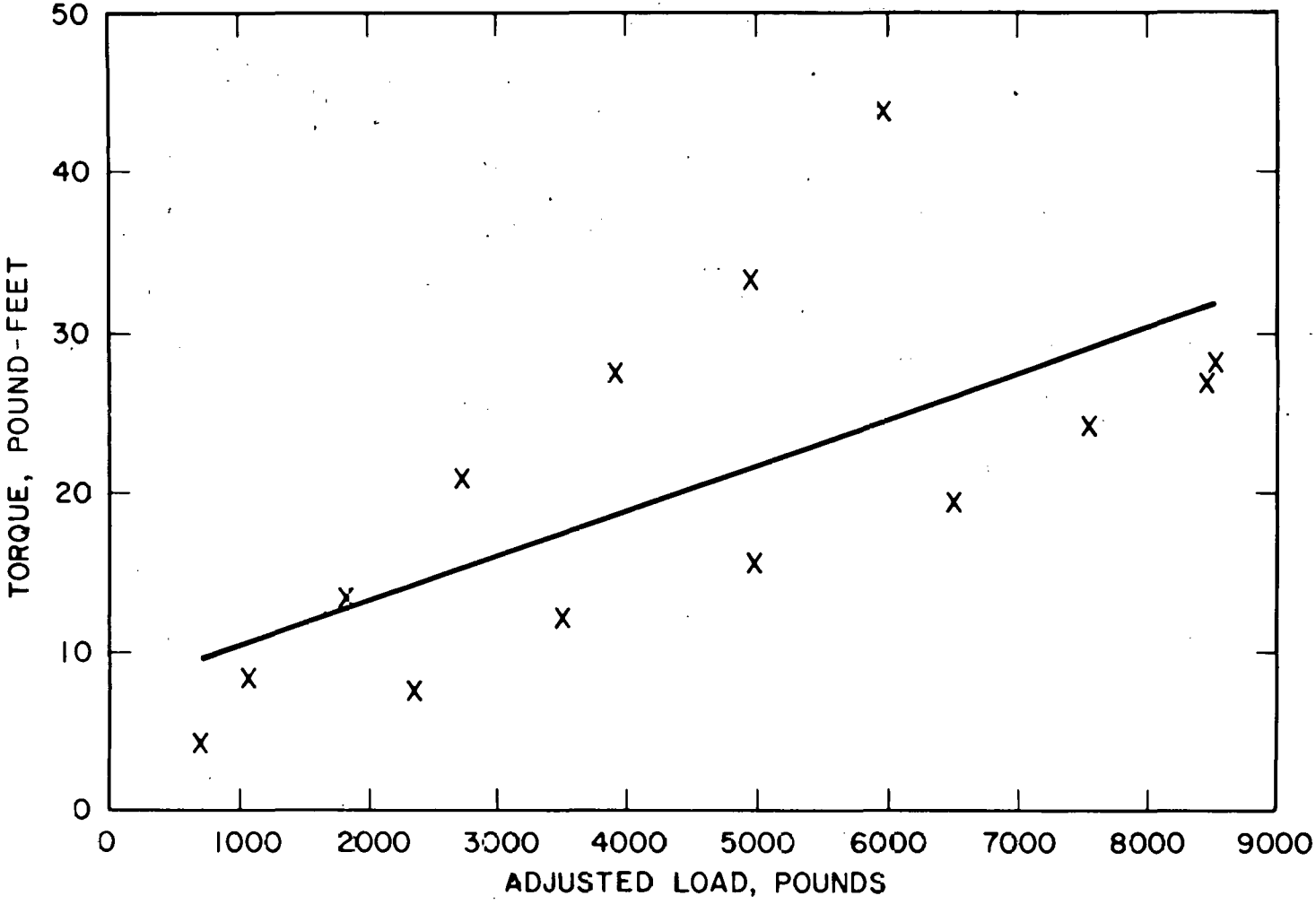

Figure 14. Torque-Preload Test, Pooled Data for Blanket Guide Tube Extension Joint

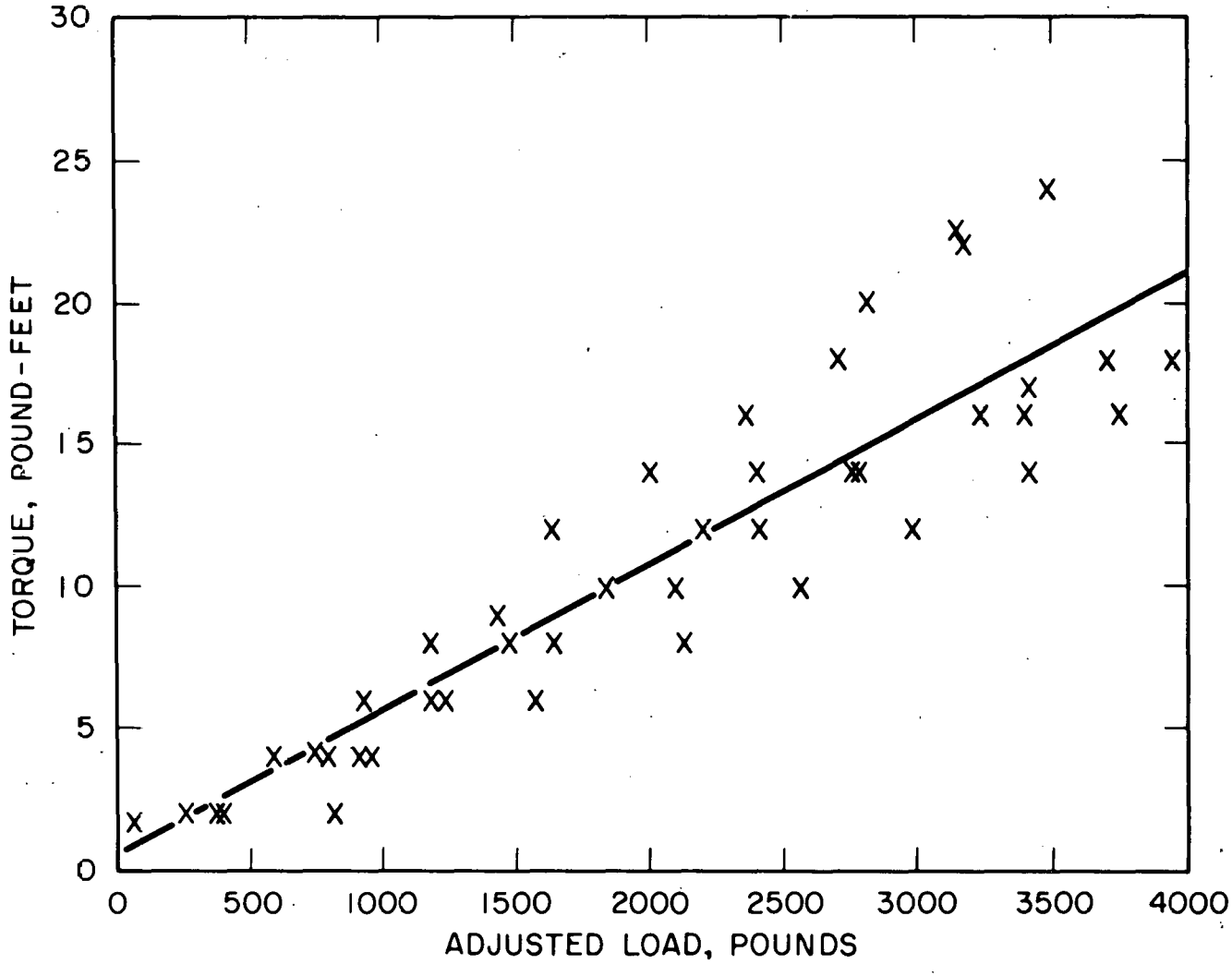

Figure 15. Torque-Preload Test, Pooled Data for Blanket Shear Key Joint

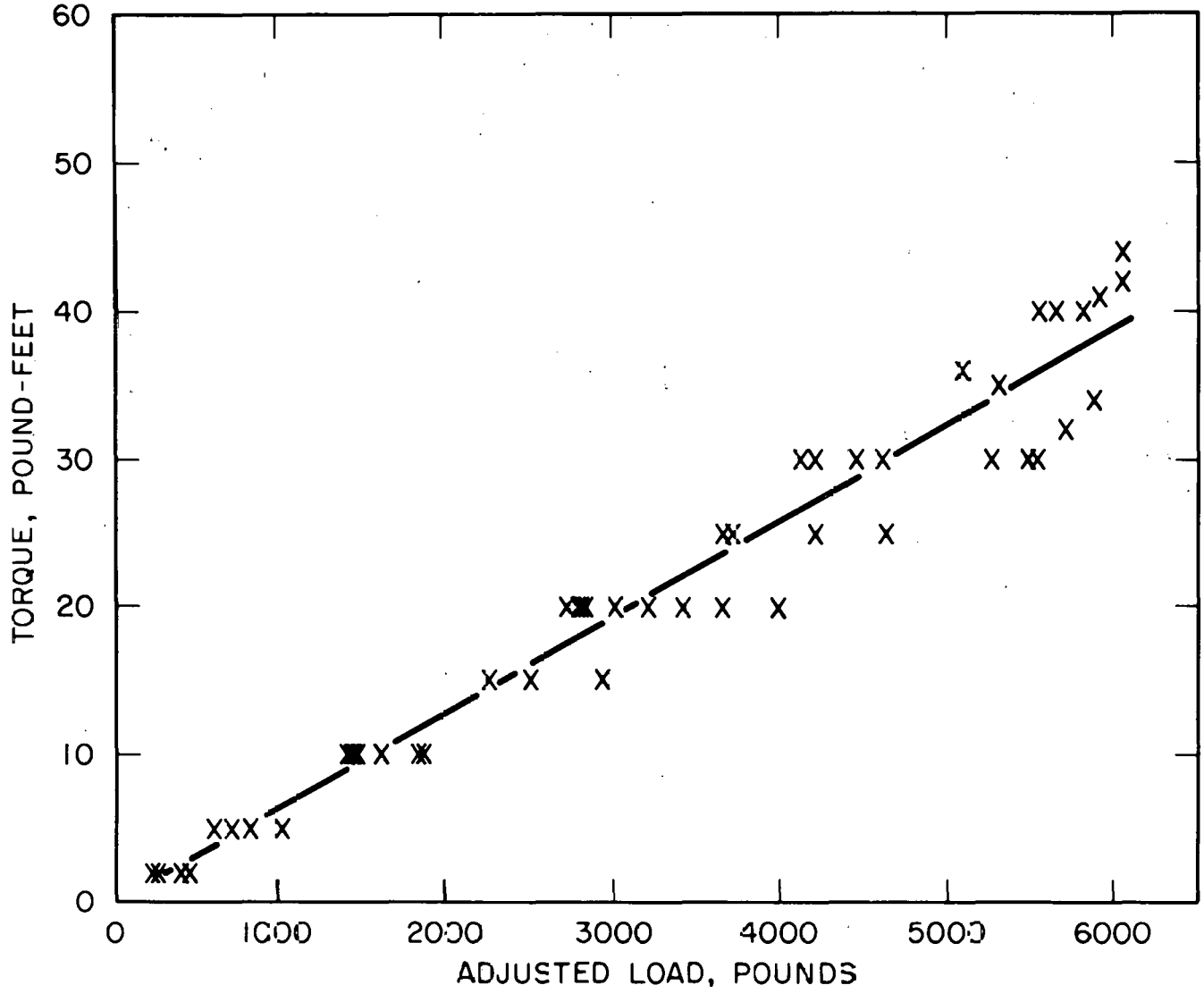

Figure 16. Torque-Preload Test, Pooled Data for Movable Fuel Top Ease Plate Joint

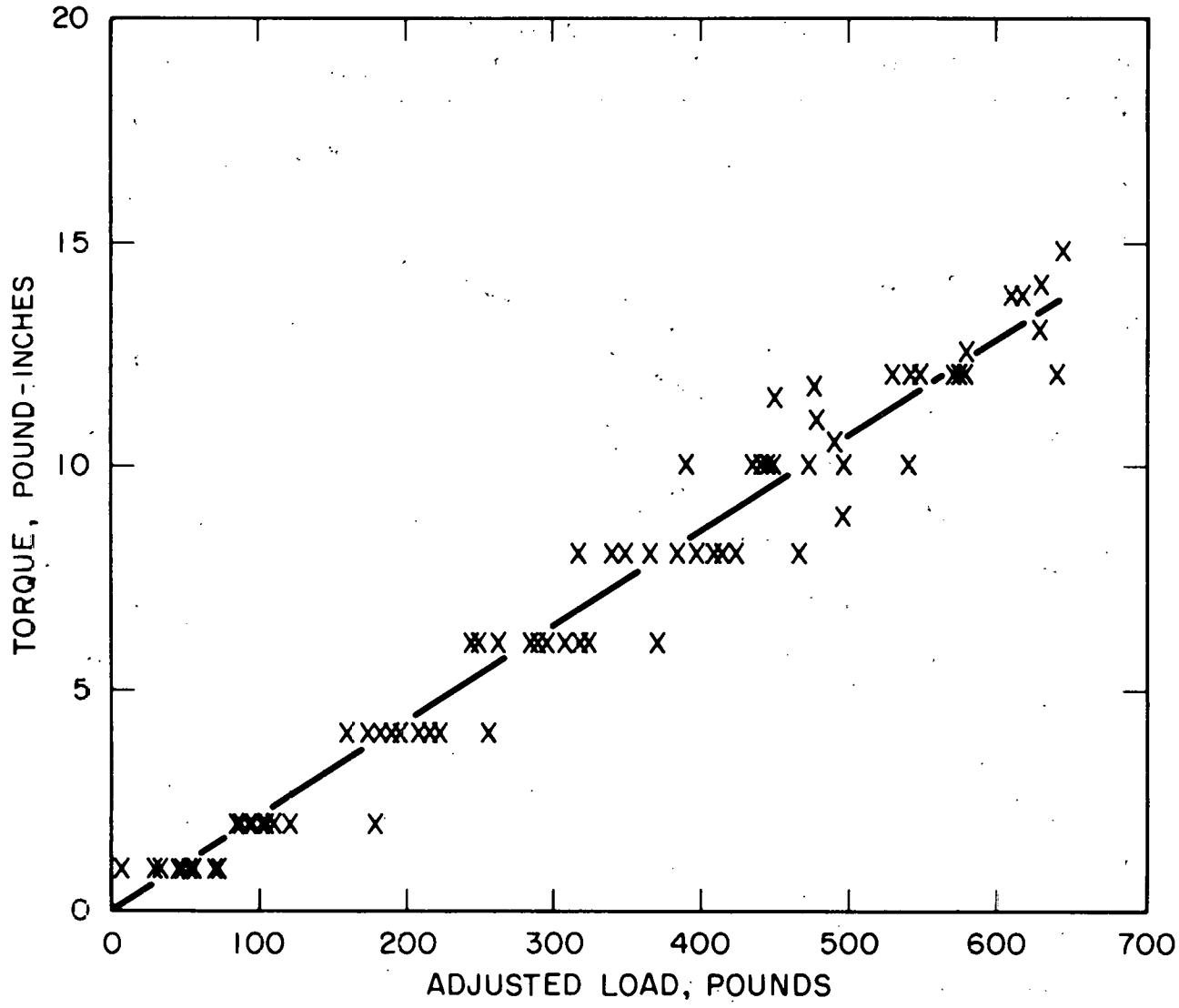

Figure 17. Torque-Preload Test, Pooled Data for Movable Fuel Grid Joint

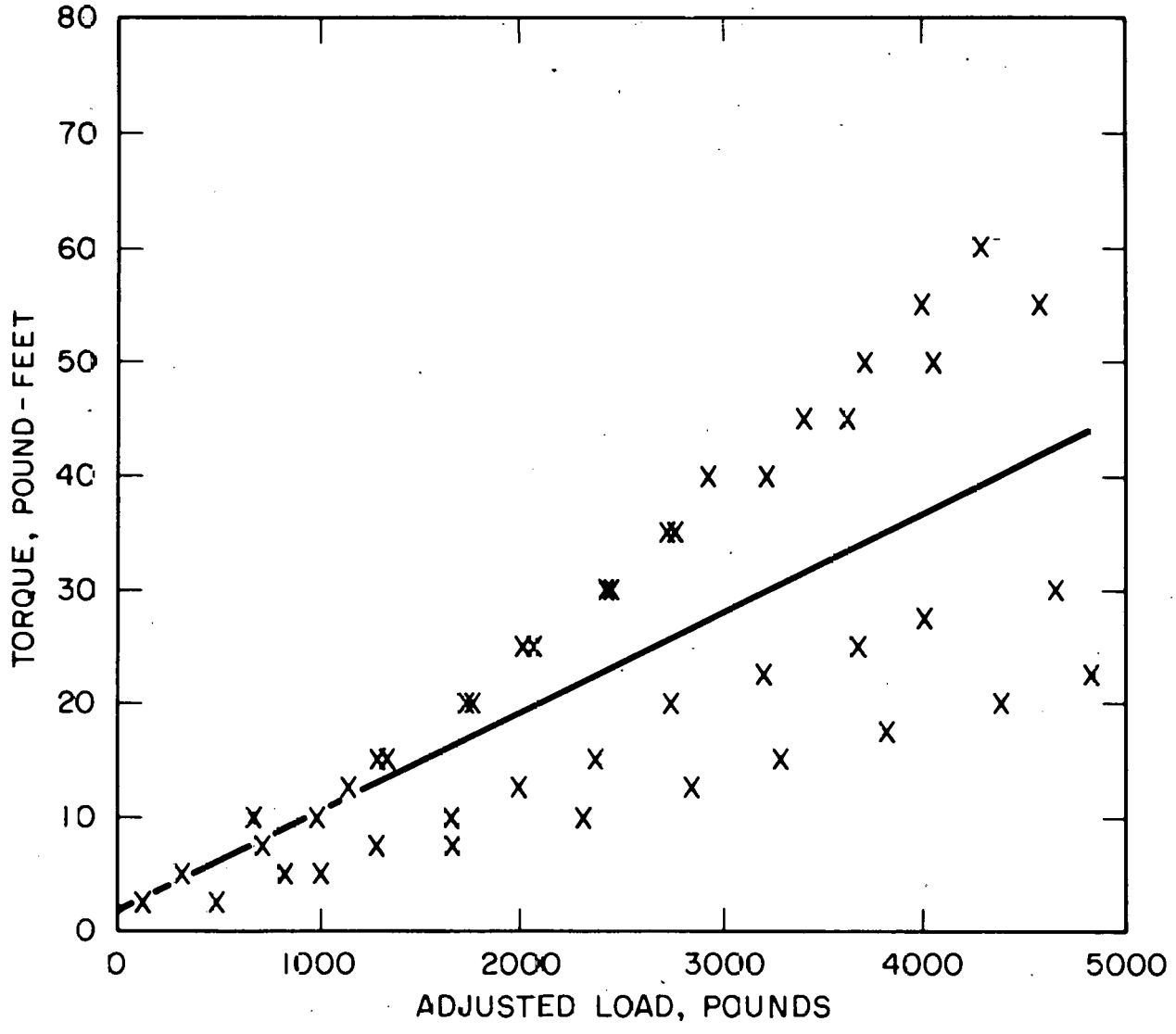

Figure 18. Torque-Preload Test, Pooled Data for Reflector Seal Block Joint

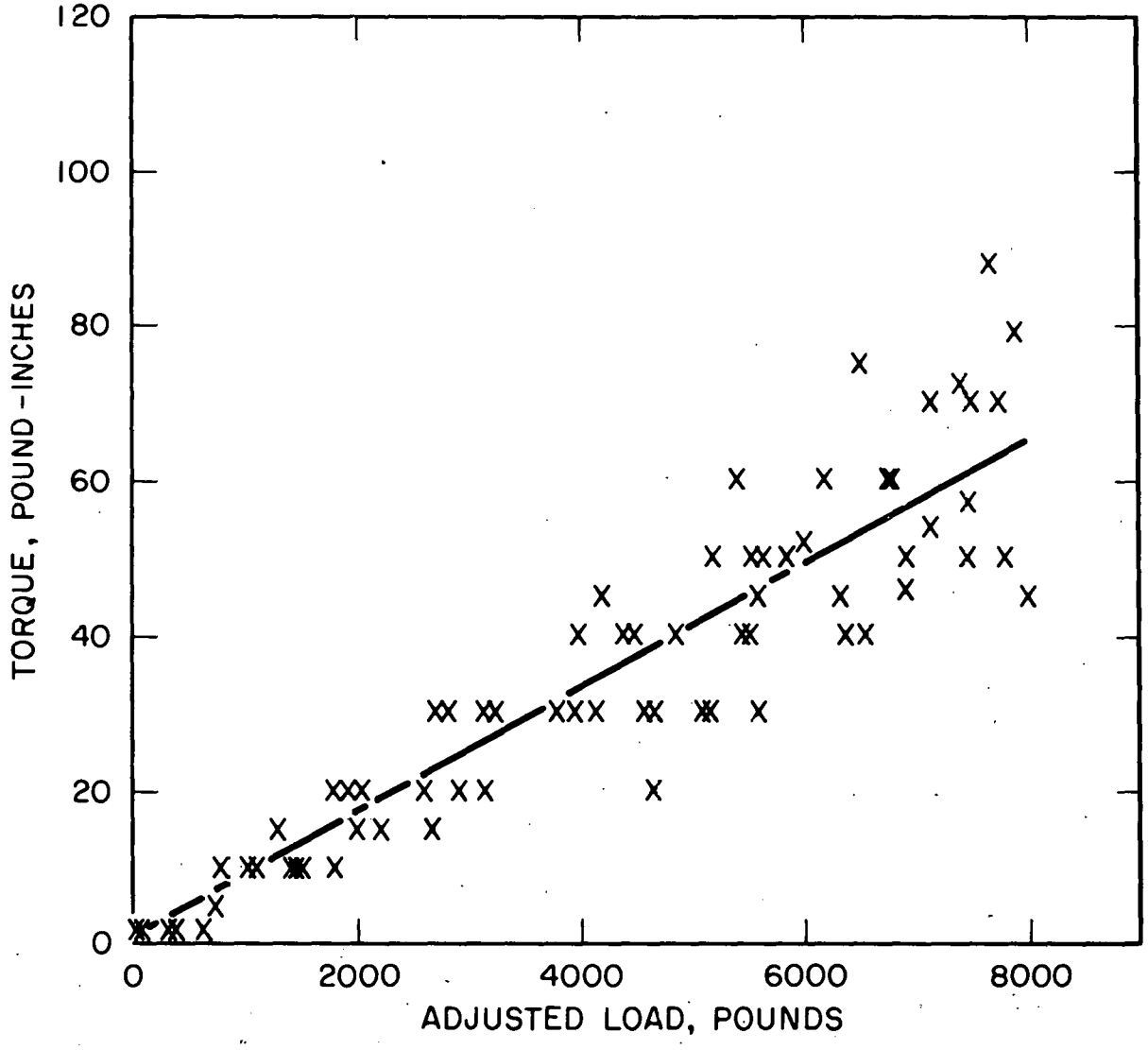

Figure 19. Torque-Preload Test, Pooled Data for Reflector Stub Tube Joint

Table 1. Test Summary of Torque-Preload Assembly Coefficients and Friction Coefficients

Bolted Joint	Figure Number	Screw Thread	Head Dia. / Hole Dia.	Sliding Materials		Assembly* Coefficient Min/Max	Ave. Friction Coefficient Min/Max
				Bolt/Nut	Head/Hole		
Blanket, Top Base Plate	10	0.750-10	1.315 / 0.770	INCO-X-750 / INCO-600	INCO-X-750 / INCO-600	0.090 / 0.290	0.056 / 0.217
Blanket, Guide Tube Extension	11	0.500-13	0.860 / 0.545	INCO-X-750 / INCO-600	INCO-X-750 / SS-304	0.075 / 0.175	0.041 / 0.122
Blanket, Bottom Base Plate	12	0.375-24	0.626 / 0.436	INCO-X-750 / INCO-600	INCO-X-750 / INCO-600	0.085 / 0.260	0.054 / 0.193
Blanket, Shear Key	13	0.500-13	0.775 / 0.530	INCO-X-750 / SS-17-4PH	INCO-X-750 / INCO-600	0.095 / 0.175	0.060 / 0.128
Movable Fuel, Top Base Plate	14	0.500-13	0.840 / 0.520	SS-17-4PH / INCO-600	SS-17-4PH / SS-304	0.130 / 0.180	0.087 / 0.129
Movable Fuel, Grid-to-Support Post	15	0.164-32	0.240 / 0.170	AM-350 / SS-304	AM-350 / AM-350	0.110 / 0.160	0.070 / 0.114
Reflector, Seal Block	16	0.438-14	0.798 / 0.453	INCO-X-750 / INCO-600	INCO-X-750 / SS-340	0.120 / 0.390	0.076 / 0.285
Reflector, Stub Tube	17	0.438-14	0.610 / 0.513	SS-304 / INCO-600	SS-304 / SS-304	0.125 / 0.265	0.085 / 0.206

*It should be noted that the assembly coefficients were determined using Equation (30) with torques expressed in lb-in, which is necessary for consistent units in the equation. Also, it is noted that these are the maximum and minimum values indicated by measurements as illustrated in Figures 10 through 17.

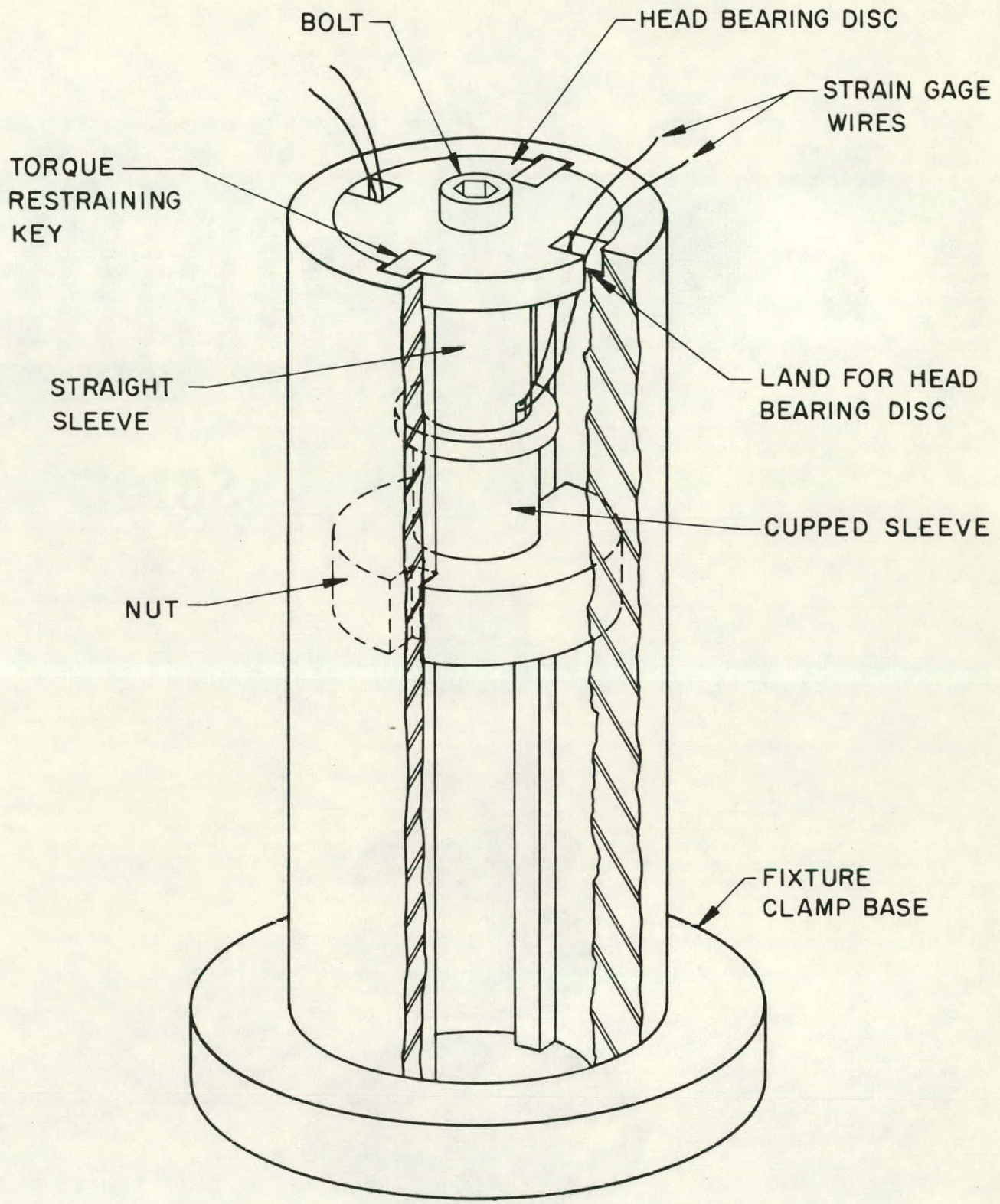

Figure 20. Universal Tightening Fixture with Typical Joint Test Assembly, SCC Test Joints

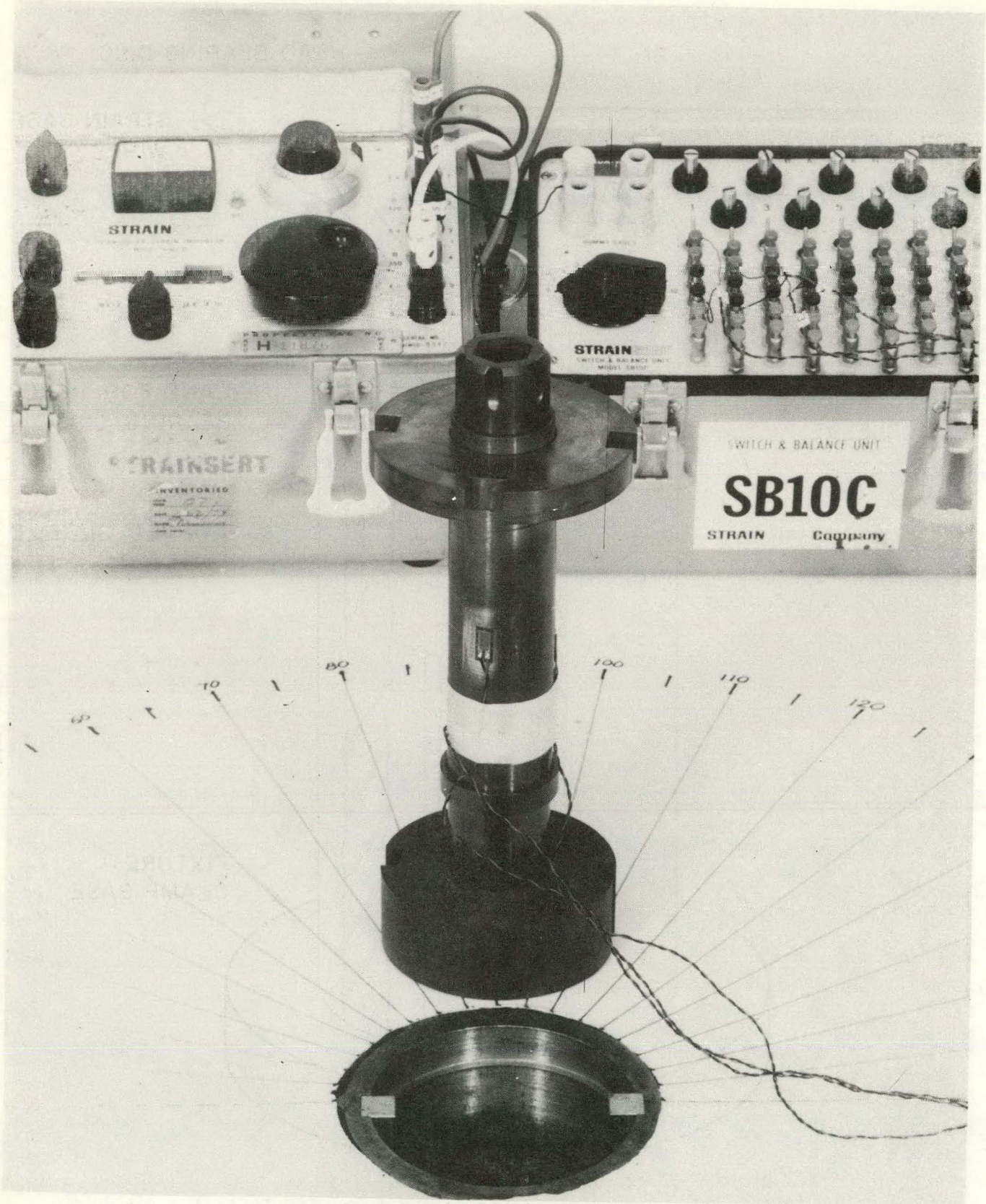

Figure 21. Actual Test Assembly, SCC Test (Neg. No. 52358-3)

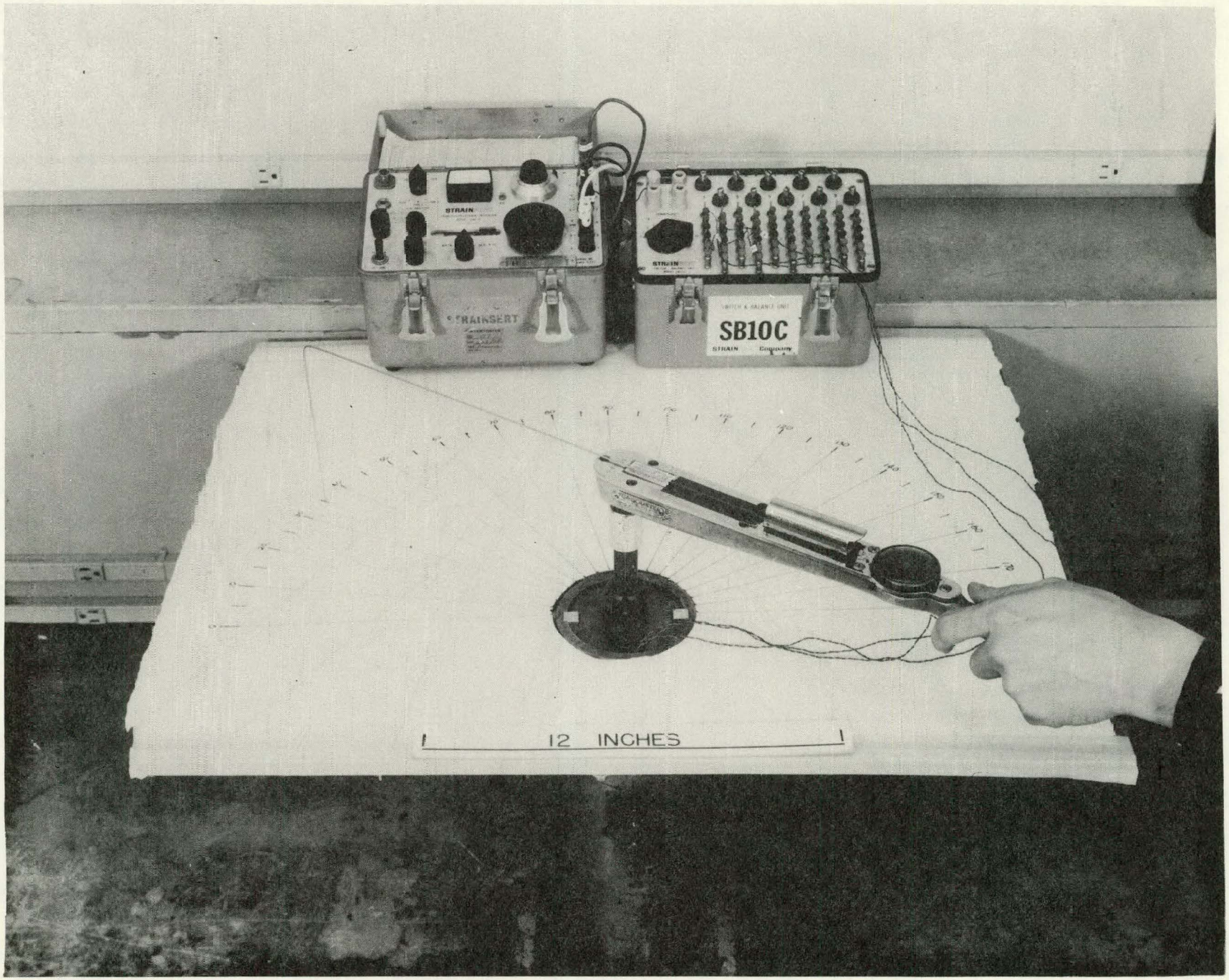

Figure 22. Test Set-up for Tightening Bolted Joints, SCC Test
(Neg. No. 52358-1)

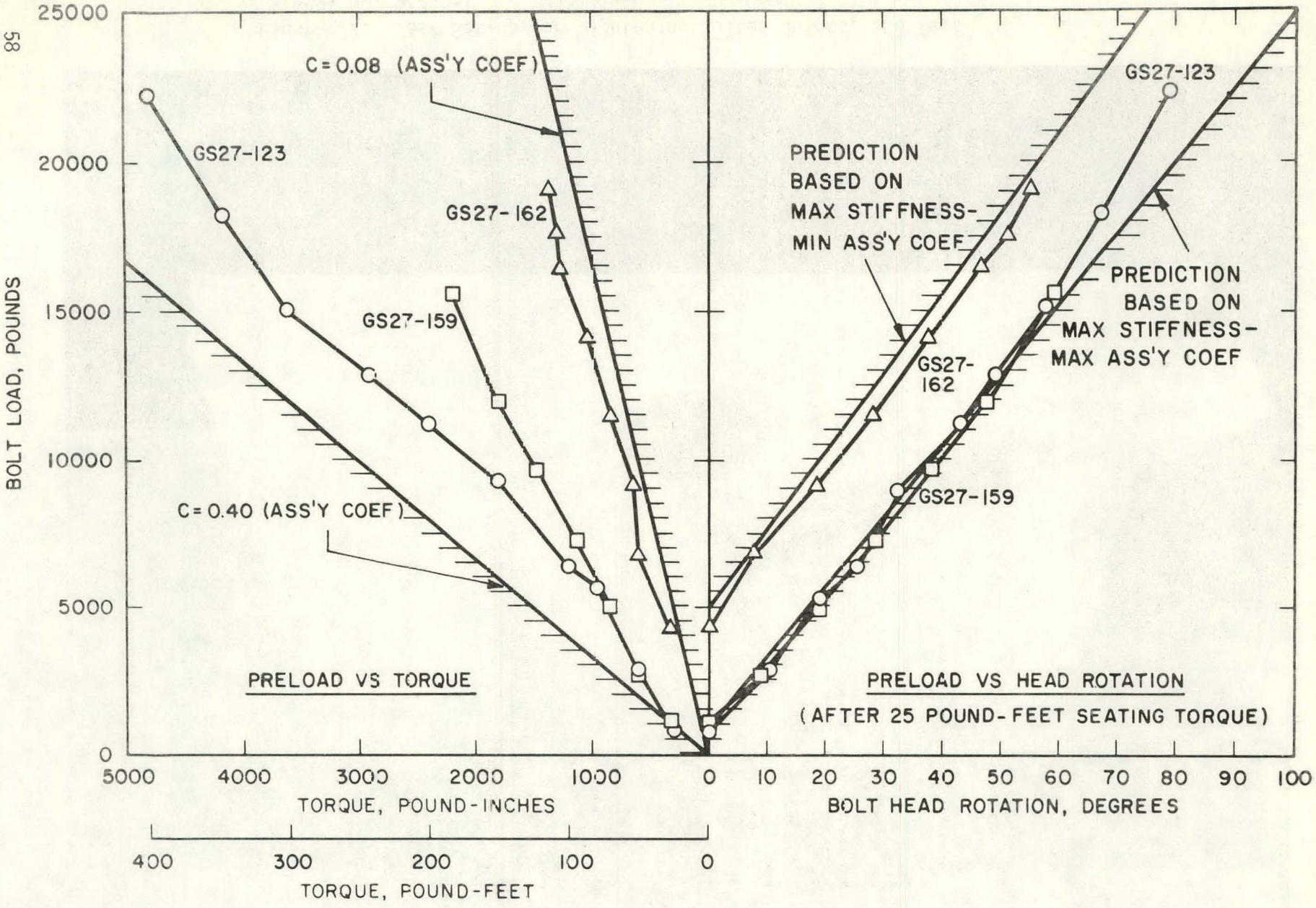

Figure 23. Typical Experimental Data for Blanket Top Base Plate Joint (3/4-10 THD)

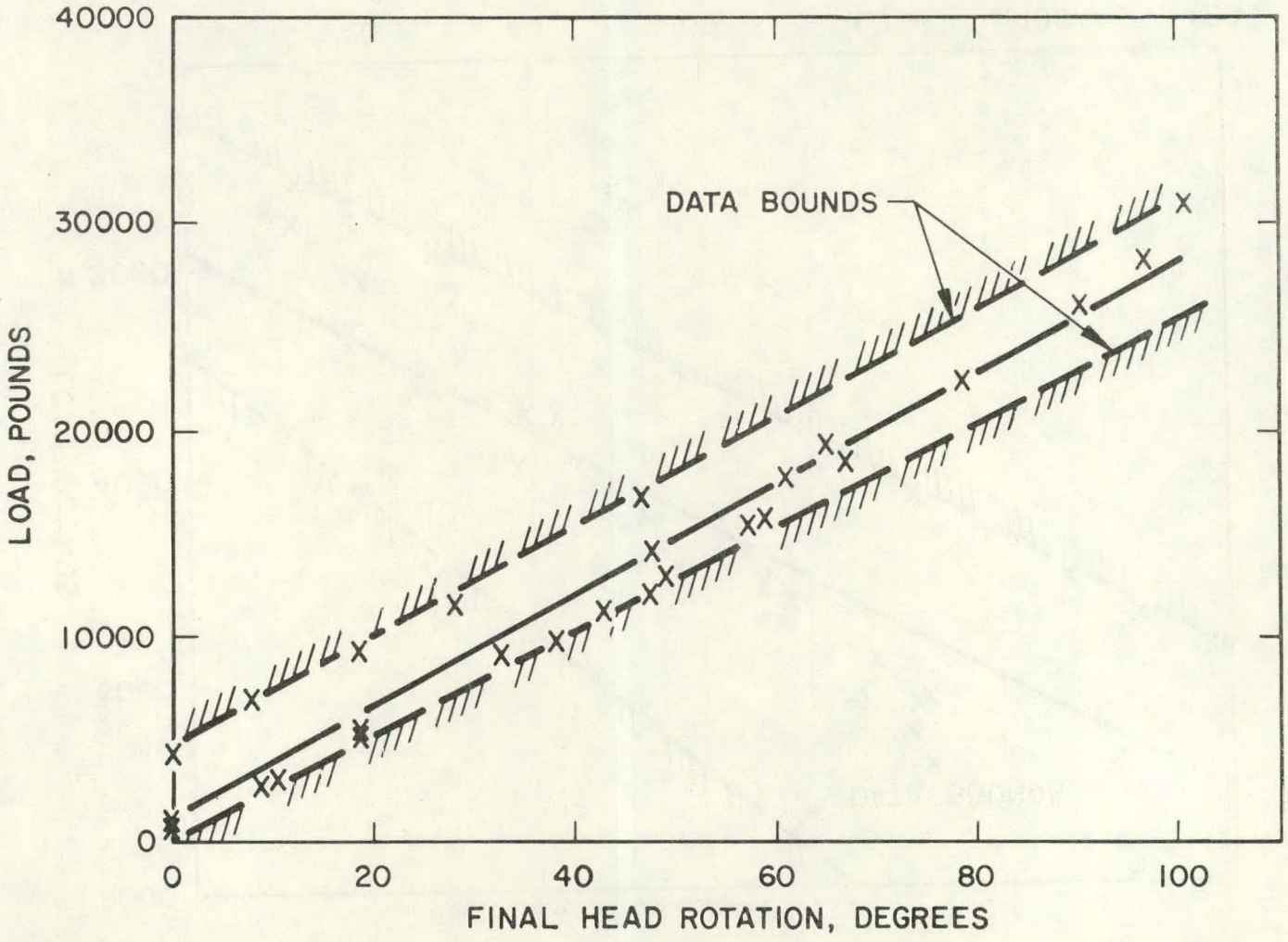

Figure 24. Preload-Head Rotation Test, Pooled Data for Blanket Top Base Plate Joint

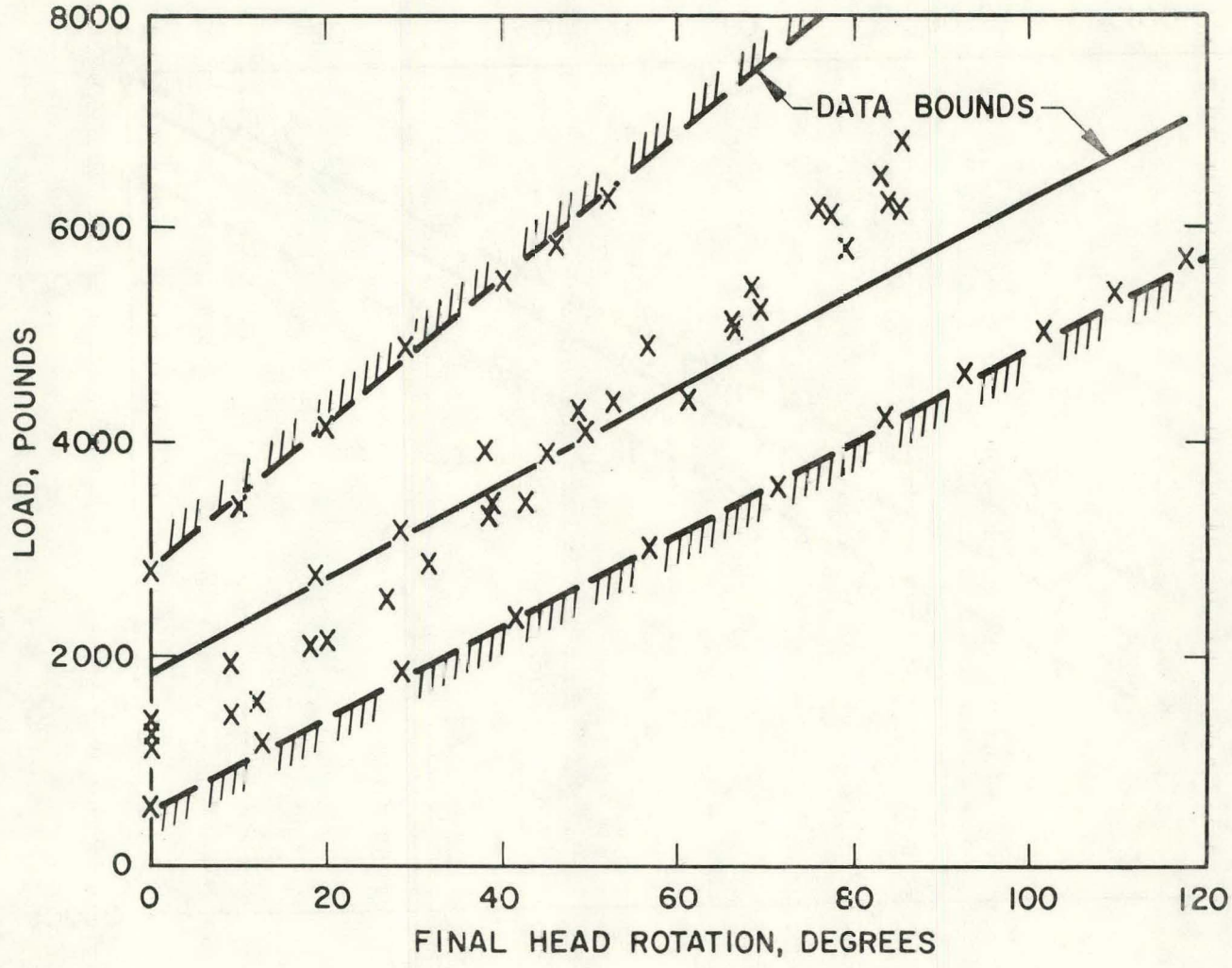

Figure 25. Preload-Head Rotation Test, Pooled Data for Blanket Bottom Base Plate Joint

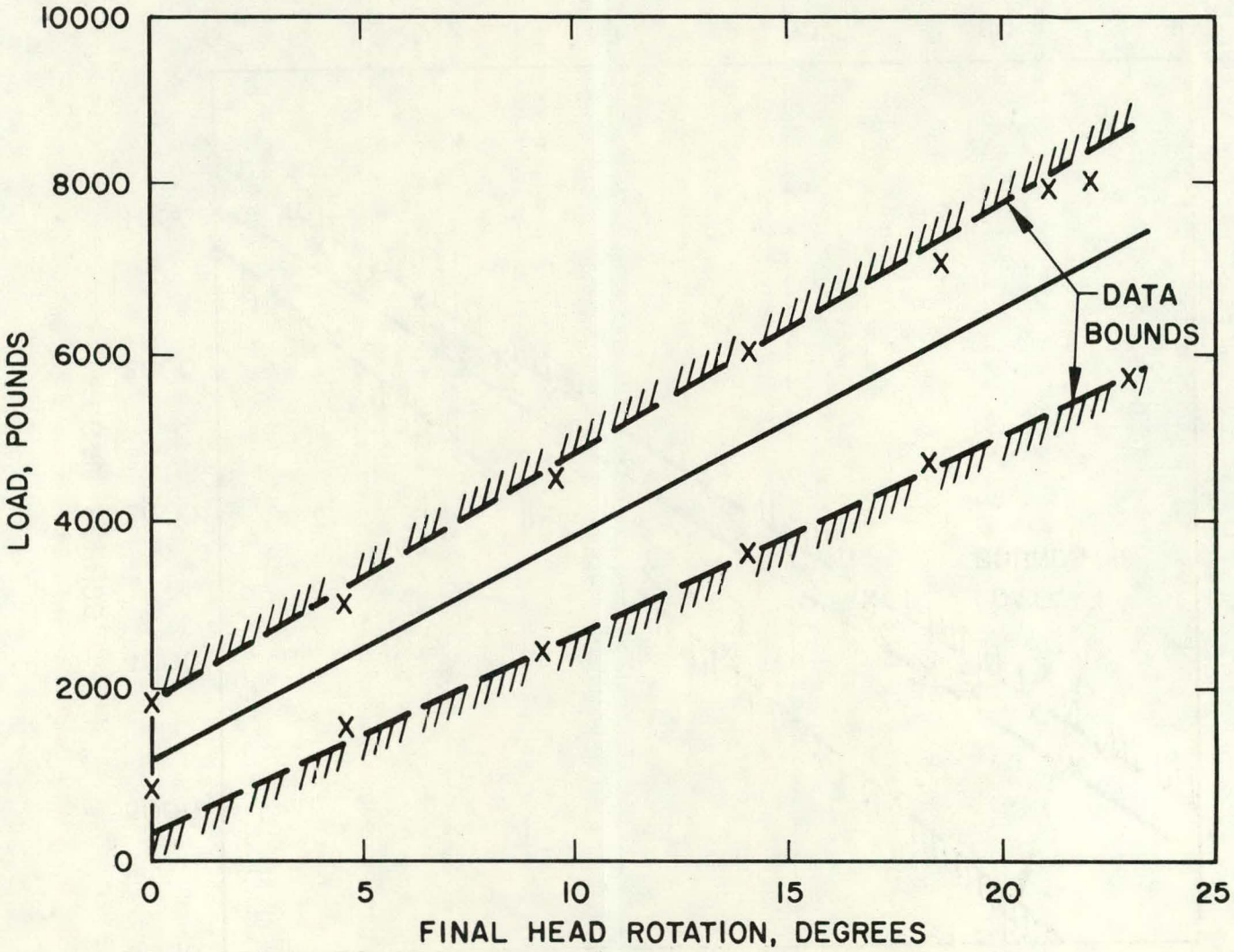

Figure 26. Preload-Head Rotation Test, Pooled Data for Blanket Guide Tube Extension Joint

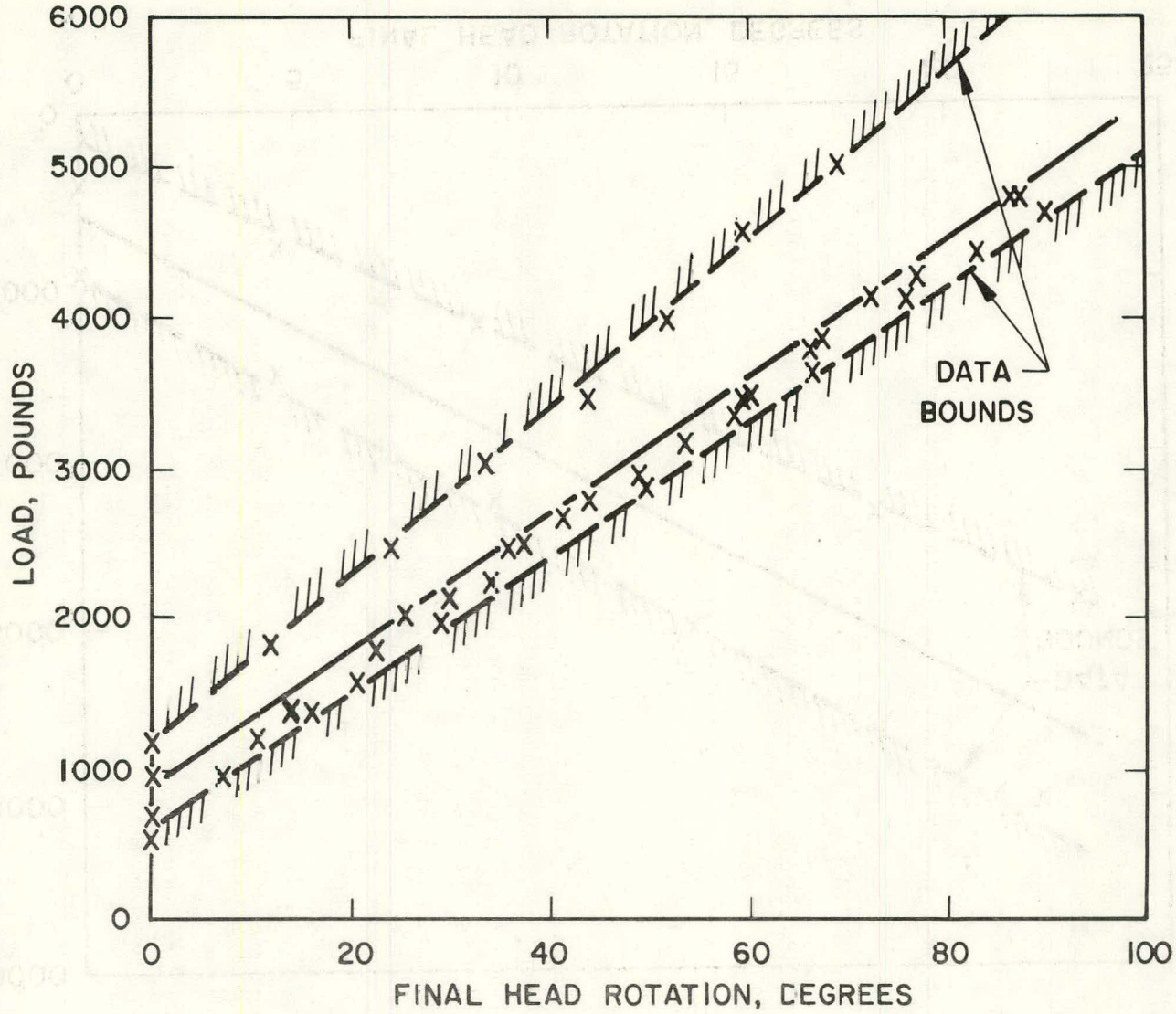

Figure 27. Preload-Head Rotation Test, Pooled Data for Reflector Seal Block Joint

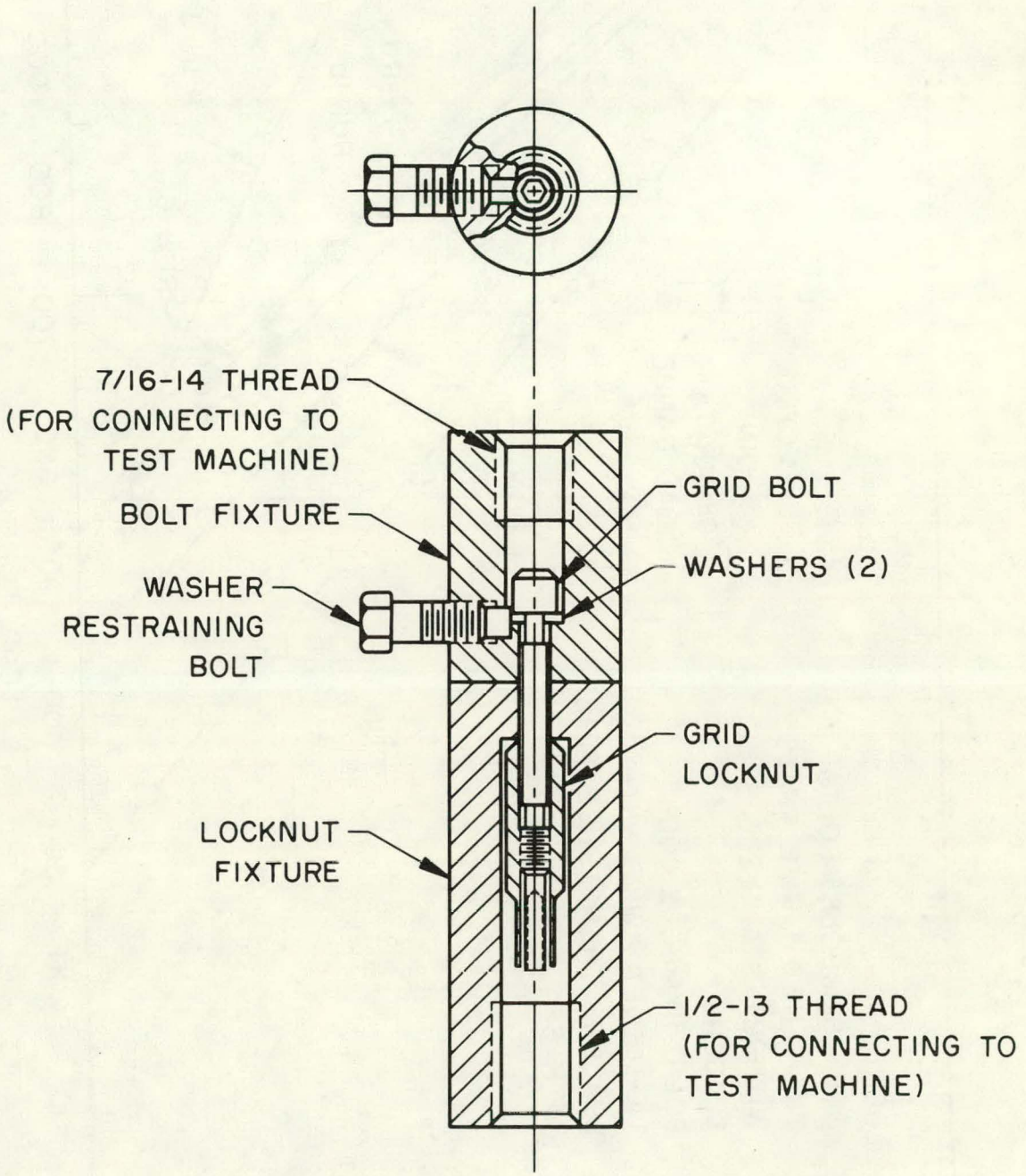

Figure 28. Test Assembly for Joint Separation Test

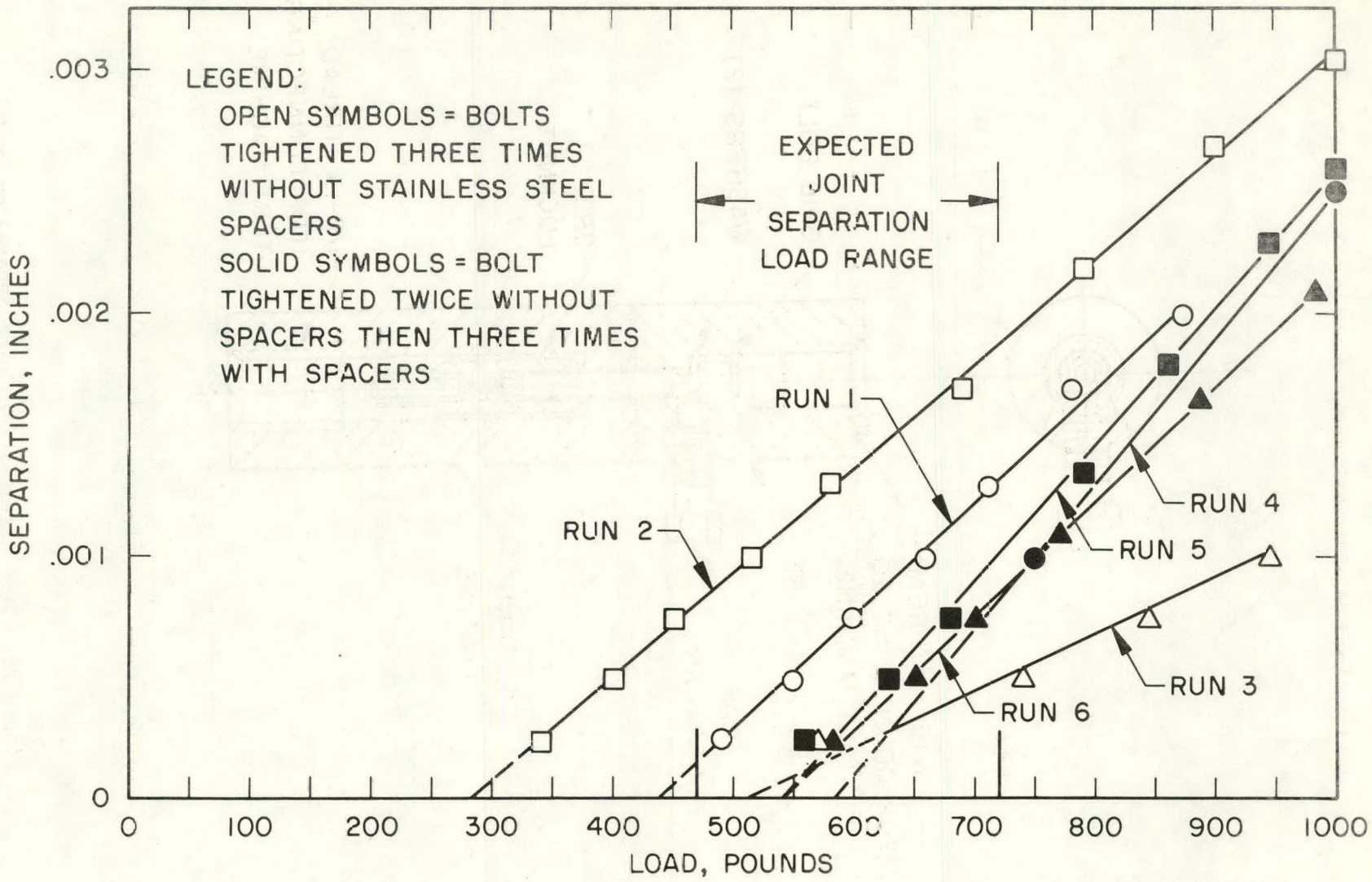

Figure 29. Blanket Grid to Post Joint Separation Test Data

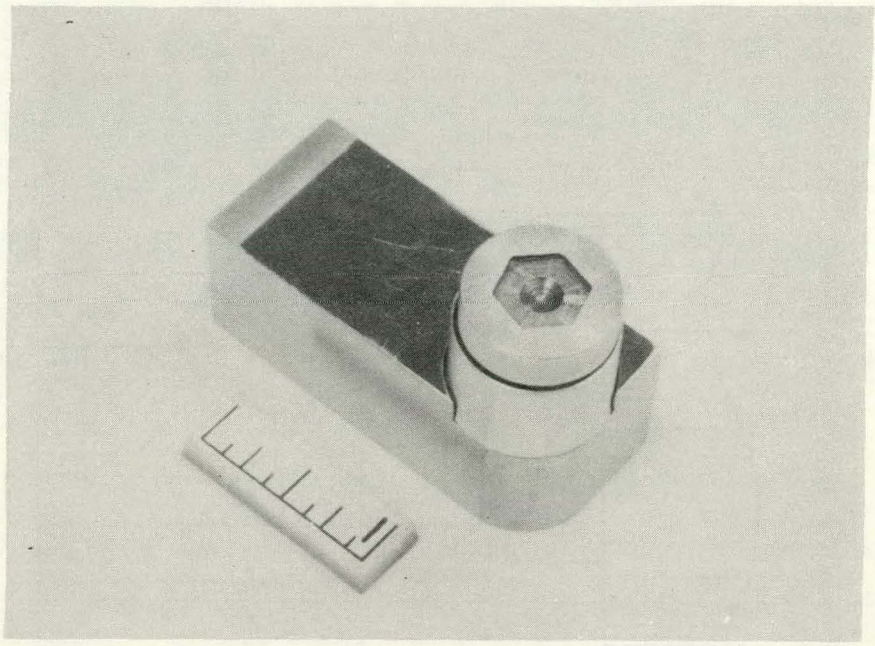

(a) Neg. No. 52358-4

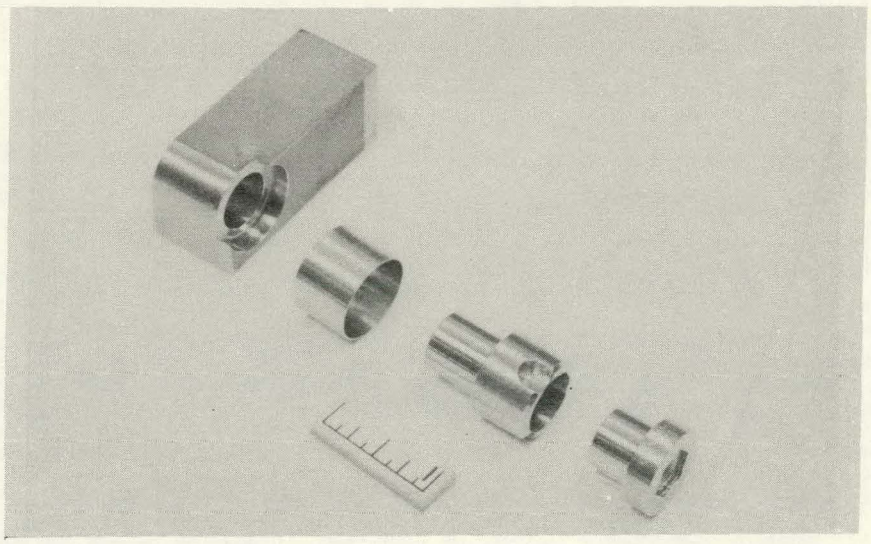

(b) Neg. No. 52358-6

Figure 30. Bearing Load Test Assembly - Support Post Joint (Neg. Nos. 52358-4 and 52358-6)

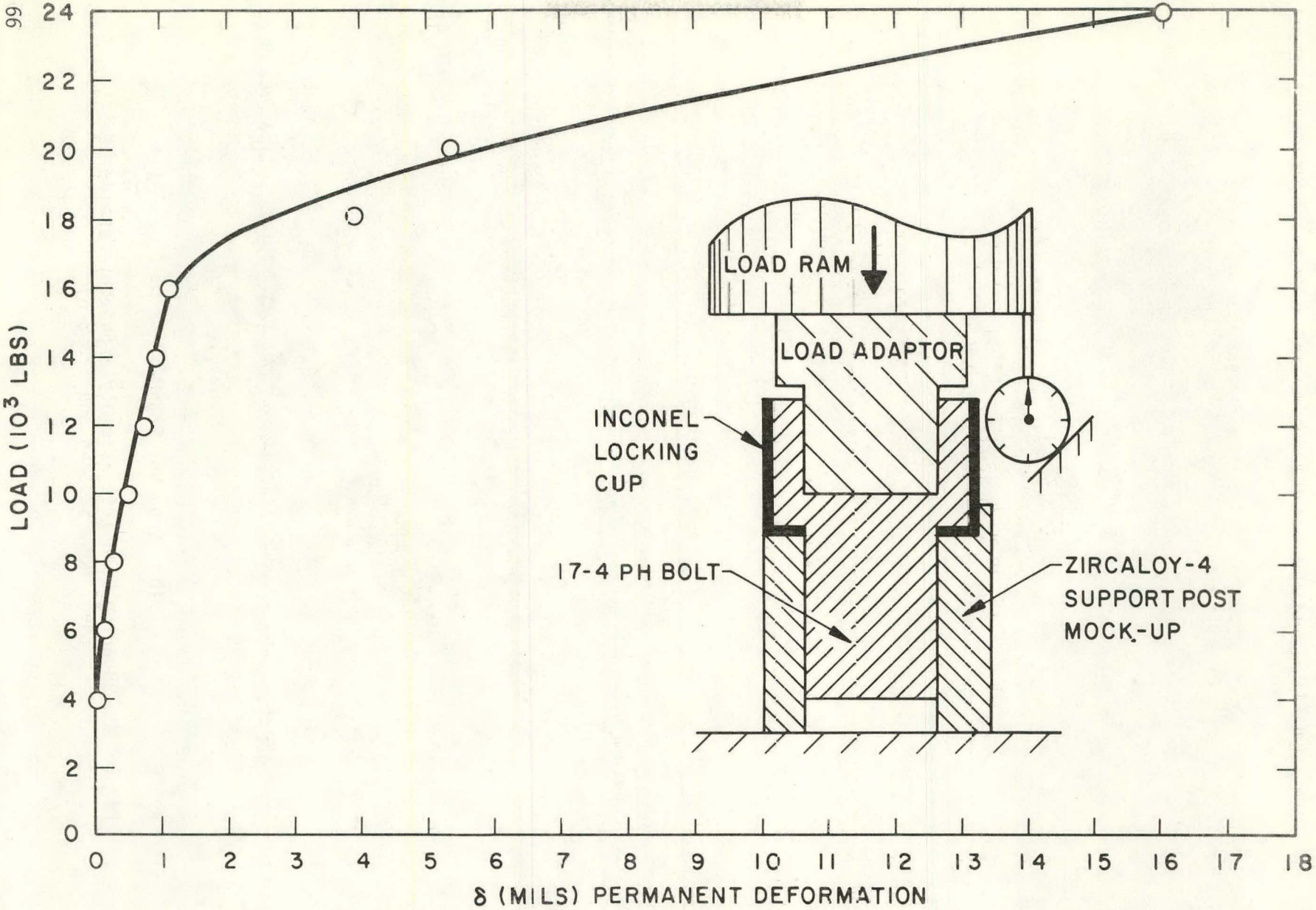

Figure 31. Bearing Test Data - Support Post Joint

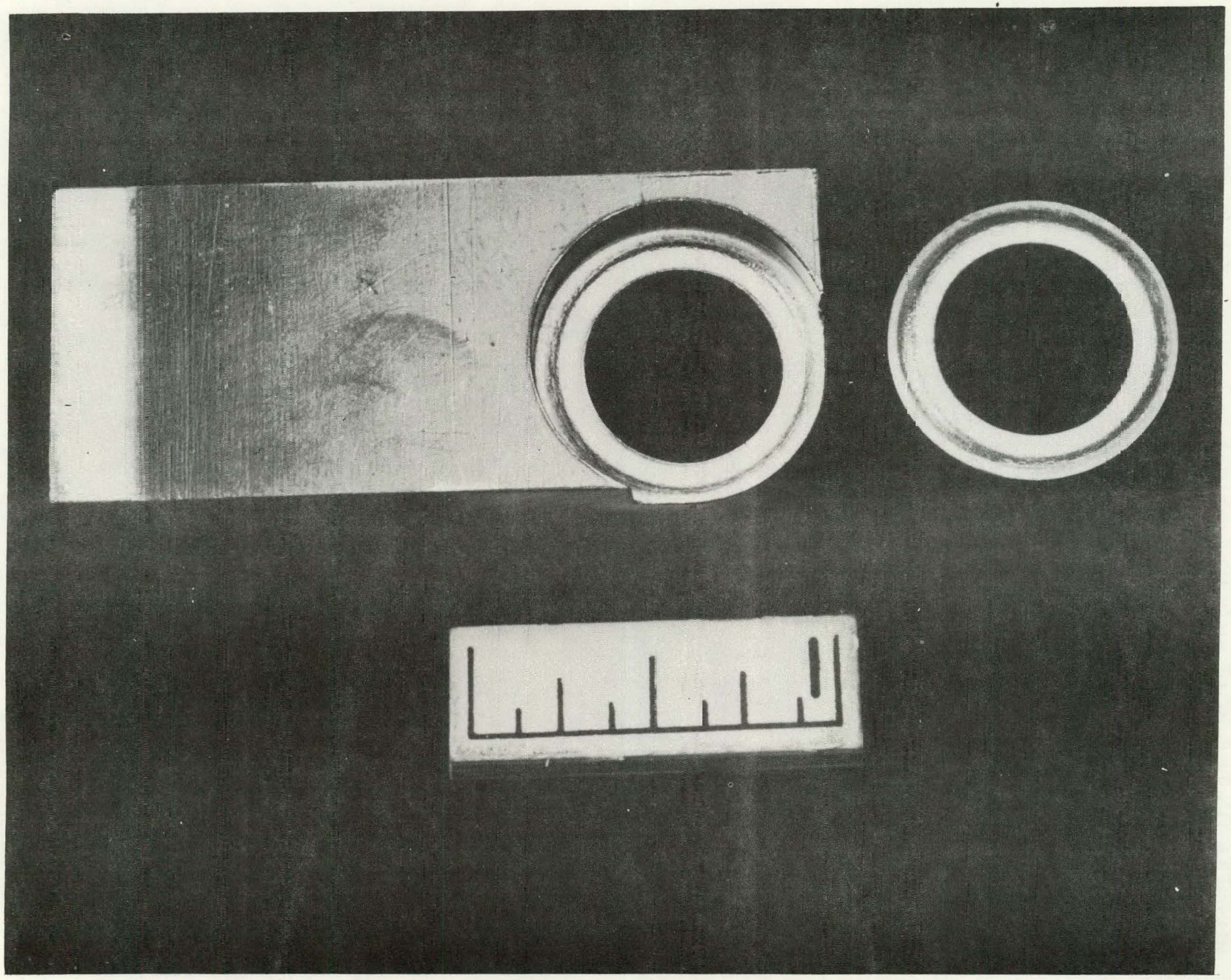

Figure 32. Plastic Deformation of Test Specimen Due to Bearing Loads
(Neg. No. 52358-7)

(a) DIRECTIONS OF THE STRAIN ROSETTE ON THE BOLT SHANK

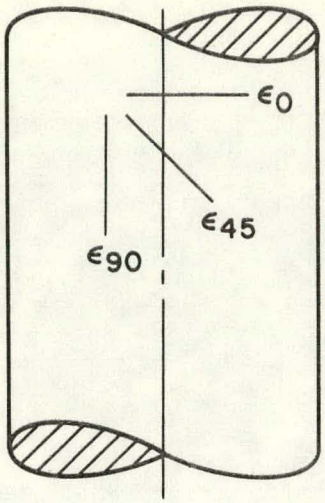

(b) MOHR CIRCLE FOR THE STATE OF STRAIN ON THE SURFACE OF THE SHANK

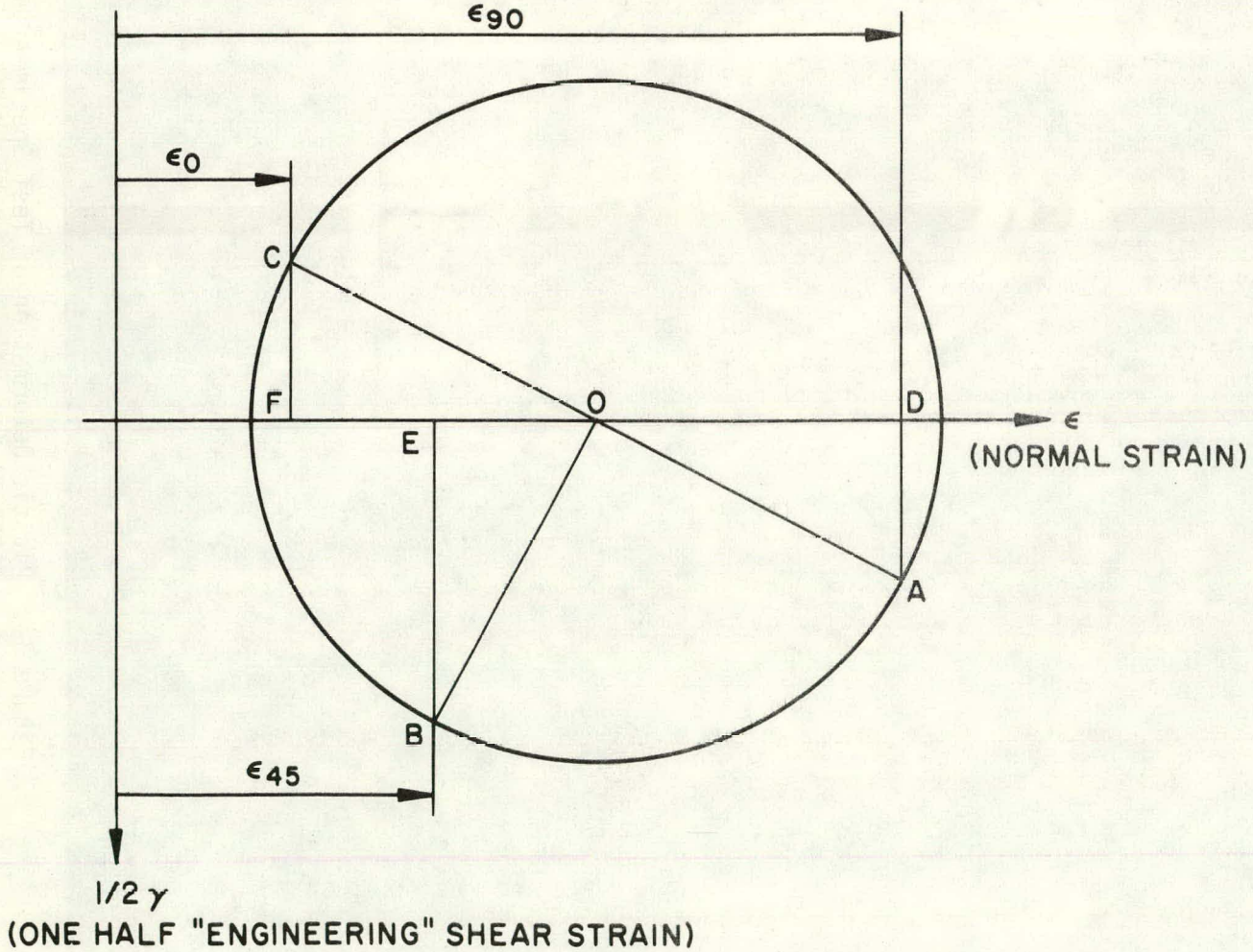

Figure 33. Strains on the Surface of a Bolt Shank

APPENDIX A

DESIGN STRESSES IN BOLTED JOINTS

1. MEMBRANE AND BENDING STRESSES IN THE BOLT

Membrane tensile and shear stresses (uniform stresses over a cross section) are computed for the minimum cross-sectional area of the bolt. If the minimum cross section occurs in the threaded region of the bolt, the cross-sectional area can be computed using the expression shown in Equation (A1) (which was obtained from Reference f). For both circumstances, the minimum cross-sectional area for the bolt may be calculated as follows:

$$A_c = \frac{\pi}{4} D_c^2, \quad D_c = \begin{cases} \text{diameter of minimum cross section, or} \\ \left[D_p - \dfrac{0.32476}{n} \right] \text{ for threaded region} \end{cases} \qquad \text{(A1)}$$

where,

D_c = (effective) diameter for min. cross-sectional area

D_p = basic pitch diameter

n = threads per inch.

Consequently, the membrane stresses produced by the tensile force, F_b, and shear force, Q_b, are

$$\sigma_M = \frac{F_b}{A_c}$$

and

$$\tau_M = \frac{Q_b}{A_c} \ ,$$

respectively.

If external loading of the joint results in a bending moment, M_b, acting on the bolt, the maximum linear elastic bending stress may be computed using the equality, $\sigma_B = (8\ M_b\ D)/(A_c D_c^2)$, where D is either the minimum diameter D_c or the minimum root diameter, D_r, if the minimum cross-sectional area occurs in the threaded region.

2. AVERAGE BEARING STRESS AND AVERAGE THREAD SHEARING STRESSES

In a bolted joint, bearing stresses in the clamped region and shear stresses over the thread engagement region are examples of stresses that are

distributed in a highly nonlinear fashion. However, gross failure from these two phenomena is observed to occur when averaged values of these stresses over defined sections exceed critical values. In the discussion that follows, relations are presented which can be used to compute these average stresses.

For the average bearing stress the minimum contact area, B_b, is computed from part drawings considering the effects of chamfers and dimensional tolerances. Wherever the minimum contact area might be (typically under the bolt head, although it could occur elsewhere depending on the joint design), this area is compressed by the preload or possibly a force of different magnitude when a working force, W, is present. Assuming that one or the other of these conditions leads to a maximum compressive force, F_j, acting on the bearing area, the average bearing stress is computed using the following equation:

$$\sigma_b = F_j / B_b \quad .$$

To compute the average thread shear stress two calculations are required: one for shear of the external (bolt) thread, and the other for the internal (nut) thread. The length of thread engagement, I_e, is taken as the minimum which can occur within drawing tolerances if the end of the screw protrudes from the internal thread (as in a bolt-nut combination), or may be taken as the minimum drawing length minus 1/2n (half the thread pitch) if the bolt thread does not protrude. From thread form and dimensional tolerancing information presented in Reference (f), the following minimum shear areas for threads may be obtained:

(1) Bolt and nut of same material, shearing at basic pitch diameter, the shear area is

$$B_{sb} = B_{sn} = \pi D_p \frac{I_e}{2} \qquad (A2)$$

(2) Bolt threads stronger, shearing in nut threads only, the shear area is,

$$B_{sn} = \pi n I_e V_s \left[\frac{1}{2n} + (V_s - U_n) \tan \alpha \right] \qquad (A3)$$

(3) Shearing in bolt threads only, nut threads stronger, the shear area is,

$$B_{sb} = \pi\, n\, I_e\, V_n \left[\frac{1}{2n} + (U_s - V_m) \tan \alpha\right] \qquad (A4)$$

where

n = threads per inch
I_e = engagement length
D_p = basic pitch diameter
U_s = minimum pitch diameter of bolt
U_m = maximum pitch diameter of nut
V_s = minimum major diameter of bolt
V_n = maximum minor diameter of nut
α = 1/2 thread profile angle (30° for standard threads).

With these areas, the average thread shear stress computed is

$$\tau_t = F_b/B_{sb} \text{ or } \tau_t = F_b/B_{sn}$$

to assess the strengths of the bolt and nut materials respectively. F_b is the maximum bolt load applicable to the type stress being computed (from primary loads or from primary-plus-secondary loads).

3. LOCAL AND AVERAGE STRESS INTENSITIES OVER BOLT TENSILE AREA

The assembly methods used to tighten bolted joints in the LWBR core, discussed in Section II.B, caused a residual torque along with an axial preload. Although some methods of bolt tightening do exist which produce preloads without a residual bolt torque, their use is generally restricted to special applications. For the vast majority of bolted joints, residual torque is virtually assured because of the methods of joint tightening normally applied. Since control of stresses is of widespread interest in bolts, account must often be taken of the simultaneous action of this torque and axial loading. For ductile bolting materials, the average stress intensity level across the smallest cross section of the bolt can be viewed as a measure of the bolts' capacity to safely withstand service loading even if the stress is beyond yield at the surface of the section. Hence an important stress limit for bolts to satisfy is the average stress intensity limit. In addition, fluctuations of the maximum stress intensity caused by cyclic loading can affect the fatigue response of the bolt

material. In the following discussion, therefore, a formulation for the stress intensity and its area weighted mean (or "average") value are presented.

To compute the stress intensity at the loaded shank (or thread) region with the minimum section, it is first assumed that the cross section is circular with radius R, and solid, so the following applies for the area and polar moment of inertia:

$$A = \pi R^2, \; J = 1/2 \; \pi R^4 \quad . \tag{A5}$$

Given that the maximum axial force supported by this section is F (which may exist when the preload joint supports a working load), and that the section is simultaneously supporting the torque T, the distribution of normal and torsional shear stresses is given by

$$\sigma(r) = \frac{F}{A} = \text{const}, \; \tau(r) = \frac{T}{J} r, \; 0 \leq r \leq R \quad . \tag{A6}$$

Representing the complete state of stress for any point at distance "r" from the shank axis by a Mohr-circle, it can be shown that the principal stresses for this combined state of stress are

$$\sigma_1 = \frac{\sigma(r)}{2} + \sqrt{\left[\frac{\sigma(r)}{2}\right]^2 + \tau^2(r)} \; ,$$

$$\sigma_2 = \frac{\sigma(r)}{2} - \sqrt{\left[\frac{\sigma(r)}{2}\right]^2 + \tau^2(r)} \; ,$$

and

$$\sigma_3 = 0$$

for which the greatest stress intensity must be $S(r) = \sigma_1 - \sigma_2$, or

$$S(r) = \sqrt{\sigma(r)^2 + 4 \; \tau(r)} \quad .$$

By expressing this stress in terms of the axial force, the torque, and the cross-sectional properties, the following result is obtained,

$$S(r) = \frac{2}{J} \sqrt{\left[\frac{J}{2A}\right]^2 F^2 + T^2 \; r^2} \; , \tag{A7}$$

which takes on a maximum value when r = R. Defining the average stress intensity by

$$\overline{S} = \frac{\int_A S(r)\, dA}{\int_A dA} = \frac{2\pi \int_0^R S(r)\, r\, dr}{2\pi \int_0^R r\, dr}$$

or

$$\overline{S} = \frac{2}{R^2} \int_0^R S(r)\, r\, dr \quad ,$$

evaluation of the integral then yields

$$\overline{S} = \frac{J^2}{6\, A^3\, R^2} \frac{F^3}{T^2} \left[\left[1 + \left[\frac{2AR}{J} \frac{T}{F} \right]^2 \right]^{3/2} - 1 \right] .$$

But, from Equation (A5), it is found that

$$\frac{J^2}{6\, A^3\, R^2} = \frac{1}{24\, \pi} \, , \quad \frac{2AR}{J} = \frac{4}{R} = \frac{8}{D}$$

where D is the diameter of the section of interest, hence the average stress intensity becomes, upon substituting F_b for F and T_r for T*,

$$\overline{S} = \frac{1}{24\, \pi} \frac{F_b^3}{T_r^2} \left[\left[1 + \left(\frac{8\, T_r}{D\, F_b} \right)^2 \right]^{3/2} - 1 \right] . \qquad \text{(A8)}$$

In evaluating Equation (A8) it should be noted that F_b and T_r are the total axial bolt force and residual torque, respectively, that exist simultaneously in the bolt shank. Hence, at the time of joint assembly, if the greatest bolt force is the preload, which takes on its maximum value when the lowest

---

*It is presumed that the highest axial bolt force occurs when the residual torque is present, which is the normally encountered condition after joint assembly. However, during the initial joint tightening itself, a higher shank torque may be present, and it is this torque which must be considered with the attained peak axial load when computing the average stress intensity applicable to joint assembly.

applicable coefficient of friction exists, the residual torque will be based on this same coefficient of friction and must be a "minimum" residual torque. To be realistic the force and torque must be consistent in this fashion. Additionally, temperature and stress relaxation changes in the joint will not only affect the axial stiffness of the joint but it must also similarly influence the torsional stiffness of the bolt. Hence, accounting for elastic modulus reductions with increased temperature, or the stress relaxation affecting the bolt material, the residual torque will drop along with the bolt preload. But other factors may be present which affect the axial bolt load alone as thermal expansion and working loads, and have no influence on the torque. Appreciation of these considerations allow one to maintain a consistent pairing of these quantities.

Alternate forms of Equation (A8) are sometimes used in which the variables are preload, P, and friction coefficient, μ, instead of F_b and T_r. Such alternate forms have the undesirable feature that the maximum coefficient of friction could be inadvertently coupled with the maximum preload, which is inconsistent. Further, in this form, the residual torque is implicitly presumed to be related to what may possibly be inconsistent values of preload and friction coefficient, which is another inconsistency. In addition to this, no provision is made for increased values of axial force under the action of a working load. Because of these potential difficulties when $\overline{S}$ is expressed as a function of P and μ, the formula provided in Equation (A8) is preferred since it clearly identifies the proper coefficients and parameters to be considered together, thereby insuring a consistent analysis.

APPENDIX B

EXAMPLE OF A BOLTED JOINT PRELOAD ANALYSIS

Use of the results presented in Sections II and III is best demonstrated by a preload analysis of a bolted joint. To this end, the LWBR guide tube extension joint has been chosen because it is a rather typical core joint, and it also possesses sufficient complexity to illustrate many analytic features of general interest. A cross-sectional drawing of this joint in Figure B.1 shows an Inconel X-750 bolt clamping five distinct 304 SS joint members against an Inconel 600 structure. Since a variety of materials are employed in the joint, particular attention must be given to such matters as elastic stiffness, material strength, thermal expansion, and stress relaxation effects. In addition, the bolt and individual joint members are shaped differently, and this will have an effect on local stresses and on the elastic stiffness of each member. For example, other than the spacer which is in the form of a simple washer, the clamped members are in the form of bolting lugs of various shapes and sizes. By assuming that the structures to which the lugs are appended are significantly more flexible than the individual lugs themselves, the clamping force in the joint will be determined primarily by the elastic deformability of the bolt and joint members (lugs) rather than by any deformation in the structures to which they are attached. This assumption is valid for the application at hand, and allows attention to be focused exclusively on the joint itself as an isolated elastic structure; the only communication with regions outside the joint is through a working force, W.

As stated earlier, the clamped lugs are each different in size and shape and hence the distribution of stresses throughout each lug under load is likely to be complicated, which makes the precise determination of each lug's elastic flexibility (or stiffness) no trivial matter. However, for many bolted joints (including the one currently being considered), most of the system flexibility resides in the bolt itself. In this situation, some lack of precision in the flexibility associated with individual joint members is tolerable and will not markedly affect the magnitudes of the computed joint forces. It is therefore considered appropriate to treat the loaded volumes of the joint as cylindrical regions whose length and effective cross-sectional areas are as given in

Figure B.1. With this portrayal of the joint members, and the fact that the bolt actually is a cylindrical body, the individual region stiffnesses listed in Table B.1 were computed.

The treatment of the bolt in this table is noteworthy since the table values are based on two slightly different bolt lengths. For the elastic flexibility, the length of the threaded region was artificially increased to account for the flexibility of the engaged threads. The increase follows the recommendation of Reference (a) which suggests that an increased length of approximately 2/3 D_c may be employed (where D_c represents the effective diameter of the threaded region). However, in accounting for thermal expansion effects the actual grip length of the bolt was used (e.g., in the product $\bar{\alpha}L$ the true value of L was used, not the effective value employed in the stiffness computations).

The treatment of stress relaxation factors includes both thermal and irradiation induced effects. Although the experimentally observed irradiation induced relaxation is developed at operating temperature, the thermal and irradiation induced effects are treated as sequential events. This is done because thermal relaxation rises to maximum levels very quickly and essentially stays at this level independent of further time exposure at temperature. Irradiation induced effects however become sensibly evident long afterwards, and generally increase at a much slower rate. To explain the relaxation expressions presented in Table B.1, consider the following argument. For brevity suppose that constant total strain tests for material "i" show a drop in stress level from an initial value, σ_{i0}, to a value, σ_{i1}, as a consequence of thermal relaxation effects. Then, under the influence of neutron irradiation, suppose a further drop in stress takes place to the value σ_{i2}. Since the relaxation factor is defined as the ratio of the drop in stress to the initial stress, the relaxation factors for these sequential events are expressed,

$$R_{i1} = \frac{\sigma_{i0} - \sigma_{i1}}{\sigma_{i0}} \text{ and } R_{i2} = \frac{\sigma_{i1} - \sigma_{i2}}{\sigma_{i1}} .$$

Accordingly, the gross relaxation factor defining the final condition to the initial condition must be expressed,

$$R_i = \frac{\sigma_{i0} - \sigma_{i2}}{\sigma_{i0}} .$$

From Section II.A.3 it is seen that the parameter $(1-R_i)$ is needed for each material region in the bolted joint. This is determined in a straightforward fashion by noting that

$$(1-R_i) = \frac{\sigma_{i2}}{\sigma_{i0}} \quad ,$$

$$(1-R_{i1}) = \frac{\sigma_{i1}}{\sigma_{i0}} \quad ,$$

and

$$(1-R_{i2}) = \frac{\sigma_{i2}}{\sigma_{i1}} \quad ,$$

so that the desired quantity is computed from the values R_{i1} and R_{i2}, determined from relaxation test results, using the following equality:

$$(1-R_i) = (1-R_{i1})\,(1-R_{i2}) \quad .$$

The results of this computation are listed in Table B.1. Also shown in this table is the quotient which represents the composite effect of the relaxation for all materials present in the bolted joint, namely

$$(1-\overline{R}) = \frac{\sum \frac{(1-R_i)}{K_i}}{\sum \frac{1}{K_i}} \quad ,$$

which is needed for the computations indicated in Equations (27) and (28).

In Table B.2 the initial preloads are determined by using the applicable maximum and minimum assembly coefficients (Table 1). Employing the calculated stiffnesses, thermal expansion sums, and the overall relaxation multiplier, a sequence of forces (preload, total bolt force, and separation load) and stresses are computed. These results reveal the critical performance conditions for the bolted joint (highest bolt stresses on one hand and closest proximity to joint separation on the other). This table portrays a specific sequence of events common to many bolted joints in service: cold assembly, heatup, relaxation at hot operating conditions, and cooldown to assembly temperature after relaxation has occurred. As an aid in following Table B.2, the source (table or equation numbers) for each entry or computation is given.

Tables B.1 and B.2 should be viewed as something more than just an illustration to display the major results of this analysis. It is true that if entries in these tables are carefully examined, the intended objective of this example calculation shall have been fulfilled. But these tables mean more. They contain an orderly listing of preliminary information and provide, in addition, an efficient calculational sequence for the performance of joint analyses. The organization of information in these tables has evolved from numerous joint evaluations, and it is recommended as a practical aid for the analyst. Model work sheets based on the formats of Tables B.1 and B.2 can be found immediately before the back cover of this document. They are suitable for making duplicate forms which can be used in engineering analyses of bolted joint designs.

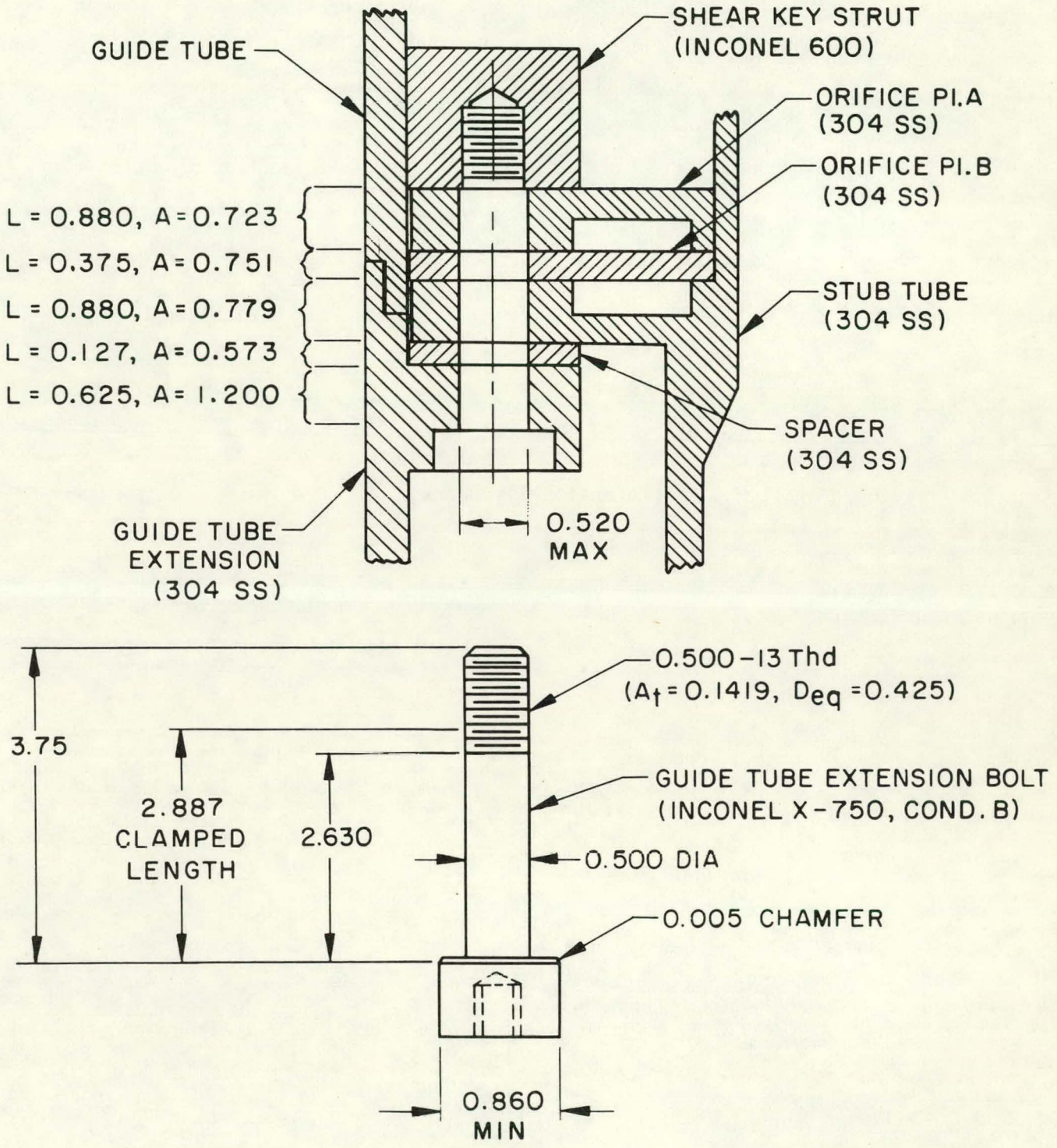

Figure B.1. Guide Tube Extension Joint

(Intentionally Blank)

Table B.1. Stiffness Calculation Work Sheet

Member Material	GT Ext 304 SS	Spacer 304 SS	Stub Tube 304 SS	Orif. B 304 SS	Orif. A 304 SS	Shank I-X750	Thread I-X750
A (D_h)*	1.20	0.573	0.779	0.751	0.723	0.1964	0.1419
(D_n)*	-	-	-	-	-	-	-
(D_n/D_h)*		-	-	-	-	-	-
L (L/D_h) or $2L/D_h$)*	0.625	0.127	0.880	0.375	0.880	2.63	0.540**
(β^o, cone angle)*	-	-	-	-	-	-	-
(ρ from TM-1105)*	-	-	-	-	-	-	-
A/L	1.92	4.51	0.885	2.00	0.822	7.47×10^{-2}	2.63×10^{-1}
t_c	70°F →						→
E_c	28.3×10^6 →				→	31.0×10^6	→
$K_c = E_1 A/L$ ($=E_1 D_h \rho$)*	5.43×10^7	1.28×10^8	2.50×10^7	5.66×10^7	2.33×10^7	2.31×10^6	8.15×10^6
$1/K_c$	18.4×10^{-9}	7.83×10^{-9}	39.9×10^{-9}	17.7×10^{-9}	43.0×10^{-9}	4.32×10^{-7}	1.23×10^{-7}
$\bar{\alpha}_c$	8.7×10^{-6} →				→	7.2×10^{-6}	→
$\underline{\alpha}_c$	5.44×10^{-6}	1.10×10^{-6}	7.66×10^{-6}	3.26×10^{-6}	7.66×10^{-6}	18.9×10^{-6}	1.85×10^{-6}†
Region Totals: $\Sigma \underline{1}/K_c$	0.126×10^{-6}					0.555×10^{-6}	
$\Sigma \underline{\alpha}_c L$	2.51×10^{-5}					2.08×10^{-5}	

Table B.1. (Cont)

Member Material	GT Ext 304 SS	Spacer 304 SS	Stub Tube 304 SS	Orif. B 304 SS	Orif. A 304 SS	Shank I-X750	Thread I-X750
t_h	535°F →						→
E_h	25.5×10^6 →				→	28.0×10^6	→
$K_h = E_2 A/L$ $(E_2 D_h \rho)$*	4.90×10^7	1.15×10^8	2.26×10^7	5.10×10^7	2.10×10^7	2.09×10^6	7.36×10^6
$1/K_h$	20.4×10^{-9}	8.70×10^{-9}	44.3×10^{-9}	19.6×10^{-9}	47.7×10^{-9}	4.78×10^{-7}	1.36×10^{-7}
$\bar{\alpha}_h$	9.6×10^{-6} →				→	7.7×10^{-6}	→
$\bar{\alpha}_h L$	6.00×10^{-6}	1.22×10^{-6}	8.45×10^{-6}	3.60×10^{-6}	8.45×10^{-6}	20.3×10^{-6}	1.98×10^{-6}†
Region Totals: $\Sigma\ 1/K_h$	0.141×10^{-6}					0.614×10^{-6}	
$\Sigma\ \bar{\alpha}_h L$	2.77×10^{-5}					2.23×10^{-5}	
$(1-R) = (1-R_{th})(1-R_{irrad.})$	0.51 →				→	0.80	→
$(1-R)/K_h$	1.00×10^{-8}	4.26×10^{-9}	2.17×10^{-8}	9.60×10^{-9}	2.34×10^{-8}	9.57×10^{-8}	2.72×10^{-8}
$(1-\bar{R}) = \frac{\Sigma\ (1-R)/K_h}{\Sigma\ 1/K_h}$	0.75						

*Items in parentheses used if joint stiffness computed by methods of TM-1105 (Reference a) or equivalent.

**0.257 + 2/3 D_{ec} = 0.540; increased length to estimate thread flexibility.

†Based on length of 0.257 only.

Table B.2. Bolt Load Calculation Sheet

Operational Condition	Item	Source (Definition or Equation)	Minimum Preload	Maximum Preload
	T(lb-in) or P_o(lb)	-	278.	314.
	C or M	-	0.175	0.075
	D_m(in) or θ(deg.)	-	0.50	0.50
	t_c(°F)	-	70°	70°
Cold Condition	P_c(lb)	Eq. (30) or (37)	3180.	8370.
No Relaxation	W(lb)	-	-	-
	F_b(lb)	Eq. (19) or (16)	-	-
	T_r(lb-in)	-	139.	157.
	$\bar{S}$(psi)	Eq. (A7)	-	-
	$[1/K_b + 1/K_j]_c$	Table B.1	0.681×10^{-6}	0.681×10^{-6}
	Δ_c	Eq. (21)	2.16×10^{-3}	5.70×10^{-3}
	$\delta_b = \Sigma \bar{\alpha}_b L_b$	Table B.1	2.23×10^{-5}	2.23×10^{-5}
	$\delta_j = \Sigma \alpha_j L_j$	Table B.1	2.77×10^{-5}	2.77×10^{-5}
	t_h(°F)	-	535°	535°
Hot Condition	$(t_h - t_c)$	-	465°	465°
	$(\delta_b - \delta_j)(t_h - t_c)$	-	-2.51×10^{-3}	-2.51×10^{-3}
No Relaxation	Δ_h	Eq. (24)	4.67×10^{-3}	8.21×10^{-3}
	$[1/K_b + 1/K_j)]_h$	Table B.1	0.755×10^{-6}	0.755×10^{-6}
	P_h (lb)	Eq. (21)	6190.	10,900.
	W(lb)	Design External Load	3400.	3400.
	F_b(lb)	Eq. (19) or (16)	6820.	11,500.
	T_r(lb-in)	(= E_h/E_c T_r cold)	126.	142.
	$\bar{S}$ (psi)	Eq. (A8), thread region, Deq. = 0.425	49,500.	82,100.

Table B.2. (Cont)

Operational Condition	Item	Source (Definition or Equation)	Minimum Preload	Maximum Preload
Hot Condition With Relaxation	$(1-\bar{R})$	Table B.1	0.75	0.75
	$P_{rh} = (1-\bar{R})P_h$	Eq. (28)	4640.	8180.
	W_{sep}	Eq. (13), (15)	5710.	10,100.
	Δ_{rh}	Eq. (21) or (27)	3.50×10^{-3}	6.16×10^{-3}
Cold Condition With Relaxation	Δ_{rc}	Eq. (24)	0.99×10^{-3}	3.65×10^{-3}
	P_{rc}	Eq. (21)	1450.	5360.
	W_{sep}	Eq. (13), (15)	1780.	6580.

Basic Relations:

$$P_c = \begin{cases} T/(C\ D_m) \\ \text{or} \\ P_c \div M\theta \end{cases} \qquad \Delta_h = \Delta_c - (\alpha_b - \alpha_j)(t_h - t_c)$$

$$\Delta_c = [1/K_b + 1/K_j]_c P_c \qquad P_h = \frac{\Delta_h}{[1/K_b + 1/K_j]_h}$$

APPENDIX C

CONSIDERATION OF AXIAL AND BENDING FLEXIBILITIES IN A COAXIAL JOINT

1. RELATIONS FOR ELASTIC INTERNAL FORCES AND MOMENTS

In Section II.A.1, the bolted joint relations were derived for a rather general bolted connection considering only the effects of linear axial flexibility. In this appendix the same model is considered with the additional complication that the three fundamental structural elements acting in the connection (the bolt and the two joint regions) possess bending as well as axial flexibility. As before, only a completely coaxial system is considered so that bending effects are totally uncoupled from axial effects. This is accomplished by assuming that axial effects are caused only by changes in length along the coaxial neutral axes of all bolted joint members, and that bending effects (flexure) cannot influence axial displacements because of the coaxiality restriction. However, related axial and rotational displacements (or forces and moments) may be introduced to this system from an external source (external loads or structures). An idealized mechanical model to portray this type of bolted joint appears in Figure C.1(a), which shows the bolt and joint members at nodes A and C separated for purposes of illustrative clarity. The flexibility for each region of the connection is indicated schematically by a coil spring with linear stiffness K, and a spiral spring with angular stiffness H. In the assembled (and fully seated) condition the axial and rotational displacements are continuous at each node, hence faces in contact develop the same axial motion and tilt at the contact points (see points A, B, and C in Figure C.1(a)). If the system is imagined in its disengaged state (in the sense that the restraining forces are removed and all elements are allowed to revert to an unloaded configuration), the bolt and joint elements may be viewed as shown in Figure C.1(b), which presents the linear and angular mismatches (Δ_ℓ and Δ_r) that exist between the bolt and joint members in the connection (see Section II.A.1 for definition of mismatch). Also shown in Figure C.1(b) are the bolt elongation and the bolt angle of flexure as point C' is brought to its loaded position, point C in Figure C.1(a). The extension and flexure angles for the bolt are indicated in Figure C.1(b) by the symbols δ_b and ϕ_b: they

represent the differences in the linear and rotational displacements respectively of the bolt extremities (points A and C'). In a similar fashion, the end point displacements of the joint regions are used to determine elongation and flexure angles for those members. The displacements of all node points are labeled in Figure C.1(c), the positive sense for each displacement being indicated by the arrows shown in the figure. The elongations and flexure angles are expressed in terms of these displacements as follows:

$$\left.\begin{aligned} \delta_b &= x_3 - x_0 & \phi_b &= \theta_3 - \theta_0 \\ \delta_{j1} &= x_1 - x_0 & \phi_{j1} &= \theta_1 - \theta_0 \\ \delta_{j2} &= x_2 - x_1 & \phi_{j2} &= \theta_2 - \theta_1 \end{aligned}\right\} \qquad \text{(C1)}$$

The forces, F, and moments, M, in the respective bolted joint elements arise as a consequence of the element elastic stiffnesses and their corresponding elongation and flexure angles, as expressed in the following relations.

1. Stiffness Relations

$$\left.\begin{aligned} F_b &= K_b\,\delta_b, & \delta_b &\geq 0; & M_b &= H_b\,\phi_b \\ F_{j1} &= K_{j1}\,\delta_{j1}, & \delta_{j1} &\leq 0; & M_{j1} &= H_{j1}\,\phi_{j1} \\ F_{j2} &= K_{j2}\,\delta_{j2}, & \delta_{j2} &\leq 0; & M_{j2} &= H_{j2}\,\phi_{j2} \end{aligned}\right\} \qquad \text{(C2)}$$

From Figure C.1(b), in order for the assembled joint to be in continuous contact, the cumulative joint compression and rotation at point C" must make up the deficit between the bolt motions and the respective linear and angular mismatches. This requirement leads to the following condition for compatible elongations and flexure angles in an unseparated joint.

2. Compatibility of Member Displacements

$$\delta_{j1} + \delta_{j2} = -(\Delta_\ell - \delta_b)$$

$$\phi_{j1} + \phi_{j2} = -(\Delta_r - \phi_b)$$

or

$$\left.\begin{aligned} \delta_b - \delta_{j1} - \delta_{j2} &= \Delta_\ell \\ \phi_b - \phi_{j1} - \phi_{j2} &= \Delta_r \end{aligned}\right\} \qquad \text{(C3)}$$

Lastly, for a connection that is in static equilibrium, the following results must be fulfilled at nodes A, B, and C in Figure C.1(a).

$$\Sigma F_A = F_1 + K_b (x_3 - x_0) + K_{j1} (x_1 - x_0) = 0$$

$$\Sigma M_A = M_1 + H_b (\theta_3 - \theta_0) + H_{j1} (\theta_1 - \theta_0) = 0$$

$$\Sigma F_B = F_2 - K_{j1} (x_1 - x_0) + K_{j2} (x_2 - x_1) = 0$$

$$\Sigma M_B = M_2 - H_{j1} (\theta_1 - \theta_0) + H_{j2} (\theta_2 - \theta_1) = 0$$

$$\Sigma F_c = F_3 - K_b (x_3 - x_0) - K_{j2} (x_2 - x_1) = 0$$

$$\Sigma M_c = M_3 - H_b (\theta_3 - \theta_0) - H_{j2} (\theta_2 - \theta_1) = 0 \quad .$$

Because the entire joint must also be in static equilibrium, the following additional relations involving the external forces and moments must also apply:

$$\left.\begin{aligned} F_1 + F_2 + F_3 &= 0 \\ M_1 + M_2 + M_3 &= 0 \end{aligned}\right\} \qquad \text{(C4)}$$

Hence, making use of the local elongations and flexure angles defined in Equations (C1), and replacing F_1 and M_1 by their equivalents per Equations (C4), the equations for the static equilibrium of forces and moments may be reduced to the following linearly independent set of equalities:

3. Static Equilibrium of Forces and Moments

$$\left.\begin{aligned} K_b \delta_b + K_{j2} \delta_{j2} &= F_3 \\ K_{j1} \delta_{j1} - K_{j2} \delta_{j2} &= F_2 \\ H_b \phi_b + H_{j2} \phi_{j2} &= M_3 \\ H_{j1} \phi_{j1} - H_{j2} \phi_{j2} &= M_2 \quad . \end{aligned}\right\} \qquad \text{(C5)}$$

The governing equations relating the system forces (or moments) to the system linear (or angular) displacements, Equations (C5), and the displacement compatibility equations, Equations (C3), may be expressed in matrix form as follows:

$$\left[\begin{array}{ccc|ccc} 1 & -1 & -1 & 0 & 0 & 0 \\ K_b & 0 & K_{j2} & 0 & 0 & 0 \\ 0 & K_{j1} & -K_{j2} & 0 & 0 & 0 \\ \hline 0 & 0 & 0 & 1 & -1 & -1 \\ 0 & 0 & 0 & H_b & 0 & H_{j2} \\ 0 & 0 & 0 & 0 & H_{j1} & -H_{j2} \end{array}\right] \left[\begin{array}{c} \delta_b \\ \delta_{j1} \\ \delta_{j2} \\ \phi_b \\ \phi_{j1} \\ \phi_{j2} \end{array}\right] = \left[\begin{array}{c} \Delta_\ell \\ F_3 \\ F_2 \\ \Delta_r \\ M_3 \\ M_2 \end{array}\right] . \qquad \text{(C6)}$$

The dashed line partitioning of the coefficient matrix in Equation (C6) clearly shows that axial and bending effects are uncoupled in this bolted joint model. If the bolted joint model did not contain a coaxiality requirement, then there would have to be some non-zero entries in the off-diagonal submatrices of Equation (C6) to reflect the additional complexity of coupled axial and bending effects. However, the current discussion pertains only to uncoupled axial and bending effects, and consequently only the system portrayed in Equation (C6) will be analyzed. Obtaining the member displacements in Equation (C6) under the assumed coaxiality restriction is relatively simple and follows identically the steps outlined in Section II.A.1, since only two algebraically identical sets of three equations in three unknowns need to be solved. This yields the following results upon substitution of the resulting forces and moments in Equations (C2).

$$
\left.
\begin{aligned}
F_b &= \frac{\left[\frac{1}{K_{j1}}\right] F_2 + \left[\frac{1}{K_{j1}} + \frac{1}{K_{j2}}\right] F_3 + \Delta_\ell}{\left[\frac{1}{K_b} + \frac{1}{K_1} + \frac{1}{K_{j2}}\right]}, \\
M_b &= \frac{\left[\frac{1}{H_{j1}}\right] M_2 + \left[\frac{1}{H_{j1}} + \frac{1}{H_{j2}}\right] M_3 + \Delta_r}{\left[\frac{1}{H_b} + \frac{1}{H_{j1}} + \frac{1}{H_{j2}}\right]} \\
F_{j1} &= \frac{\left[\frac{1}{K_b} + \frac{1}{K_{j2}}\right] F_2 + \left[\frac{1}{K_b}\right] F_3 - \Delta_\ell}{\left[\frac{1}{K_b} + \frac{1}{K_{j1}} + \frac{1}{K_{j2}}\right]}, \\
M_{j1} &= \frac{\left[\frac{1}{H_b} + \frac{1}{H_{j2}}\right] M_2 + \left[\frac{1}{H_b}\right] M_3 - \Delta_r}{\left[\frac{1}{H_b} + \frac{1}{H_{j1}} + \frac{1}{H_{j2}}\right]} \\
F_{j2} &= \frac{-\left[\frac{1}{K_{j1}}\right] F_2 + \left[\frac{1}{K_b}\right] F_3 - \Delta_\ell}{\left[\frac{1}{K_b} + \frac{1}{K_{j1}} + \frac{1}{K_{j2}}\right]}, \\
M_{j2} &= \frac{-\left[\frac{1}{H_{j1}}\right] M_2 + \left[\frac{1}{H_b}\right] M_3 - \Delta_r}{\left[\frac{1}{H_b} + \frac{1}{H_{j1}} + \frac{1}{H_{j2}}\right]}
\end{aligned}
\right\} \qquad \text{(C7)}
$$

From Equations (C7) it is noted that when the external forces and moments are not present, the bolt force becomes

$$
F_o = \frac{\Delta_\ell}{\left[\frac{1}{F_b} + \frac{1}{K_{j1}} + \frac{1}{K_{j2}}\right]}, \qquad \text{(C8)}
$$

which is identical to the system preload defined earlier (Section II, Equation (12)). In a similar vein the bolt moment becomes

$$
M_o = \frac{\Delta_r}{\left[\frac{1}{H_b} + \frac{1}{H_{j1}} + \frac{1}{H_{j2}}\right]}, \qquad \text{(C9)}
$$

which shall be called, for uniformity, the system premoment.

To further simplify the results presented in Equations (C7) the following stiffness ratios are defined:

$$r_1 = \frac{K_b}{K_{j1}} \ , \ r_2 = \frac{K_b}{K_{j2}} \ , \ \rho_1 = \frac{H_b}{H_{j1}} \ , \ \rho_2 = \frac{H_b}{H_{j2}} \ . \qquad \text{(C10)}$$

With Equations (C8), (C9), and (C10), the results presented in Equations (C7) may be more compactly expressed,

$$\left.\begin{aligned}
F_b &= F_o + \frac{r_1}{(1+r_1+r_2)} F_2 + \frac{(r_1+r_2)}{(1+r_1+r_2)} F_3 \\
F_{j1} &= -F_o + \frac{(1+r_2)}{(1+r_1+r_2)} F_2 + \frac{1}{(1+r_1+r_2)} F_3 \\
F_{j2} &= -F_o - \frac{r_1}{(1+r_1+r_2)} F_2 + \frac{1}{(1+r_1+r_2)} F_3 \\
M_b &= M_o + \frac{\rho_1}{(1+\rho_1+\rho_2)} M_2 + \frac{(\rho_1+\rho_2)}{(1+\rho_1+\rho_2)} M_3 \\
M_{j1} &= -M_o + \frac{(1+\rho_2)}{(1+\rho_1+\rho_2)} M_2 + \frac{1}{(1+\rho_1+\rho_2)} M_3 \\
M_{j2} &= -M_o - \frac{1}{(1+\rho_1+\rho_2)} M_2 + \frac{1}{(1+\rho_1+\rho_2)} M_3
\end{aligned}\right\} \qquad \text{(C11)}$$

which, it must be recalled, are applicable relations only if joint separation has not occurred.

For a bolted connection having axial and flexural member displacements, the term "joint separation" is taken to mean that the internal resisting force and moment have both become zero for some member in the connection. When this condition occurs it is clear that the unloaded member cannot transmit forces and moments to adjacent members (or external load sources).

For the joint model under consideration this can mean that F_b and M_b are zero (complete separation between bolt and joint), that F_{j1} and M_{j1} are zero (a joint interface completely separates and the bolt supports the external load), or that simultaneously F_b, F_{j1}, M_b, and M_{j1} are all zero (a joint region is squeezed by external joint loads to such an extent that both bolt and joint

interface contact is lost at the same time). To illustrate these concepts observe that when Equations (C11) is applicable, that is when the connection is in full and continuous contact, the equation for bolt force may be expressed in the form,

$$F_b - \frac{r_1}{(1+r_1+r_2)} F_2 - \frac{(r_1+r_2)}{(1+r_1+r_2)} F_3 = F_o \quad ,$$

which is perceived to represent a plane in a space represented by coordinates F_b, F_2, F_3. From the model shown in Figure C.1(a), it is also noted that when $F_{j1} = 0$, the bolt supports the axial loads F_2 and F_3 directly so that this condition can be expressed

$$F_b - F_2 - F_3 = 0$$

which also represents a plane in the aforementioned coordinate space. Lastly, when the loads reverse in such a fashion that they merely compress the joint elements, and the bolt becomes unloaded, this condition is expressed simply by $F_b = 0$, which again can be visualized as a plane in F_b, F_2, F_3 space. An illustration of these planes and their intersections in this coordinate system is presented in Figure C.2 for the purposes of clarifying this concept. It may be noted that the wedge-shaped plane portrayed in this figure represents the bolt load when no separation has taken place: the conditions for separation are portrayed in the oblique plane that corresponds to the conditions that $F_{j1} = 0$, and the horizontal plane corresponding to $F_b = 0$. The intersection line between the oblique and horizontal planes, outside of the wedge apex, represents the combination of loading forces F_2 and F_3 which result in joint separation from the squeezing of region "j2" in the joint.

Figure C.2 is consistent with the results presented earlier for the bolt in Figure 2. It will be seen that the characteristic shape of the curve in Figure 2 is the same as that shown by A-B-C-D and A'-B'-C'-D' in Figure C.2, where the point P (pierce-point in the wedge-shaped plane) is none other than the bolt preload, F_o.

The projection of line MN onto the F_2, F_3 coordinate plane, and line MK already lying in that plane, define a wedge-like region there. The combination of values F_2 and F_3 which plot as coordinate points within this region represent the condition of joint continuity (no separation). Conversely, those

combinations which plot as coordinate points outside the "wedge" represent the conditions for joint separation when only axial effects are present. This is illustrated in Figure C.3(a). Since the preceding development for linear effects could have been completely duplicated for bending effects (see Equations (C11)), it is concluded that a wedge region with similar implications could be derived for bending effects. If this is done, a portrayal of the type illustrated in Figure C.3(b) could be evolved. If the requirement is imposed that the numerical scale of the coordinates for both Figures C.3(a) and C.3(b) be made identical, it would then be meaningful to project one on the other to get Figure C.3(c). In this last figure the conditions for separation of the joint subjected to both effects simultaneously can be illustrated. For example, from this figure the shaded regions represent those combinations of either (F_2, F_3) or (M_2, M_3) which imply joint separation as previously defined. In addition, this figure also shows the combination of external forces and moments for which Equations (C11) are valid, namely the completely unlined region. This is the most practical form to portray the rather complex combination of external loading that defines whether or not separation in the elastic system of Figure C.1 occurs, and for which load combination Equations (C11) are valid.

2. APPLICATION TO THE LWBR GRID-TO-SUPPORT POST JOINT

A cut-away view of the LWBR grid-to-support post bolted joint appears in Figure C.4.(a), showing a member (grid connector foot) clamped in an eccentrically loaded joint. Due to this eccentricity the connector foot could rotate off its seat if the applied grid force is high enough, although the maximum rotation is limited by a spacer. To be conservative in the assessment of this joint, the maximum possible rotation of this member was assumed. This rotation was represented in the joint analysis by the addition of a hinge element to the standard model of Figure C.1, as shown in Figure C.4.(b).

Although this hinge element causes a coupling between axial and rotational effects, this coupling can be expressed by a simple relation for Δ_ℓ in terms of Δ_r, which could be treated as an additional constraint (on these parameters) without reformulating Equation (C6). To derive this relation, the effect of the hinge opening angle on bending rotations of the joint elements was analyzed. This analysis can be described using the sketches shown in Figure C.5. Greatly exaggerated for purposes of graphic illustration, Figure C.5.(a) shows the displacement of the system as the hinge element is opened. With the long

solid-line element in the figure portraying the bolt, the bending rotation, ϕ_b, accumulated over the length of the bolt, is given by the angular difference in tangents from the bolt extremities. By lines drawn perpendicular to these tangent lines through the hinge opening (lines EG and FG in Figure C.5.(a)), it is also reasoned that the interior angle EGF must be equal to ϕ_b. To consider the hinge in greater detail, an enlarged view of the hinge is shown in Figure C.5.(b). In this view a line is drawn through EF, and a perpendicular to this line is drawn through point G. The two right triangles thus formed have apex angles α_1 and α_2, the sum of which is ϕ_b. By comparison of Figure C.5.(a) and Figure C.5.(b), it is perceived that the relative rotation of the joint members from A to F and E to B are ϕ_{j1} and ϕ_{j2} respectively, and they are as indicated in Figure C.5.(b). Since the dashed line terminating at point E is given to be parallel to BD, it must also be perpendicular to EG. By a similar argument the dashed line terminating at point F is perpendicular to line FG. Hence angles ϕ_{j1} and ϕ_{j2} are seen to be equal to angles CEG and CFG respectively. Summing the angles (measured in radians) of triangle CEF one obtains,

$$\phi_c + \left[\phi_{j1} + \frac{\pi}{2} - \alpha_1\right] + \left[\phi_{j2} + \frac{\pi}{2} - \alpha_2\right] = \pi$$

or

$$\phi_c + \phi_{j1} + \phi_{j2} - (\alpha_1 + \alpha_2) = 0 \quad .$$

But since

$$\phi_b = \alpha_1 + \alpha_2$$

the hinge angle, ϕ_c, is

$$\phi_c = \phi_b - \phi_{j1} - \phi_{j2}$$

which is also the definition for angular mismatch (Equation (C3)). Consequently, with ϕ_c expressed in radians,

$$\phi_c = \Delta_r \quad . \tag{C12}$$

From Figures C.4.(a) and C.4.(b) it is observed that the hinge opening force and moment cause a unique hinge angle (or system angular mismatch to be developed), provided that the foot rotation has not fully consumed the clearance, s. If the foot has moved through this clearance and the spacer has seated against the stop, the applied force and moment may be loading the stop in

addition to keeping the foot rotated. In this case the developed angular mismatch is not a function of the applied loads, instead it is a function of the clearance s, which for small displacements can be expressed,

$$\Delta_r = \phi_c = \frac{s}{q_2} \quad .$$

To obtain Δ_r for the case when the loaded connector foot has not fully rotated through the spacer clearance, take first the sum of moments about the hinge pivot point (Figure C.4.(b)) to get,

$$q_1 F_{j2} + M_{j2} = -q_2 F_2 - M_2 \quad .$$

By substituting for F_{j2} and M_{j2} from Equation (C7) one obtains

$$q_1 \frac{\left[-\frac{1}{K_{j1}} F_2 - \Delta_\ell\right]}{\sum \frac{1}{K_i}} + \frac{\left[-\frac{1}{H_{j1}} M_2 - \Delta_r\right]}{\sum \frac{1}{H_i}} = -q_2 F_2 - M_2 \quad ,$$

where (for this problem),

$$\sum \frac{1}{K_i} = \frac{1}{K_b} + \frac{1}{K_{j1}} + \frac{1}{K_{j2}} \quad , \quad \sum \frac{1}{H_i} = \frac{1}{H_b} + \frac{1}{H_{j1}} + \frac{1}{H_{j2}} \quad . \tag{C13}$$

But the mismatches Δ_ℓ and Δ_r are related since the hinge opening angle is numerically equal to the angular mismatch, thus from Figure C.4.(b)

$$\Delta_\ell = q_1 \Delta_r \tag{C14}$$

so that an expression only in terms of Δ_r can be obtained. Solving for Δ_r yields the desired equality, which is summarized as follows:

$$\left.\begin{aligned} \Delta_r &= \frac{\left[q_2 - q_1 \frac{\frac{1}{K_{j1}}}{\sum \frac{1}{K_i}}\right] F_2 + \left[1 - \frac{\frac{1}{H_{j1}}}{\sum \frac{1}{H_i}}\right] M_2}{\frac{q_1^2}{\sum \frac{1}{K_i}} + \frac{1}{\sum \frac{1}{H_i}}} \quad , \text{ no contact with stop} \\ \text{or} \\ \Delta_r &= \frac{s}{q_2} \quad , \text{ contact with stop.} \end{aligned}\right\} \tag{C15}$$

From calculations for this joint, it was estimated that the connector foot rotations could result in pivot point depressions varying from 0.0009 inch (min. preload) to 0.0013 inch (max. preload), and that the corner deformation for the spacer could result in an effective increase of the spacer gap by approximately 0.0008 inch. Since the maximum allowable clearance determined to be present after core assembly was 0.0042 inch, it was concluded that a connector foot could rotate through an effective clearance of 0.0059 inch (min. preload) to 0.0063 inch (max. preload).

The nature of the materials employed in this joint are such that stress relaxation (both thermal and radiation induced) can occur while the bolted joint is loaded. To derive the unique relaxation relations pertinent to this joint design, a definition of the geometric features of the pivot point were required. The idealized configuration, shown in Figure C.6, is assumed to define these features. In this figure the joint is presumed to possess a local indentation (permanent deformation) left by the corner of the connector foot* as it pivots at point C under the influence of the peak joint loads. Upon removal of the joint loads, the connector foot is shown in contact with a new pivot point, C', under the assumption that the internal bolt and joint forces dissipated in the course of material relaxation are insufficient to fully restore seating of the joint. The development of force and moment relations leading to this possible final result are outlined in the following steps.

a. Suppose the initial preload is F_o (no premoment is present) then by application of Equations (C8), (C9), and (C13),

$$\Delta_r = 0$$

$$\Delta_{\ell o} = F_o \sum \frac{1}{K_i} \quad . \tag{C16}$$

*In this application the foot was made of a harder material than the member on which it pivots.

b. Applying the external load, any plastic deformation at the pivot must lie in the range $0 \leq \delta_{pl} < \Delta_{\ell o}$, where hinge angle is ϕ_c in radians. Thus,

$$\Delta_r = \phi_c = \text{(See Equation (C12))}$$

$$\Delta_\ell = (\Delta_{\ell o} - \delta_{pl}) + q_1 \phi_c \quad . \tag{C17}$$

c. Stress relaxation occurs while the joint loads are acting. Using the form of Equation (27) for both linear and angular effects one obtains,

$$\Delta_{r,R} = \phi_c \frac{\sum \frac{(1-R_i)}{H_i}}{\sum \frac{1}{H_i}} \tag{C18}$$

$$\Delta_{\ell,R} = (\Delta_{\ell o} - \delta_{pl}) \frac{\sum \frac{(1-R_1)}{K_i}}{\sum \frac{1}{K_i}} + q_1 \phi_c \frac{\sum \frac{(1-R_1)}{H_i}}{\sum \frac{1}{H_i}} \quad . \tag{C19}$$

d. Upon subsequent removal of the joint loads assume* that a hinge angle equal to ϕ'_c is attained (Figure C.6), such that $\phi'_c < \phi_c$. Then,

$$\Delta'_{r,R} = \phi_c \frac{\sum \frac{(1-R_i)}{H_i}}{\sum \frac{1}{H_i}} - (\phi_c - \phi'_c) \tag{C20}$$

$$\Delta'_{\ell,R} = (\Delta_{\ell o} - \delta_{pl}) \frac{\sum \frac{(1-R_i)}{K_i}}{\sum \frac{1}{K_i}} + q_1 \phi_c \frac{\sum \frac{(1-R_i)}{H_i}}{\sum \frac{1}{H_i}} - q_o(\phi_c - \phi'_c) \tag{C21}$$

where the final mismatches $\Delta'_{r,R}$ and $\Delta'_{\ell,R}$ may approach zero simultaneously or be oppositely signed due to unequal net effects in bending and extension.

---

*If $\phi'_c = \phi_c$ upon removal of joint loads, Equations (C20) and (C21) will still be valid, although the pivot point required in the derivation that follows will not be present.

e. Let the finally developed "preload" and "premoment" be F_o and M_o respectively. These loads act on the connector foot as shown in Figure C.6. With external joint loads absent the condition for static equilibrium requires that

$$M_o + q_o F_o = 0^* \quad ,$$

where it is understood that $\phi'_c < \phi_c$. By applying the definition for M_o and F_o, these parameters are expressed,

$$M_o = \frac{\Delta'_{r,R}}{\sum \frac{1}{H_i}} \quad , \quad F_o = \frac{\Delta'_{\ell,R}}{\sum \frac{1}{K_i}} \quad .$$

Substituting $-q_o F_o$ for M_o in the premoment equation, and utilizing the expression for angular mismatch in Equation (C20), the reduced elastic range of the hinge is,

$$\phi_c - \phi'_c = \phi_c \frac{\sum \frac{(1-R_i)}{H_i}}{\sum \frac{1}{H_i}} + q_o F_o \sum \frac{1}{H_i}$$

Substitution of this expression, along with the above expression relating $\Delta'_{\ell,R}$ to F_o, into Equation (C21) leads to the equality,

$$F_o \sum \frac{1}{K_i} = (\Delta_{\ell o} - \delta_{pl}) \frac{\sum \frac{(1-R_i)}{K_i}}{\sum \frac{1}{K_i}} + q_1 \phi_c \frac{\sum \frac{(1-R_i)}{H_i}}{\sum \frac{1}{H_i}}$$

$$- q_o \phi_c \frac{\sum \frac{(1-R_i)}{H_i}}{\sum \frac{1}{H_i}} - q_o^2 F_o \sum \frac{1}{H_i} \quad .$$

---

*If this assumption does not apply, that is if $\phi'_c = \phi_c$, then the joint seats flat, $M_o = 0$, and the force F_o is in equilibrium with the net force produced by the resisting contact pressure acting at the joint interface.

Solving for F_o, this yields

$$F_o = \frac{(\Delta_{\ell o} - \delta_{p1}) \dfrac{\sum \frac{(1-R_i)}{K_i}}{\sum \frac{1}{K_i}} + (q_1 - q_o)\,\phi_c \dfrac{\sum \frac{(1-R_i)}{H_i}}{\sum \frac{1}{H_i}}}{\sum \frac{1}{K_i} + q_o^2 \sum \frac{1}{H_i}} \quad .$$

Having thus established the magnitude of the residual preload, F_o, the residual premoment, M_o, is computed as follows,

$$M_o = q_o F_o \quad . \tag{C23}$$

Utilizing the definition for angular mismatch, the final hinge angle is solved from Equation (C20), which yields the following result:

$$\phi_c' = \phi_c \left[1 - \frac{\sum \frac{(1 R_i)}{H_i}}{\sum \frac{1}{H_i}} \right] + M_o \sum \frac{1}{H_i} \quad . \tag{C24}$$

The parameters in Equations (C22) and (C23) are as defined in Equations (C15), (C16), (C17) and Figure C.6. It should be noted that the quantity, q_o, in Figure C.6 is determined by δ_{p1}, q_1, and ϕ_c in accordance with the following relation:

$$q_o = q_1 - \frac{\delta_{p1}}{\tan \phi_c} \approx q_1 - \frac{\delta_{p1}}{\phi_c} \quad . \tag{C25}$$

In the preceding paragraphs all the individual features of interest in this joint analysis have been discussed, and derivations of important results have been provided where needed. Putting all these results together, the analysis performed for this joint will be briefly described.

Using the relations presented in Figure C.7, the axial and rotational stiffness of the bolt and joint members were computed at room and design operating temperatures. A conservative range of assembly coefficients were then selected from the test results obtained for this bolted joint (as presented in Section III). Given that an assembly torque of 13.5 lb-in is attained, the maximum and minimum preloads were calculated for the joint at the assembly temperature. With the computed bolt and joint stiffnesses, the system flexibility was

determined and the liner mismatches corresponding to the range of preloads were computed. Assuming the residual torque to be one half the applied value (see Section II.B.2.c.), an assessment of the stresses and stress intensities was made. A summary of calculated results is shown in Table C.1 for the grid-to-support post joint illustrated in Figure C.4.

To account for the consequence of elevating joint temperature to the design condition, and the consequences produced by hinge loading and "end-of-life" stress relaxation, the following general procedure was employed. Considering the chronological order in which events and effects were expected to develop, the analysis started with the effect of the temperature change. From the determination of material thermal expansion, the correct mismatches at operating temperature were computed along with the corresponding adjusted preloads. Using the available geometric information about the system configuration and the magnitude of the external hinge loads, the appropriate angular and linear mismatches were computed for the joint under load. From these mismatches, the moments and forces acting at critical regions in the bolted joint were determined. Since these were computed prior to relaxation of the joint, the stresses calculated from this loading represented the highest joint stresses. These stresses were required to satisfy the allowable design limits.

The next phase was consideration of the various effects of stress relaxation. Here the minimum load aspect of the analysis was generally the most meaningful in answering whether or not joint tightness had become questionable because of preload loss. In the type of joint considered in this appendix, particular attention was paid to the relaxation developed under load, since excessive loss in elastic mismatch can cause the joint to become loose when the external loads are removed.

The two calculational phases just discussed for the grid-to-support post bolted joint are summarized in Table C.2. These calculations show an interesting result. Comparing Items 4 and 5 in the tabulated summary, it is seen for the "minimum load" part of the analysis that a drop in preload occurs when the external loads on the hinge are removed, which is to be expected. Hence, upon removal of the hinge loads, the connector foot pivots out of the indentation since it will seek the lower preload state. But, as shown in the table, the value of ϕ_c' is greater than zero, therefore the joint will not fully reseat.

For the "maximum load" part of the analysis the reverse situation exists. Here a greater load is indicated when the connector foot tends to pivot out of the indentation. (Note that a negative value is computed for the q_0 dimension of the indentation. See Item 3 in Table C.2.) Since the elastic system will seek its lowest load state upon removal of the hinge loads, movement will not occur and the connector foot will remain fully "cocked" into the indentation.

The preceding results show the necessity for carefully conducting the analysis of a complex joint since many elastic and plastic effects may be operative, and the order in which they occur, sequentially or simultaneously, can be quite important in the final result. (Consider the unloaded hinge state portrayed in Item 6 of Table C.2, for which no "cocking" of the connector foot is implied, yet comparable "end-of-life" preloads are developed.)

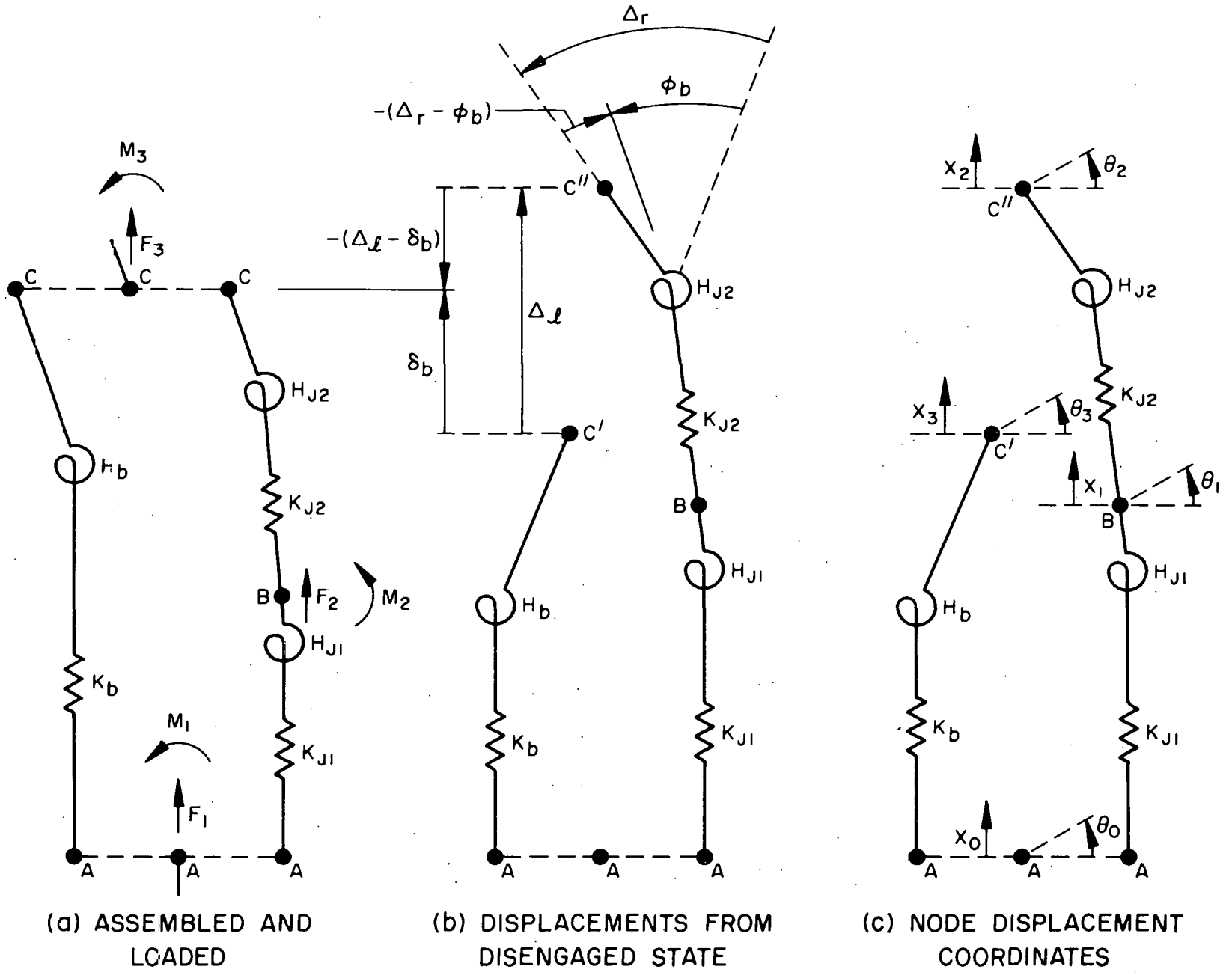

Figure C.1. Generalization of a Coaxial Joint with Axial and Bending Flexibilities (Three Nodes with Two Degrees of Freedom per Node)

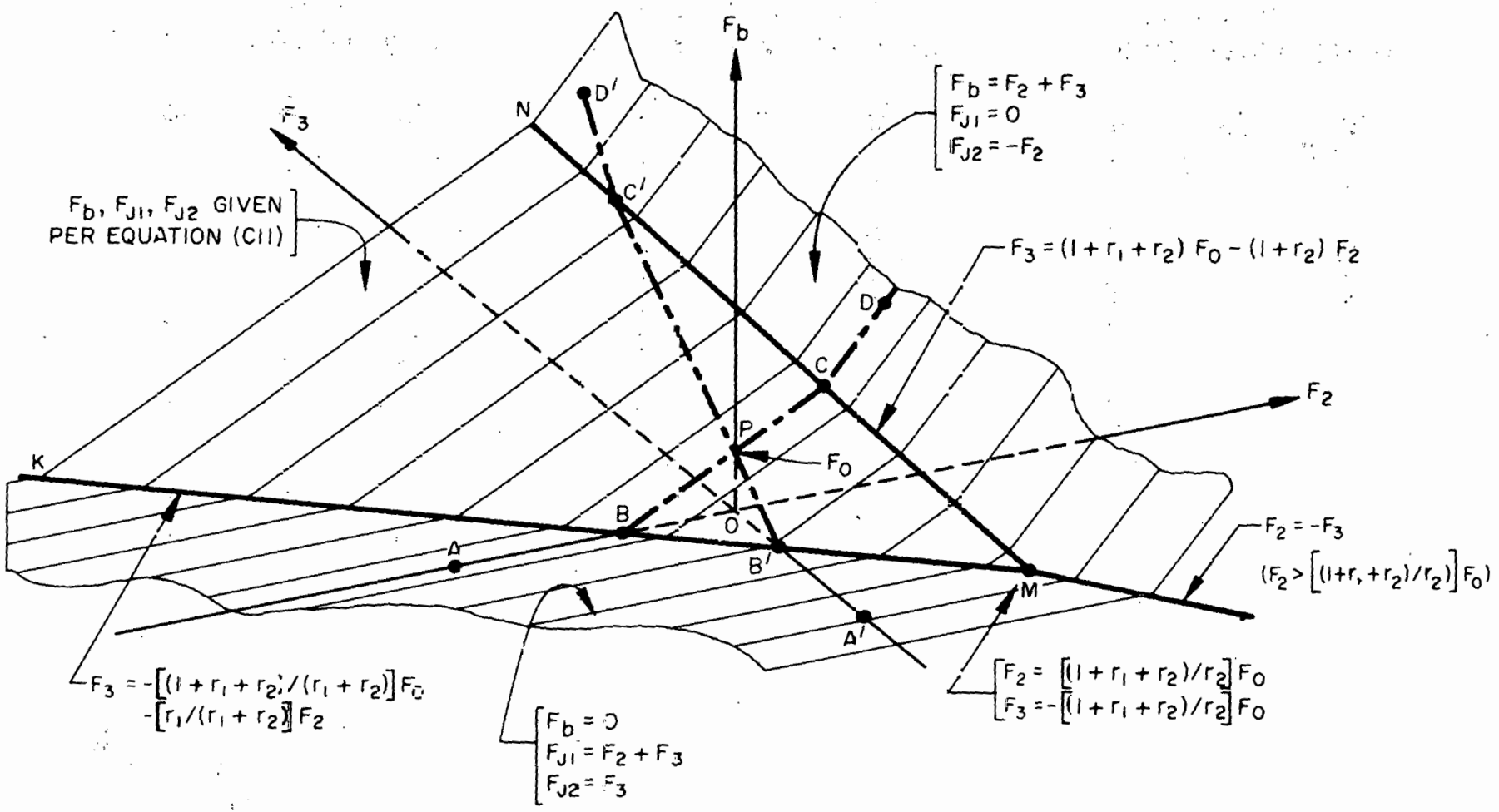

Figure C.2. Sufaces Defining Axial Bolt Force as a Function of External Forces F_2 and F_3

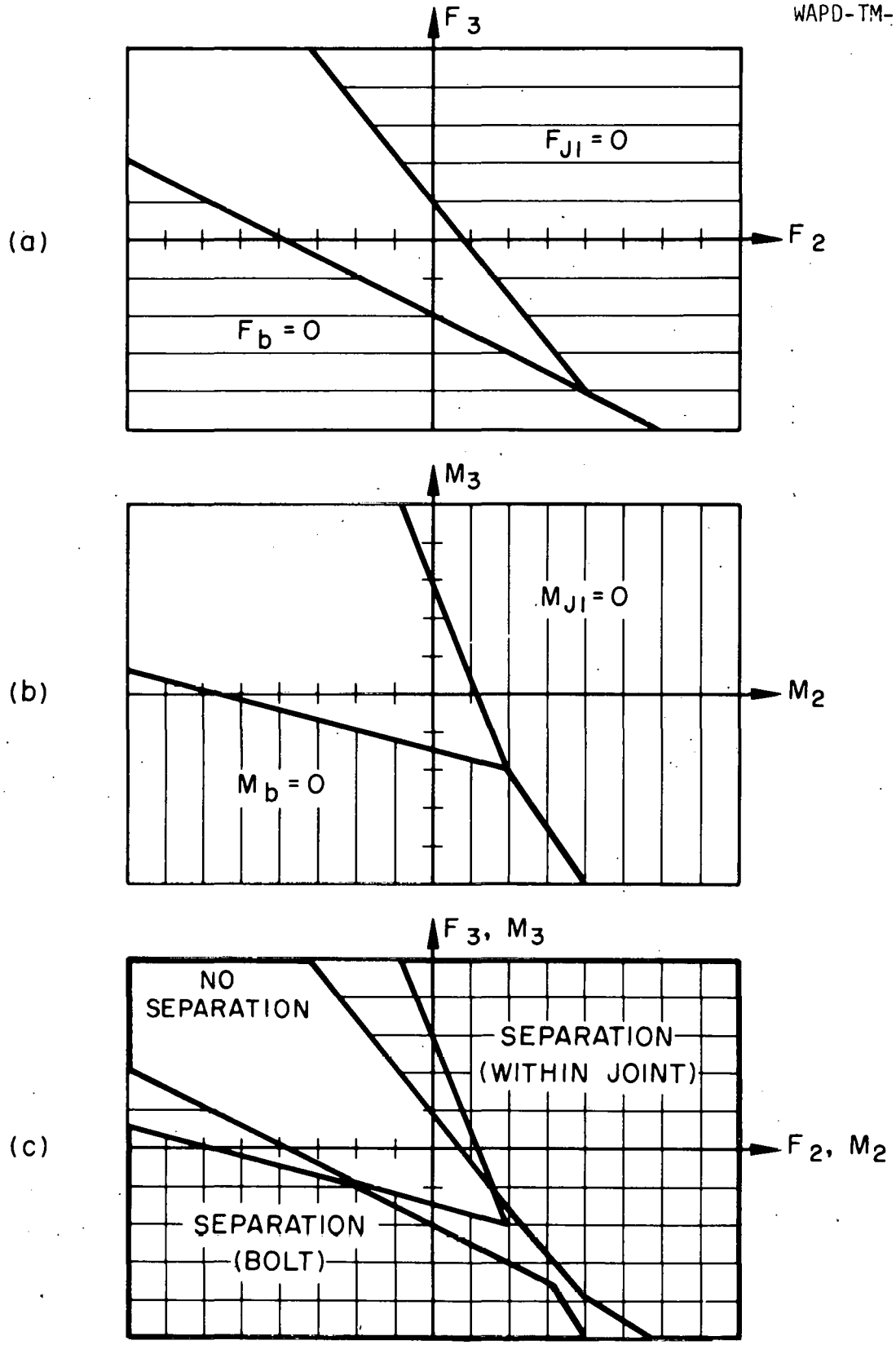

Figure C.3. Bolted Joint Separation Zones

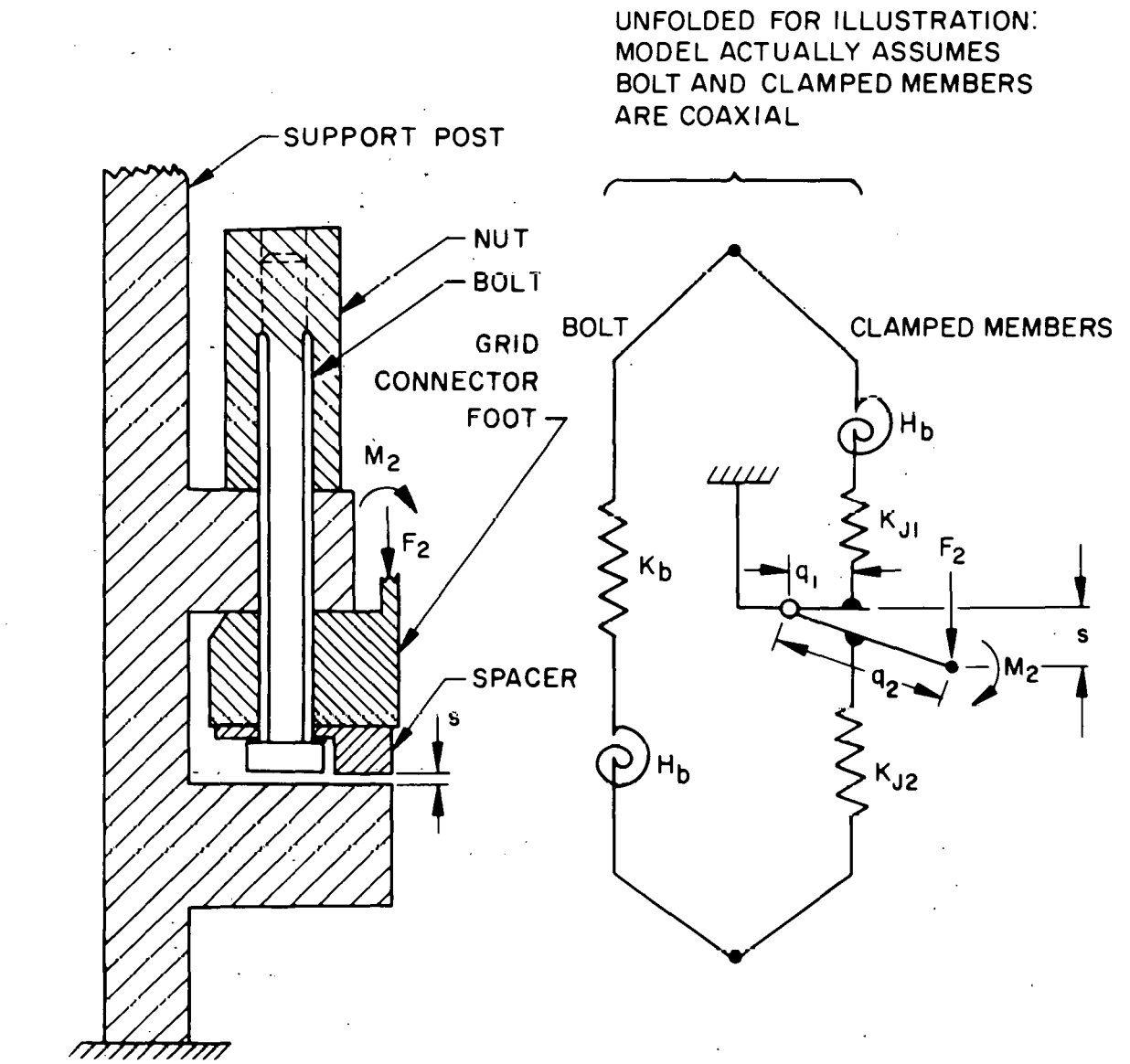

(a) PHYSICAL ILLUSTRATION JOINT
(ROTATION NOT SHOWN)

(b) ANALYTICAL IDEALIZATION
(INDICATING ROTATION FROM LOAD)

Figure C.4. Idealization of Blanket Grid Joint

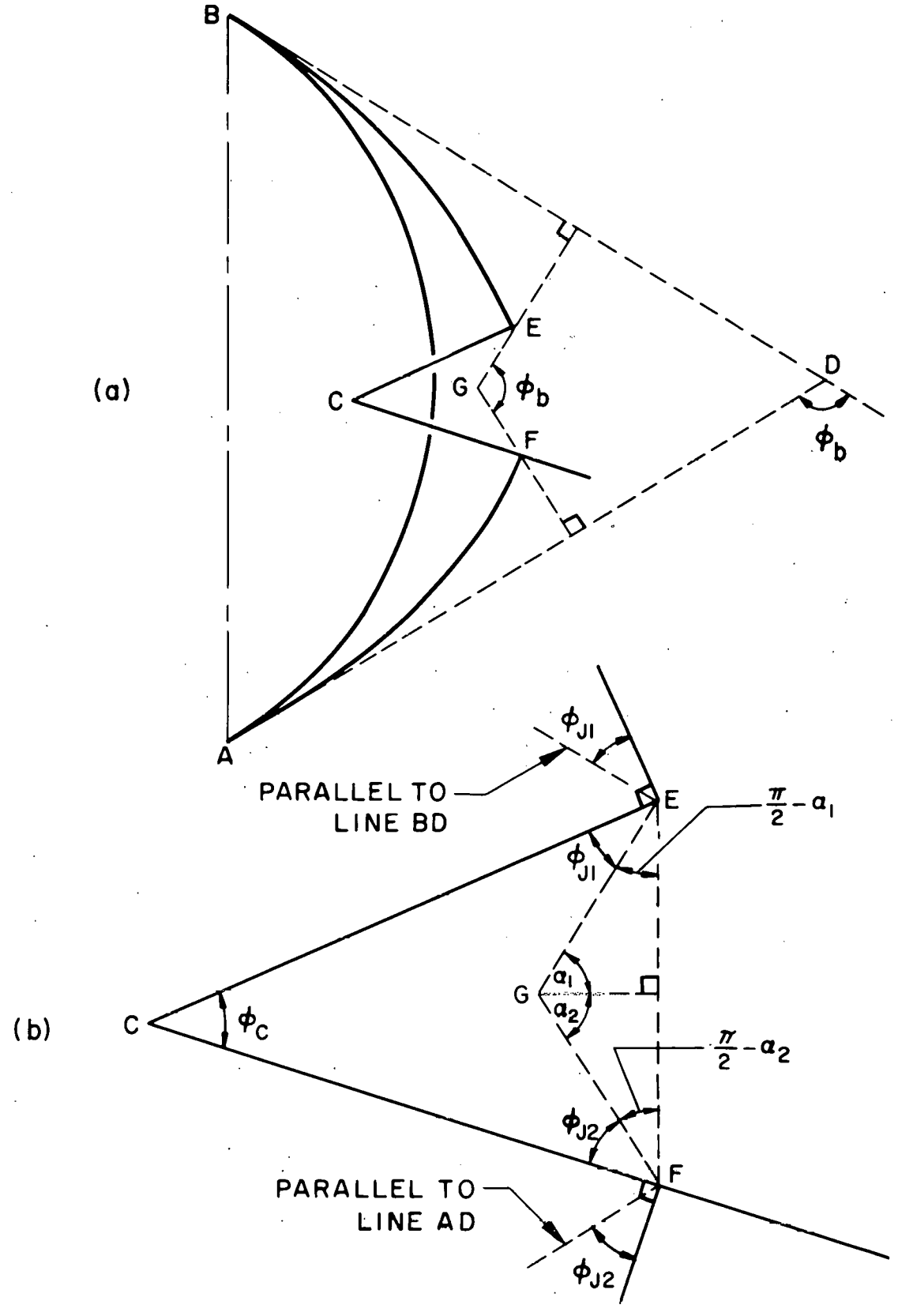

Figure C.5. Relation Between Hinge Angle and Flexural Rotation of Bolted Joint Elements

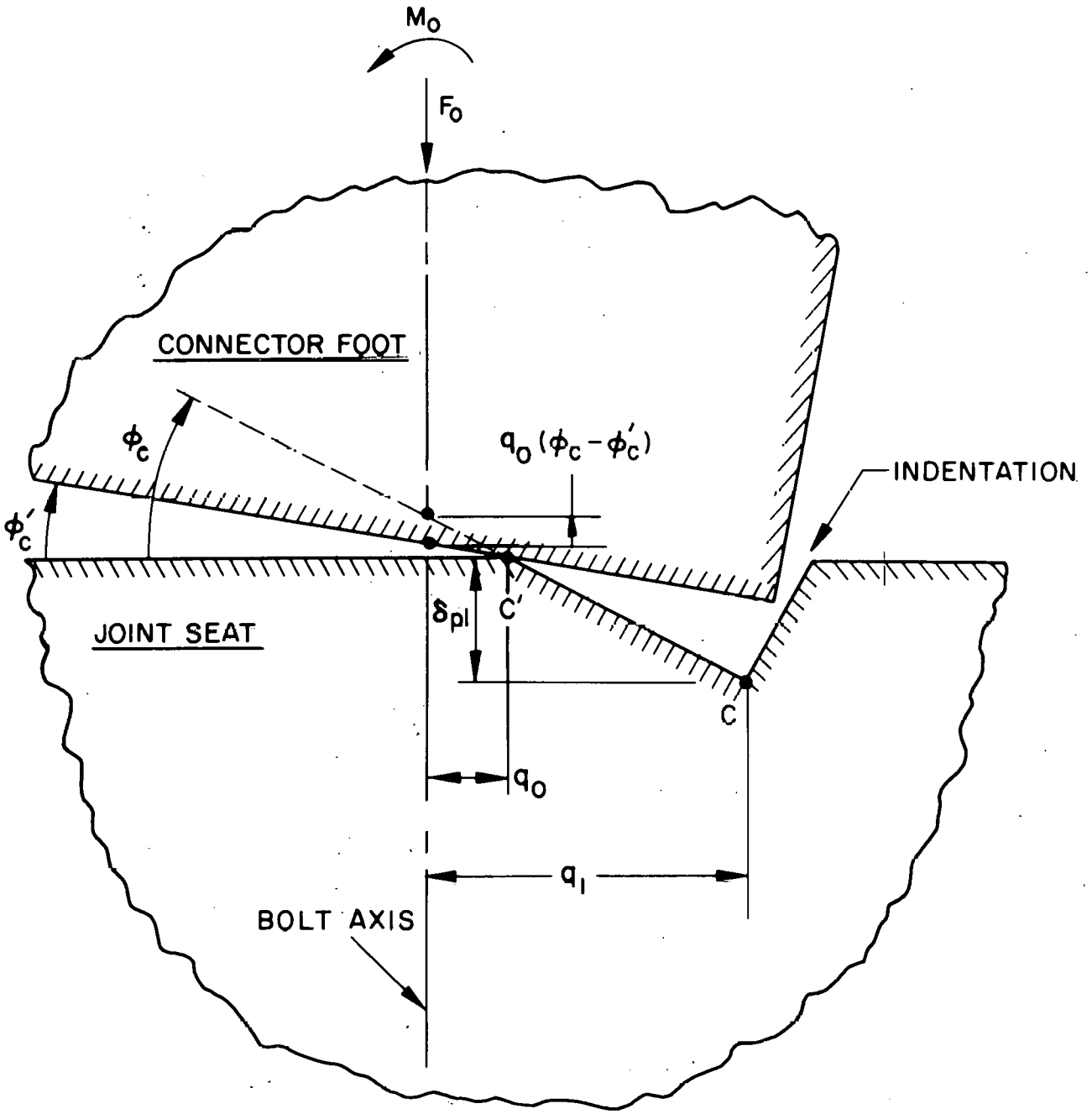

Figure C.6. Pivot Point Detail

AXIAL EFFECTS

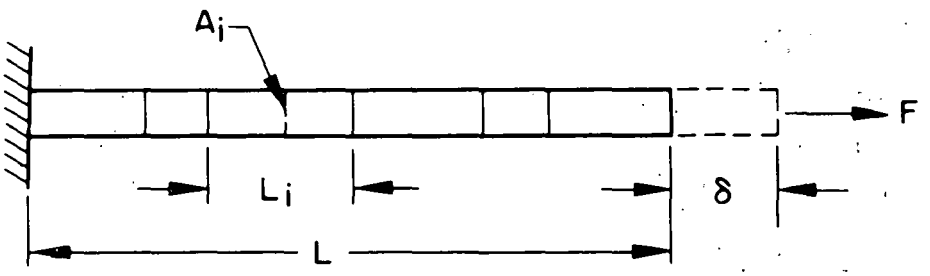

$$L = \sum_{i=1}^{N} L_i \quad ; \text{ N SEGMENTS}$$

$$\frac{1}{K} = \sum_{i=1}^{N} \frac{L_i}{EA_i} \quad ; A_i \text{ IS CROSS-SECTIONAL AREA}$$

$$F = K\delta$$

ROTATIONAL EFFECTS

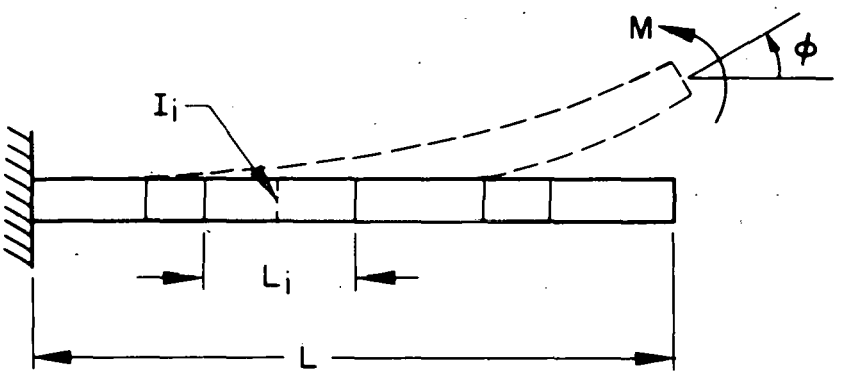

$$L = \sum_{i=1}^{N} L_i \quad ; \text{ N SEGMENTS}$$

$$\frac{1}{H} = \sum_{i=1}^{N} \frac{L_i}{EI_i} \quad ; \quad \begin{cases} \text{b} \square \text{h} & I_{rect} = \dfrac{bh^3}{12} \\ \bigcirc \text{D} & I_{cir} = \dfrac{\pi D^4}{64} \end{cases}$$

$$M = H\phi$$

Figure C.7. Useful Relations for Determining Elastic Flexibilities (or Stiffnesses)

Table C.1. Loads and Stresses at 70°F

	Minimum Load	Maximum Load
1. Joint Assembly		
Assembly Torque, T_{max} (lb-in)	13.5	13.5
Assembly Coef, C*	0.16	0.11
Preload, F_o (lb-in)	514.	748.
2. Linear Flexibility		
Σ $1/K_j$, Eq. (C13), (in/lb)	3.69×10^{-6}	3.69×10^{-6}
3. Initial Linear Mismatch		
$\Delta_{\ell o}$, Eq. (C8), (in)	1.90×10^{-3}	2.96×10^{-3}
4. Stresses at Min. Diam. (Shank)		
D min	--	0.120
Residual Torque, Tr (lb-in)	--	6.75
Membrane Stress, σ_m (psi)	--	66,100.
Torsional Shear Stress, τ (psi)	--	19,900.
Max. Stress Intensity, S_{max} (psi)	--	77,200.
Ave. Stress Intensity per Eq. (44), $\bar{S}$ (psi)	--	71,800.

*For illustrative purposes the values listed in Table 2 were used.

Table C.2 Loads and Stresses at 600°F

	Minimum Load	Maximum Load
1. Angular and Linear Flexibility		
$\Sigma\ 1/H_i$, Eq. (C13), (rad./lb-in)	2.44×10^{-3}	2.44×10^{-3}
$\Sigma\ (1-R_i)/H_i$, EOL Relaxation (rad./lb-in)	6.70×10^{-4}	6.70×10^{-4}
$\Sigma\ 1/K_i$, Eq. (C13), (in/lb)	4.26×10^{-6}	4.26×10^{-6}
$\Sigma\ (1-R_i)/K_i$, EOL Relaxation, (in/lb)	9.99×10^{-7}	9.99×10^{-7}
2. Initial Condition (no hinge load)		
Thermal Expansion: $(\ell_b - \ell_j)$ (600°-70°)	0.19×10^{-3}	0.19×10^{-3}
$\Delta_{\ell o}$, Eq. (24), (in)	1.71×10^{-3}	2.77×10^{-3}
F_o, Eq. (C8), (lb)	401.	650.
3. Hinge Loaded (No Relaxation)		
a. Loads and Mismatches		
q_1, Figure C.4(b), (in)	0.090	0.090
q_2, Figure C.4(b), (in)	0.470	0.470
Spacer Gap (in)	4.2×10^{-3}	4.2×10^{-3}
Spacer Deformation (in)	0.8×10^{-3}	0.8×10^{-3}
Pivot Deformation, δ_{p1} (in)	0.9×10^{-3}	1.3×10^{-3}
Effective Gap, s (in)	5.9×10^{-3}	6.3×10^{-3}
ϕ_c, Hinge Angle (rad.)	1.26×10^{-2}	1.34×10^{-2}
Δ_r, Eq. (C15) (rad.)	1.26×10^{-2}	1.34×10^{-2}
q_o, Eq. (C22) (in)	0.0186	-0.007
Δ, Eq. (C17) (in)	1.94×10^{-3}	2.68×10^{-3}
M_o, Eq. (C9) (lb-in)	5.16	5.49
F_o, Eq. (C8), (lb)	455.	629.
b. Stresses at Min. Diam. (Shank)		
D min	0.120	0.120
Residual Torque, Tr, (lb-in)	5.85	5.85
Membrane Stress, σ_M, (psi)	40,200.	55,600.
Max. Bend. Stress, σ_B, (psi)	30,400.	32,400.
Torsional Shear Stress, τ (psi)	17,200.	17,200.
Max. Stress Intens., S_{max} (psi)	78,500.	94,500.
Ave. Intens., Eq. (A8), $\bar{S}$ (psi)	46,900.	60,700.

Table C.2. (Cont)

	Minimum Load	Maximum Load
4. Hinge Loaded (EOL Relaxation)		
$\Delta_{r,R}$, Eq. (C18), (rad.)	3.46×10^{-3}	3.68×10^{-3}
$\Delta_{,R}$, Eq. (C19), (in)	5.01×10^{-4}	6.76×10^{-4}
M_o, Eq. (C9), (lb-in)	1.42	1.51
F_o, Eq. (C8), (lb)	118.	159.
5. Hinge Unloaded (EOL Relaxation)		
(Assumes pivoting at distance q_0 per Figure C.9. See values in 3.a of this table.)		
F_o, Eq. (C22), (lb)	85.6	160.2
M_o, Eq. (C23), (lb-in)	-1.59	1.12
ϕ_c, Eq. (C24), (rad.)	5.26×10^{-3}	1.25×10^{-2}
6. No Hinge Load Throughout Core Life (EOL Relaxation)		
Δ_ℓ, Eq. (27), (in)	4.01×10^{-4}	6.50×10^{-4}
F_o, Eq. (C8), (lb)	94.1	152.5

APPENDIX D

AN ENGINEERING ANALYSIS OF TIME INDEPENDENT PLASTIC DEFORMATION ON BOLT AND JOINT FORCES

Situations arise in some bolted joint applications where time independent material plasticity effects reduce the preload attainable from a given mismatch. For example, suppose an assembled bolt and joint fabricated of the same material are tightened to a very high preload and then heated. If all the deformation during assembly was elastic and remained that way during heatup, then there would be only a slight reduction in preload due to the change in elastic modulus. However, since the material yield strength can also change with temperature (usually at a faster rate than the elastic modulus) the elevated temperature preload, if plastic deformation takes place, could actually be lower than the value computed on a linear-elastic basis. This additional preload reduction is attributed to the lost "mismatch" (Section II.A.1) caused by the plastic deformation (Figure D.1). If several materials had been employed in this bolted joint, thermal expansion effects could also contribute to the plastic deformation that might occur (assuming the joint design had not been compensated for such effects). Thus, it is perceived that unless judicious design choices are made, plastic deformation can readily occur in bolted joints.

While most joints are designed to avoid plastic deformation for design operating loads and temperature ranges, it is conceivable that an assessment for the consequence of plastic deformation may be required for exceptional operating or accident conditions. To perform such assessments the following engineering analysis was developed.

Without presently defining the test or analysis required to generate appropriate force-displacement curves for the bolt and the composite joint, let it be supposed such curves have been obtained and are as illustrated in Figure D.2 (curve o-a-c for the bolt and o-a'-c' for the joint). As seen in this figure, both elastic and plastic responses for each region are portrayed, where K_b and K_j are the linear-elastic stiffness of the bolt and joint regions respectively.

Points i and i' in Figure D.2 represent the initial forces and displacements based on linear elastic calculations alone. Since these points are not on the respective curves they represent incompatible combinations of forces and

displacement. The objective is to find points on the curves which also satisfy both the static equilibrium of internal joint forces and the compatibility of joint displacements. Initially, let it be assumed that the points f and f' in Figure D.2 represent joint forces and displacements after plastic deformation has occurred. From Figure D.1 the final joint mismatch must be,

$$\Delta_f = \Delta_i - (\delta_{bp} - \delta_{jp}) \tag{D1}$$

where Δ_i is the initial mismatch corresponding to the totally elastic initial calculation, and Δ_f is the residual elastic mismatch after plastic deformation has taken place. From the definition of mismatch (Equation (3), Section II.A.1) it is seen in Figure D.2 that,

$$\Delta_f = (\delta_{bf} - \delta_{bp}) - (\delta_{jf} - \delta_{jp})$$

or

$$\Delta_f = (\delta_{bf} - \delta_{jf}) - (\delta_{bp} - \delta_{jp}) \tag{D2}$$

so that by substitution of Equation (D2) into Equation (D1) one obtains

$$\Delta_i = \delta_{bf} - \delta_{jf} \tag{D3}$$

which is the condition that must be satisfied after plastic deformation has taken place. From Figure D.2, as drawn, Equation (D3) has not been satisfied by the initial positions f and f'. Accordingly, adjustments must be made through calculational iterations until a valid combination of δ_{bf} and δ_{jf} are determined which satisfy Equation (D3) to some predetermined level of precision. An efficient calculational sequence to achieve this objective is as follows:

1. Choose some (reasonable) point f' that corresponds to the joint coordinates of a graph similar to Figure B.2, namely (δ_{jf}, F_{jf}).
2. Assuming the possibility of an external working load, W, acting under the bolt head with the joint and bolt still in contact, one obtains by application of Equation (10)*,

$$\Delta_f = -\left[\frac{1}{K_b} + \frac{1}{K_j}\right] F_{jf} + \frac{1}{K_b} W \quad .$$

*With the working force acting under the bolt head, there is no elastic Region j2. See Figure 1.

3. With this value of Δ_f, by applying Equation (9) to the joint under consideration the bolt force is given by

$$F_{bf} = \frac{\Delta_f + \frac{1}{K_j} W}{\left[\frac{1}{K_b} + \frac{1}{K_j}\right]} .$$

4. For this bolt force the point f is located on the bolt curve and δ_{bf} is read off. Subtracting the values δ_{jf} from Step 1, the following check is made:

$$(\delta_{bf} - \delta_{jf}) = \Delta_i .$$

If this equality is satisfied the procedure is stopped: if it is not satisfied another point f' is judiciously selected and the calculational sequence from Steps 1 through 4 is repeated.

Note that if the presence of a joint working force is not physically applicable during the plastic deformation process, then Steps 2 and 3 may be entirely omitted since

$$F_{jf} = -P_f \text{ and } F_{bf} = P_f$$

where P_f is the bolt preload, and hence the iteration process of Steps 1 and 4 may be performed directly on Figure B.2 without the need of calculations.

In the foregoing procedure, the availability of appropriate load-displacement curves were assumed without justification. In practice these would have to be obtained from an experiment. However, if stresses in the bolt and joint regions are uniformly distributed over individual region lengths, and stress/strain relations are available from both tension and compression tests, a valid load-displacement curve can sometimes be generated by calculational procedures alone. But sound judgment must be exercised in generating this curve, to assure that the experimental data supporting this curve are compatible with the manner and sequence of loading for the bolted joint being analyzed. For example, if a joint in its design application was plastically deformed during cold tightening and then underwent further plastic deformation upon heatup, a hot load material test without prior plastic deformation would lead to a

characteristic curve that might be inconsistent with the intended application. It would be prudent, in this case, to induce the expected initial cold plastic set before the hot load-displacement test is performed.

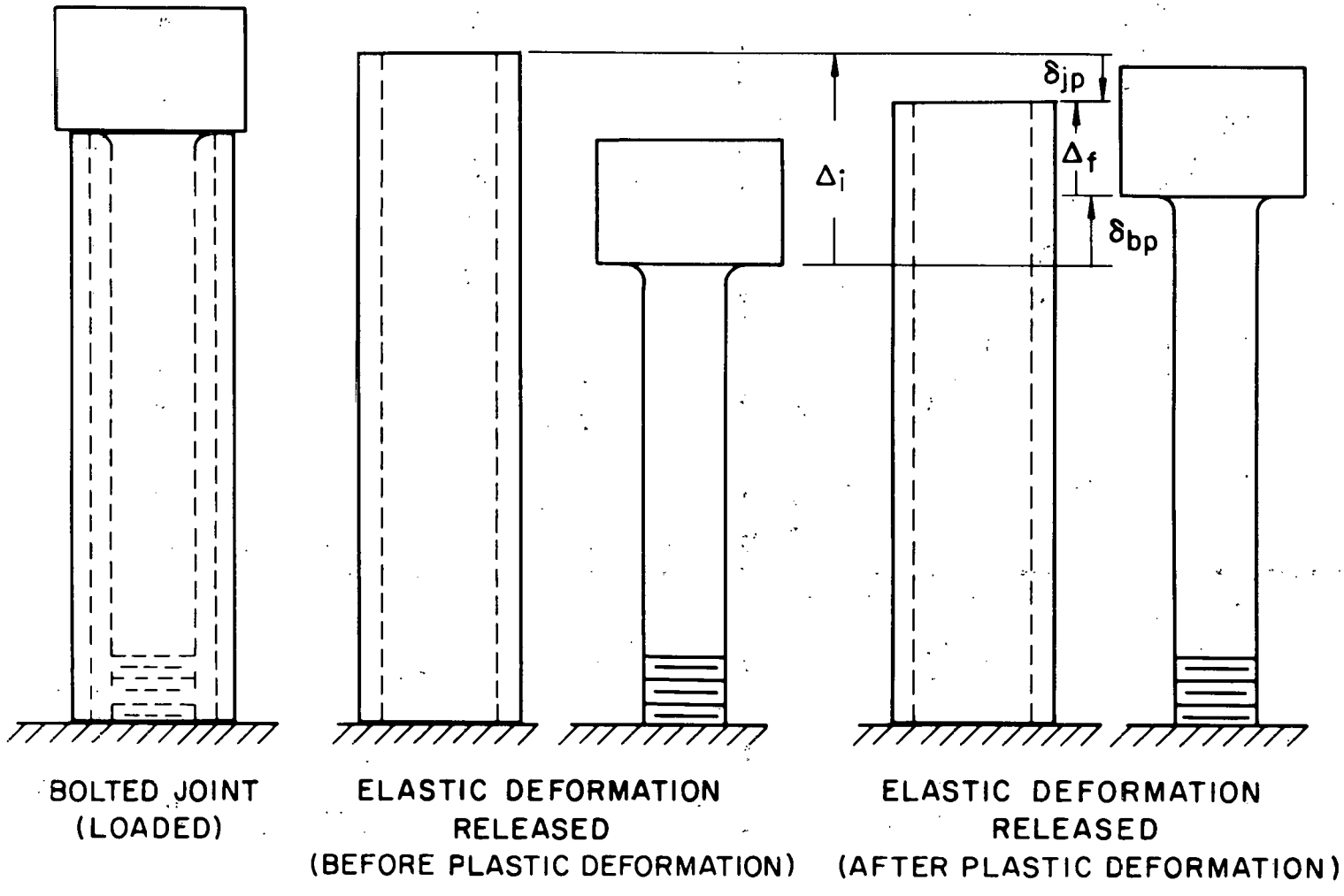

Figure D.1. Effect of Plastic Deformation on Elastic "Mismatch" - A Physical Illustration (Displacements Greatly Exaggerated)

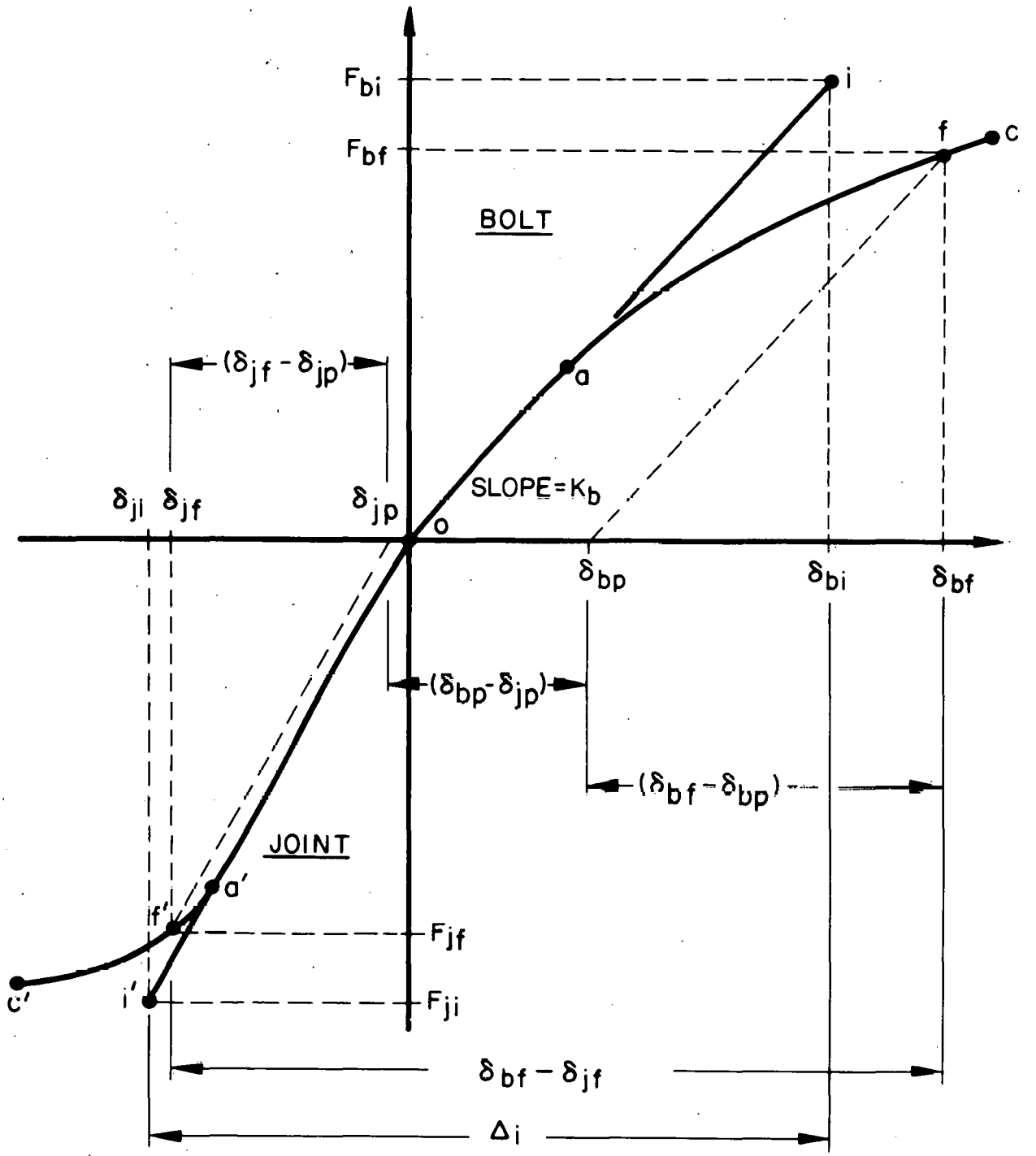

Figure D.2. Effect of Plastic Deformation on Elastic "Mismatch" - A Graphic Illustration

APPENDIX E

ASSESSING MATERIAL STRESS RELAXATION WHEN TOTAL STRAINS DO NOT REMAIN CONSTANT

In a standard stress relaxation test the specimen is elastically strained and held fixed in the test environment for an exposure time of interest. The test environment causes a fractional loss in elastic strain without changing the total strain distribution originally present. Thus a conversion of elastic to non-recoverable plastic strain occurs throughout the specimen, with a corresponding reduction in local stresses being the result.

A reduction in stresses may also develop in cases of material relaxation where the total strain distribution in the body is not held fixed, however this reduction cannot be directly deduced from a standard stress relaxation test. The purpose of this appendix is to provide a procedure for the computation of relaxation factors that are appropriate when the total strain varies during the relaxation period. Results obtained from a standard relaxation test are assumed to be available for the performance of this calculation. In the following derivation of this procedure, the integrated quantities of "force" and "displacement" shall be used in place of the corresponding local quantities of "stress" and "strain." This shall be done to relate the derived results to the specific interest of material relaxation in a bolted joint.

1. "Specific" Relaxation Factor: Defined and Derived

For a linear elastic body under uniaxial loading, the applied force and its consequent displacement are simply related by the equality,

$$F(z) = K\ \delta_e(z) \tag{E1}$$

where K represents the elastic stiffness of the body, $F(z)$ and $\delta_e(z)$ represent the force and displacement respectively, and z represents the independent variable for time or exposure level.

If plastic deformation occurs, the elastic displacement remaining in the direction of loading will be less than the total displacement of the body. This is expressed,

$$\delta_e(z) = \delta_t(z) - \delta_p(z) \tag{E2}$$

where $\delta_t(z)$ and $\delta_p(z)$ are the total displacement and "plastic displacement" respectively. When $z = 0$ it is assumed that $\delta_p(0) = 0$, hence $\delta_e(0) = \delta_t(0)$. Therefore the plastic displacement considered in this derivation is due solely to the elastic-to-plastic conversion process associated with stress relaxation. Further, since Equation (E1) is always applicable, the elastic restraining force is reduced along with the elastic displacement. This reduction, expressed in fractional form, is

$$\frac{F(z)}{F(0)} = \frac{\delta_t(z)}{\delta_t(0)} - \frac{\delta_p(z)}{\delta_t(0)} \tag{E3}$$

where the influence of the fractional plastic deformation is clearly displayed in the second term. For convenience, this term in Equation (E3) will be called the "specific" relaxation factor and shall be defined by the following equality:

$$\rho(z) = \frac{\delta_p(z)}{\delta_t(0)} \tag{E4}$$

The word "specific" is used here as a reminder that $\rho(z)$ is uniquely related to the functional form of $\delta_t(z)$. Thus this is a relaxation factor directly linked to the manner in which the total strain varies during the relaxation process. To establish this correspondence it shall be assumed that the rate of increase in plastic displacement is directly proportional to the elastic displacement present. Consequently,

$$\frac{d\,\delta_p(z)}{dz} = A\,\delta_e(z) \tag{E5}$$

where "A" is the rate controlling constant for the process. This particular relationship is both simple and physically plausible. While relationships of greater complexity may be experimentally more precise than Equation (E5), it is believed that Equation (E5) can provide a close approximation of the actual relaxation behavior experienced with a variety of materials under circumstances of practical interest.

Substituting Equation (E2) into Equation (E5), and normalizing all displacements by the initial total displacement, $\delta_t(0)$, the following governing differential equation for the specific relaxation factor is obtained:

$$\frac{d\ \rho(z)}{dz} + A\ \rho(z) = A\ \frac{\delta_t(z)}{\delta_t(0)} \tag{E6}$$

where $\rho(0) = 0$.

If the quantity "A" is assumed to be constant over the range of applicability of the variable, z, Equation (E6) becomes a linear differential equation with constant coefficients. Therefore, the general solution for $\rho(z)$ can either be expressed operationally (as in Laplace transforms) by,

$$\{\rho(z)\} = \frac{A}{(s+A)} \left\{ \frac{\delta_t(z)}{\delta_t(0)} \right\} \tag{E7}$$

where "s" is the differentiation operator and the braced expressions indicate transforms of functions. Equivalently, $\rho(z)$ can be expressed by the convolution integral,

$$\rho(z) = \int_0^z Ae^{-A(z-w)}\ \frac{\delta_t(w)}{\delta_t(0)}\ dw \quad , \tag{E8}$$

where w is the dummy variable used to carry out the integration. In both Equations (E7) and (E8) the form of the total displacement function is assumed to satisfy the usual analytic requirements for an integrable function.

A particularly simple, yet useful solution for $\rho(x)$ results from consideration of a standard relaxation test. As has been previously stated, the identifying character of this test is that the total displacement (or more precisely, total strain) remains constant.

Since the standard test has this unique feature, and is the type test that will usually be performed to establish the stress relaxation behavior of a material, another symbol shall be used for the relaxation factor obtained from this test. This factor and the corresponding fractional total strain function for the standard test are defined by the following:

$$\left.\begin{aligned} \rho(z) &= R(z) \\ \frac{\delta_t(z)}{\delta_t(0)} &= 1 \end{aligned}\right\} \qquad \text{Standard Test} \tag{E9}$$

Solving Equation (E7) (or (E8))for the specific total strain function presented in Equation (E9), one obtains,

$$R(z) = 1 - e^{-Az} \tag{E10}$$

For several other cases of common interest, the solution of Equation (E7) (or (E8)) has also been carried out. These solutions are based on general linear or exponential forms for the fractional total stain function, $\delta_t(z)/\delta_t(0)$ and they are summarized for reference in Table E.1. Figure E1 has been prepared to illustrate the nature of these solutions graphically.

2. Generalization of the Independent Variable, z

The preceding derivation was based on the independent variable, z, being a measure of "exposure". If this measure was simply time, then the rates previously discussed would be time rates. However nothing in the derivation presented necessarily limits one to this restricted interpretation. All that is really required is that the governing equation, Equation (E6), be valid for the exposure level, z, however that variable is defined.

To appreciate the significance of a more general interpretation of z than merely "time" (or something directly proportional to it) consider the type of material relaxation that can take place within a nuclear reactor. In this environment high fractional relaxation levels can be attained at relatively low stresses, in sharp contrast to thermally activated relaxation processes. The nuclear parameter that this form of relaxation appears to be a function of is the fast neutron fluence, which is defined as the "area" under a neutron flux vs. time curve over a time span of interest. The flux apparently responsible for this effect has been determined to be the total flux of neutrons with spectral energies in excess of 1.0 MEV (million electron volts). Because of the units that neutron fluxes are commonly expressed in, the quantity defined as a fluence is typically expressed in units of neutrons per square centimeter. Portrayals of experimentally determined fractional relaxation factors as a function of fluence have been approximated by many functional forms. One of these functions, which has been found to be particularly useful in empirically fitting relaxation data, is

$$R(F) = 1 - e^{-A\mathcal{F}^B} \tag{E11}$$

where the symbol $\mathcal{F}$ represents the fluence level and the parameters "A" and "B" are curve fitting constants. If the variable z is defined by the equality,

$$z = \mathcal{F}^B$$

Equation (E11) is perceived to be identical to Equation (E10). Thereby Equation (E6) may be regarded (if only approximately) as the supporting differential equation for the standard relaxation (constant total displacement) test. It is the premise of this presentation, for reasons discussed in the preceding section, that the differential equation developed in this manner will also be applicable to situations that allow the total displacement to vary during the relaxation process. In this way, a generalization of the physical significance of z has extended the scope of application for the relatively simple differential equation, Equation (E6).

From a mathematical point of view, the possibility of redefining z to be a function of a physical variable may be regarded as a "coordinate transformation" of the independent variable that dominates the relaxation process. The change of coordinate that is chosen is one that allows the governing differential equation to take on a simple form (e.g., Equation (E6)). It should be cautioned, however, that once a change is adopted, the total displacement function must also be expressed in terms of the redefined variable, z, to compute specific relaxation factors in accordance with Equations (E7) or (E8).

3. Outline for Computation of Specific Relaxation Factors

To compute the specific relaxation factors when the total displacement varies in a particular fashion during the elastic-to-plastic conversion process, the following procedure is recommended.

a. Obtain the best fit to a standard relaxation test with the general form given in Equation (E10). From this data fit assign a magnitude to the rate controlling parameter, A. Define z, noting that it could be expressed as a function of the independent test variable (see example discussed in Section 2).

b. Prepare a graph for fractional change in total displacement relative to the variable z. If desired, an analytical approximation to the graph may then be obtained for the functional form of $(\delta_t(z)/\delta_t(0))$.

c. Solve for the specific relaxation factor, $\rho(z)$, and evaluate factors for values of z which are of interest. Use Equations (E7) or (E8) as required to evaluate $\rho(z)$ by some convenient means, either analytically or graphically.

With the relaxation factors thus determined, load changes caused by the relaxation process can then be computed using Equation (E3), noting the definition of $\rho(z)$ in Equation (E4). Thus,

$$\frac{F(z)}{F(0)} = \frac{\delta_t(z)}{\delta_t(0)} - \rho(z)$$

4. Formulation For Stress Relaxation In Bolted Joints

Since a bolted connection consists of at least two regions (e.g., bolt region, joint region(s)), it is advantageous to modify the symbols used in the preceding sections in order to keep subscripts from becoming too cumbersome. The modifications shall be as follows: let the unprimed symbol, $\delta(z)$, represent the total (elastic + plastic) displacement in a region, and let the primed symbol, $\delta'(z)$, represent the residual elastic displacement in a region. Then Equation (E2) may be expressed in the following manner,

$$\delta'(z) = (\psi(z) - \rho(z))\ \delta(0) \qquad \text{(E12)}$$

where the variables $\psi(z)$ and $\rho(z)$ are defined,

$$\psi(z) = \frac{\delta(z)}{\delta(0)}\ ,\ \rho(z) = \frac{\delta_p(z)}{\delta(0)}\ .$$

These displacements and their corresponding mismatch, Δ, are illustrated for a simple two-region connection in Figure E2.

The complete set of residual elastic displacements present at one time for all regions are both necessary and sufficient to uniquely characterize the region forces present at that time. Consequently, for the basic bolted joint illustrated in Figure 1, the conditions for static equilibrium and mismatch may be stated in terms of the residual elastic displacements in exactly the same fashion that it was presented in Section II.A.1 of the main body of this

report. Doing this for the basic bolted joint model (Figure 1), one obtains the following set of equations which are similar to Equation (5) in Section II.A.1. Thus,

$$\begin{bmatrix} 1 & -1 & -1 \\ K_b & 0 & K_{j2} \\ 0 & K_{j1} & -K_{j2} \end{bmatrix} \cdot \begin{bmatrix} (\psi_b - \rho_b)\ \delta_b(o) \\ (\psi_{j1} - \rho_{j1})\ \delta_{j1}(o) \\ (\psi_{j2} - \rho_{j2})\ \delta_{j2}(o) \end{bmatrix} = \begin{bmatrix} \Delta' \\ 0 \\ W \end{bmatrix} \tag{E13}$$

where it is understood in this application that Δ', W, and all the parameters ψ and ρ are, in general, functions of a common exposure variable, z. Proceeding formally in the manner discussed in Section II.A.1, the residual elastic displacements determined by solving Equation (E13) may be expressed in the following manner:

$$\left.\begin{aligned} (\psi_b - \rho_b)\ \delta_b(o) &= \frac{1}{K_b}\left[P' + C_{j1}\ W\right] \\ (\psi_{j1} - \rho_{j1})\ \delta_{j1}(o) &= -\frac{1}{K_{j1}}\left[P' - (C_b + C_{j2})\ W\right] \\ (\psi_{j2} - \rho_{j2})\ \delta_{j2}(o) &= -\frac{1}{K_{j2}}\left[P' + C_{j1}\ W\right] \end{aligned}\right\} \tag{E14}$$

where

$$P' = \frac{\Delta'}{\left[\frac{1}{K_b} + \frac{1}{K_{j1}} + \frac{1}{K_{j2}}\right]} \tag{E15}$$

is the residual elastic preload and where the multiplicative factors are,

$$C_b = \frac{\frac{1}{K_b}}{\left[\frac{1}{K_b} + \frac{1}{K_{j1}} + \frac{1}{K_{j2}}\right]},\quad C_{j1} = \frac{\frac{1}{K_{j1}}}{\left[\frac{1}{K_b} + \frac{1}{K_{j1}} + \frac{1}{K_{j2}}\right]},\quad C_{j2} = \frac{\frac{1}{K_{j2}}}{\left[\frac{1}{K_b} + \frac{1}{K_{j1}} + \frac{1}{K_{j2}}\right]} \tag{E16}$$

The factors defined by Equation (E16) shall be referred to as the elastic redistribution factors for the external load, and as defined in Equation (E16) they apply specifically to the basic joint model portrayed in Figure 1. Naturally, any fundamental alteration of the model that changes the defining relationships portrayed in Equation (E13) will result in corresponding modifications to Equations (E14) and (E16). The overall scheme of the analysis will not have been

affected by this change, only the specific form of certain terms will have been modified. However, the specific form of Equation (E15) will always remain unchanged except for the number of factors present in the denominator.

Equation (E14) provides a condition that must be continuously satisfied by the term $(\psi - \rho)$ for each region. The general form for this condition becomes clearer if one recalls that the initial region forces are given by

$$F_b(o) = K_b\,\delta_b(o),\ F_{j1}(o) = K_{j1}\,\delta_{j1}(o),\ F_{j2}(o) = K_{j2}\,\delta_{j2}(o)\ . \qquad \text{(E17)}$$

Since the joint forces are compressive, hence negatively signed, the absolute values of the initial joint forces are expressed by $-F_{j1}(o)$ and $-F_{j2}(o)$ respectively. Consequently Equation (E14) may also be expressed,

$$\left.\begin{aligned}
(\psi_b - \rho_b) &= \frac{P'}{|F_b(o)|} + C_{j1}\,\frac{W}{|F_b(o)|} \\
(\psi_{j1} - \rho_{j1}) &= \frac{P'}{|F_{j1}(o)|} + (-C_b - C_{j2})\,\frac{W}{|F_{j2}(o)|} \\
(\psi_{j2} - \rho_{j2}) &= \frac{P'}{|F_{j2}(o)|} + C_{j1}\,\frac{W}{|F_{j2}(o)|}
\end{aligned}\right\} \qquad \text{(E18)}$$

where the equality applicable to each region is seen to be in the general form,

$$(\psi - \rho) = \frac{P'}{|F(o)|} + C\,\frac{W}{|F(o)|} \qquad \text{(E19)}$$

Another condition that the bolted joint must satisfy, is provided by the relation between the residual elastic displacements and the residual elastic mismatch. This relation, which is a statement of the definition of mismatch (Equation (3) in Section II.A.1), is given by the first row of the matrix represented in Equation (E13). Taking this relation and dividing by the initial mismatch, Δ_o, one obtains,

$$\frac{\Delta'}{\Delta_o} = (\psi_b - \rho_b)\,\frac{\delta_b(o)}{\Delta_o} - (\psi_{j1} - \rho_{j1})\,\frac{\delta_{j1}(o)}{\Delta_o} - (\psi_{j2} - \rho_{j2})\,\frac{\delta_{j2}(o)}{\Delta_o} \qquad \text{(E20)}$$

Since the effect of plastic deformation caused by relaxation is portrayed by the parameter ρ, the consequence of not subtracting this quantity in each $(\psi - \rho)$ term is to express the mismatch portrayed by the total displacements of each region. Examination of the two-region model in Figure E2 shows that this

interpretation is correct. Hence, for the basic model and Equation (E20) it is seen that the ratio of the total mismatch to the initial mismatch is given by the relation,

$$\frac{\Delta}{\Delta_o} = \psi_b \frac{\delta_b(o)}{\Delta_o} - \psi_{j1} \frac{\delta_{j1}(o)}{\Delta_o} - \psi_{j2} \frac{\delta_{j2}(o)}{\Delta_o} \quad . \tag{E21}$$

For the basic bolted joint model, Equations (E18) and (E21) must always be satisfied.

It is worth noting that some rather important simplifications arise as a consequence of letting W = o. This is, in fact, the situation that usually exists when the relaxation of bolted joints are evaluated. In this situation Equation (E21) continues to be valid as shown. But for Equation (E18) we have that

$$|F_b(o)| = |F_{j1}(o)| = |F_{j2}(o)| = P_o \text{ for } W = o$$

so that one obtains in this case,

$$(\psi_b - \rho_b) = (\psi_{j1} - \rho_{j1}) = (\psi_{j2} - \rho_{j2}) = \frac{P'}{P_o} \quad . \tag{E22}$$

Also as a consequence of W = o, it is observed from Equations (E12), and (E14) to (E16) that

$$\frac{\delta_b(o)}{\Delta_o} = \frac{\delta_b'}{\Delta'} = C_b, \quad \frac{\delta_{j1}(o)}{\Delta_o} = \frac{\delta_{j1}'}{\Delta'} = - C_{j1}, \quad \frac{\delta_{j2}(o)}{\Delta_o} = \frac{\delta_{j1}'}{\Delta'} = - C_{j2} \quad .$$

In this case, Equation (E20) takes the form

$$\frac{\Delta'}{\Delta_o} = \frac{P'}{P_o} = (\psi_b - \rho_b)\, C_b + (\psi_{j1} - \rho_{j1})\, C_{j1} + (\psi_{j2} - \rho_{j2})\, C_{j2} \tag{E23}$$

which is identical to Equation (28) in Section II.A.3 when the conditions for a standard relaxation test are applicable (i.e., $\psi_i = 1.0$, $\rho_i = R_i$, i = region index number).

Making use of Equation (E19) is exceedingly awkward since ψ is the instantaneous value of the remaining fraction of the original total displacement, whereas ρ is obtained from an integration involving the instantaneous value of ψ and all preceding values (see Equations (E8) and (E12)). This difficulty can be overcome if one makes the assumption that ρ can be suitably obtained from one of

the cases presented in Table 1. Taking an exponential variation of $\psi(z)$ with respect to z as being the most generally applicable form, ψ and ρ are expressed

$$\psi = e^{-nz}, \quad \rho = \frac{A}{A-n}\left(e^{-nz} - e^{-Az}\right) .$$

However, noting that the parameter "nz" can be expressed

$$nz = -\ell n\, \psi$$

the specific relaxation factor may be written

$$\rho = \frac{Az\ \psi - Az\ e^{-Az}}{\ell n\, \psi + Az}$$

where, upon noting that

$$Az = -\ell n\left(e^{-Az}\right)$$

if one defines,

$$\zeta = e^{-Az}$$

then the specific relaxation factor is expressed,

$$\rho = -\frac{(\psi - \zeta)\ \ell n\, \zeta}{(\ell n\, \psi - \ell n\, \zeta)} . \tag{E24}$$

With ρ expressed in this fashion, $(\psi - \rho)$ may be written,

$$(\psi - \rho) = \frac{(\psi\ \ell n\, \psi - \zeta\ \ell n\, \zeta)}{(\ell n\, \psi - \ell n\, \zeta)} \tag{E25}$$

Equations (E24) and (E25), evaluated over a range of values for ψ and ζ, are presented in graphical form in Figures (E3) and (E4) respectively. With the values of the functions ρ and $(\psi - \rho)$ available in this form, an analysis of relaxation in a bolted joint becomes practical. The general scheme is as follows:

(1) Determine elastic stiffnesses. Compute C_i and the initial values Δ_o, P_o, $\delta_i(o)$ and $F_i(o)$ for all i regions. Use Equations (E14) through (E16) as they apply to the initial state of the joint.

(2) From standard relaxation data for each region, i, determine A_i, and B_i or any other appropriate fitting constants (see discusion in Section 2).

(3) Determine times in the relaxation history that are of interest. For each time determine the values of Δ and W. Also determine the corresponding values of z for each region, i, (the discussion in

Section 2 of this appendix can provide guidance). Also for each region and each time in the relaxation history compute $\zeta_i = e^{-A_i z_i}$.

(4) For each time in history guess a possible value for P'. Compute region values of $P'/|F(o)| + C\ W/|F(o)|$ (refer to Equation (E18) for specifics). If W = o, only a guess for P'/P_o is required.

(5) Using Figure E4 determine the corresponding values of ψ_i for each region.

(6) With these values of ψ_i check that Equation (E21) is satisfied (to some preselected level of precision). If this equality is not satisfied, repeat Steps (4), (5), and (6) with another guess for P'. This process is stopped when Equation (E21) is satisfied for each time to be considered in the bolt relaxation history.

Using the steps just outlined, the fractional changes in the initial preload are determined throughout the relaxation period. If desired, the magnitudes of the specific relaxation factors in any member may also be established by using the final values of ψ_i in Figure E3. Before demonstrating this procedure with an example problem (which shall be presented in the section that follows), some general ideas shall be developed about the locus of points representing a relaxation history in Figure E4.

Consider a two-region bolted joint (a bolt and one joint region) which is preloaded. For simplicity, it shall be assumed that W = o. At the start of the relaxation period it is noted that $P'/P_o = 1$ (no relaxation or elastic load changes from the initial state has taken place), and initially $\psi_b = \psi_j = 1$ since z = 0. Throughout the relaxation process it shall be assumed that $\Delta/\Delta_o = 1$ so that according to Equations (E16) and (E21) the following equalities are required to be continuously satisfied:

$$\left.\begin{aligned} C_b + C_j &= 1 \\ C_b\ \psi_b + C_j\ \psi_j &= 1 \end{aligned}\right\} \qquad \text{(E26)}$$

With these requirements a variety of possible cases can be analyzed for the characteristic history loci that may be drawn on Figure E4 to satisfy Equations (E22) and (E23). For the first case consider the joint behavior when material relaxation only occurs in the bolt. This situation is portrayed in Figure E5(a), where initially both the bolt and joint regions start at the point O. Since the joint is presumed to be non-relaxing, (e.g., $\rho_j = 0$ and

consequently $\psi_j = P'/P_o$) the locus of points portraying this condition is the line corresponding to $\zeta = 1$. For a given reduction in preload this is indicated by the line OJ. However, if the locus of points relating ψ_j to P'/P_o is a straight line, it will be found that the corresponding locus for the bolt must also be a straight line in order to satisfy Equation (E26). The particular straight line applicable to this case is shown in Figure E5(a) by the line segment OB.

If the role of the joint and bolt are reversed, such that the bolt remains elastic (e.g., $\rho_b = 0$ and $\psi_b = P'/P_o$) and relaxation takes place in the joint, the situation portrayed in Figure E5(b) then applies. As shown, the bolt locus is given by the line OB, and that for the joint, by the line OJ.

Figure E5(c) shows the situation that occurs when both regions relax the same amount throughout their relaxation history. In this case, Equation (E22) requires that $\psi_b = \psi_j$ so that the only locus permitted by Equation (E26) is $\psi_j = \psi_b = 1$. Thus the loci OB and OJ are coincident in this case. It should be noted from the definition of ψ (Equation (E12)), that this is the condition where total displacements (and hence strains) remain constant during material relaxation. Hence the appropriate relaxation factors, in this case, are the standard relaxation factors. In this case Equation (E20) takes the form shown in Equation (27) of Section II.A.3, where the factors, R, are the same for all regions.

It will be recalled that Equation (28) was not limited to a common value of R for all regions. It was assumed however, in Section II.A.3, that the total displacements do not change in the course of the relaxation process. But as seen in the cases just considered, and also Equation (E26), this is not possible. That is the reason why it was stated in Section II.A.3 that the assumption of constant total displacement could be satisfied approximately if either the relaxation levels were relatively small in all participating members of the joint or if the relaxation levels in all regions were not "too dissimilar". In these cases, the loci OB and OJ are expected to remain close to the $\psi = 1$ line, thereby making departures from the theoretically exact result in Figure E5(c) relatively unimportant.

To illustrate the type of loci that could be obtained under more realistic circumstances, it will be instructive to consider the situation where both bolt and joint relax at different rates. Suppose the nature of the materials are

such that the joint relaxes rapidly at first and then slows down, just as the rate of relaxation in the bolt begins to increase dramatically. Keeping in mind that Equations (E22), (E23) and (E26) must be continuously satisifed, the curved loci illustrated in Figure E5(d) could be developed. It is noted that when the rates of relaxation are very high the locus of the relaxation history tends to be perpendicular to the lines of constant ζ levels. As the rate slows down, the locus tends to become parallel to lines of constant ζ. Since the loci are not independent, the path of one locus influences the other. When the net relaxation levels become the same, the two loci intersect. In this case they intersect at $\psi_j = \psi_b = 1$ because $\Delta/\Delta_o = 1$ (recall that Equation (E21) was used to obtain Equation (E26)). As a consequence of this response character, if the two loci are fairly "close" to the $\psi = 1$ line, then the use of Equation (28) as presented in Section II.A.3 is justifiable. However if the departure from the $\psi = 1$ line is considered to be too great, a reasonable estimate of the reduced preload cannot be found by using Equation (28). The example problem in the next section will demonstrate the type of calculation that must be performed when Equation (28) may not be appropriate to use.

5. Application To A Bolted Joint

Figure E6(a) shows a simple bolted joint with one bolt and one clamped region. The data provided in this illustration shall be used to determine the elastic stiffness of the two regions and the stress relaxation characteristics of their corresponding materials. If it is required that the joint be initially tightened to a torque of 120 lb-in, and testing has shown that an assembly coefficient of 0.165 is appropriate for this connection, then an initial preload may be calculated. As shown in Table E2, this preload is 2910 lbs. The initial mismatch corresponding to this preload, which is 3.69 mils, is also shown in this table.

The objective of this analysis, obviously, is to demonstrate the behavior of the joint as stress relaxation occurs. However to explore a variety of practical considerations, two joint conditions and two methods of analyses will be examined. The first joint condition to be considered is characterized by the total mismatch, Δ, remaining constant during the relaxation process for a joint supporting no external force. For this case the calculations will be performed using both the conventional method of analysis (which was presented in Section II.A.3) and the method of analysis developed in this appendix. The second

joint condition considered will be characterized by a linearly decreasing total mismatch during the relaxation process. This can occur if there is a slow and steady thermal contraction of the joint that exceeds the contraction of the bolt, or if a similarly slow thermal expansion of the bolt occurs that exceeds the expansion of the joint. Another process which could produce a similar effect on the joint is by directional expansions or contractions in the members of the bolted joint due to non-thermal causes such as radiation induced growth, hygroscopic swelling (as in some plastics) and metallurgical phase changes. Whatever the underlying process may be, it shall be assumed for the example problem that the stress-free thickness of the clamped member reduces linearly with increasing exposure level, y. The calculation for this case will be performed only by the methods derived in this appendix.

The results of all calculations performed are summarized in Table E2. The relations used are indicated in this table, as well as the sequence used to iteratively apply the analytical method develop in this appendix. It is seen, from this table, that the preloads computed for the constant total mismatch case are essentially identical for both the conventional and iterative methods of analysis. However, the plastic deformation predicted for each region differs between the two types of analyses, with the more realistic values being computed by the iterative procedure. This can be seen in Table E3, which presents the total, the elastic, and the "plastic" displacements calculated for both the bolt and joint regions. Comparing the two methods of analysis applied to the constant total mismatch case, this table shows that somewhat smaller levels of plastic deformation are computed with the iterative procedure. Accordingly, it is concluded that if knowledge of the allocation of plastic deformation in the joint is not an important consideration, the conventional method of analysis (using Equation (28)) is much easier to apply and may be quite satisfactory for an estimate of preload reduction. The experience developed in this example problem suggests that a judgement should be made prior to the application of these methods of bolted joint analyses (considering such factors as possible differences in material behavior, end use of the calculation, and level of precision needed) to determine which type of computation is worth performing.

In the case of a variation in the total mismatch during relaxation, the only realistic way of assessing the behavior of the joint is to use the iterative procedure developed in this appendix. The results of the calculation performed for this case is shown in the lower section of Table E2. As expected,

smaller preloads are computed than were obtained for the cases of constant total mismatch. The parameters obtained by computation for this case in Table E2 are presented graphically in Figure E6(b). The explanation for the initial increase in the total displacement fraction of the joint region is that the high initial relaxation rate of joint leads to a proportionately high increase in the compressive deformation (elastic plus plastic) of the joint compared to the elongations developed in the bolt. This is not to say that the plastic deformation is greater in the joint, but only that the fractional increase is greater in the joint. The magnitudes of the displacements computed for this case are presented in Table E3.

6. Summary

In this appendix a scheme was developed to assess the effects of relaxation when the condition of constant total strain in the relaxing member was not satisfied. The procedure developed only requires the results of a standard relaxation test for the materials being used and knowledge of the variation of total displacement (or total strain) during exposure to the relaxing environment. Results are presented for specific variations in total displacement that are of practical interest (Table E.1, Figure E.1).

The methods developed for one relaxing material member were applied to the bolted joint in which two or more members operate as a mechanical system governed by mutual elastic constraint. Formulas were derived to compute joint preloads and member displacements knowing only (a) the results of standard relaxation tests for the bolt and joint materials, (b) basic material properties such as modulus of elasticity and expansivity for the environmental conditions of interest, (c) initial conditions of the joint, and (d) a description of external forces or environmental conditions (temperature, etc.) acting during the relaxation process. A graphical procedure was developed to facilitate the computations required, and the application of this procedure to an example problem of a bolted joint was presented and discussed in detail to illustrate its use.

Table E.1. Useful Formulas For Specific Fractional Relaxation Factors

Total Displ. Variation Type	Normalized "Total" Displacements Variation	Specific Fractional Relaxation Factor
Linear	$\frac{\delta_t(z)}{\delta_t(o)} = 1 + mz$	$\rho(z) = (1 - \frac{m}{A})(1 - e^{-Az}) + mz$
Exponential $n \neq A$	$\frac{\delta_t(z)}{\delta_t(o)} = e^{-nz}$	$\rho(z) = \frac{A}{(A-n)}(e^{-nz} - e^{-Az})$
Exponential $n = A$	$\frac{\delta_t(z)}{\delta_t(o)} = e^{-nz}$	$\rho(z) = A\, ze^{-Az}$

TOTAL DISPLACEMENT IS CONSTANT

VALID Z: $0 \leq Z$

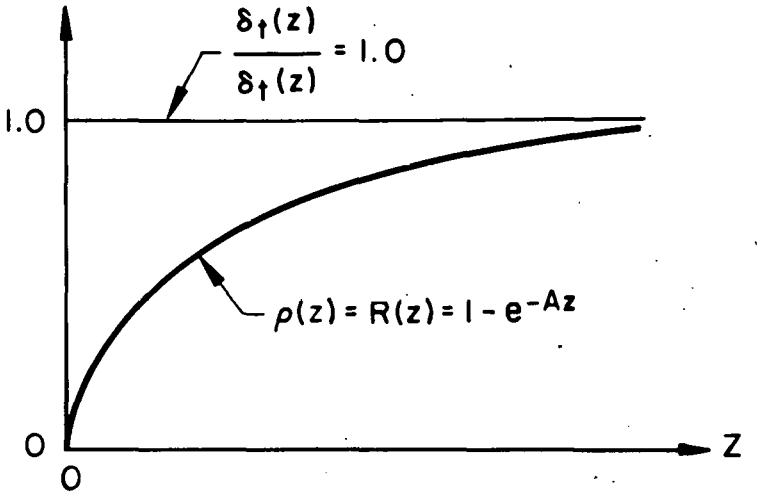

TOTAL DISPLACEMENT IS LINEARLY VARYING

VALID Z: $0 \leq Z < Z_1$

$Z_1 = \frac{1}{A} \ln\left(1 - \frac{A}{m}\right)$

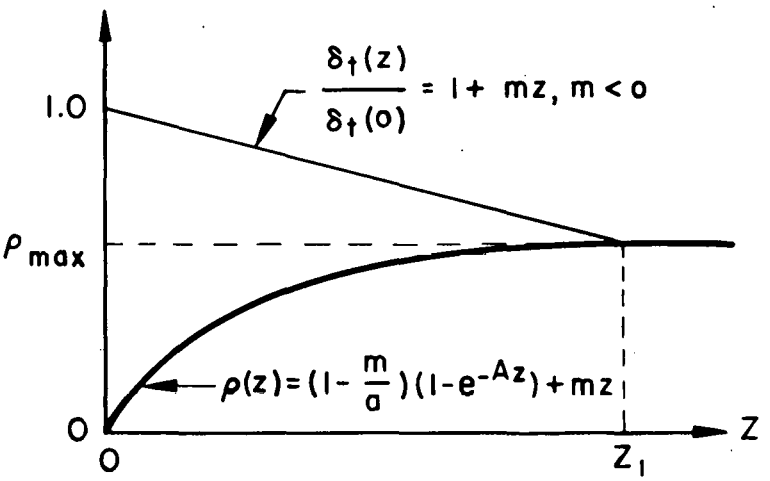

TOTAL DISPLACEMENT IS EXPONENTIALLY VARYING

VALID Z: $0 \leq Z < Z_1$

$$Z_1 = \begin{cases} \frac{1}{(A-n)} \ln\left(\frac{A}{n}\right), & n \neq A \\ \frac{1}{A}, & n = A \end{cases}$$

NOTE: WHEN; $n = A$, $\rho_{max} = e^{-1}$

$n = 0$, CONST TOT DISP CASE

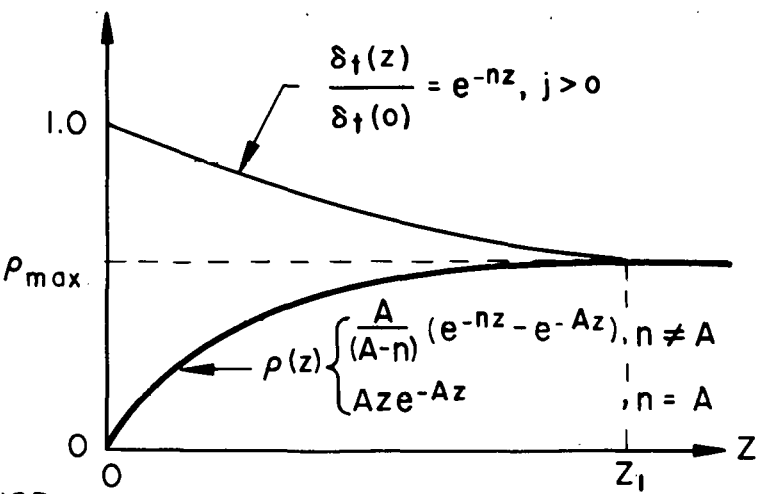

Figure E.1. Specific Relaxation Graphs for Some Cases of Interest

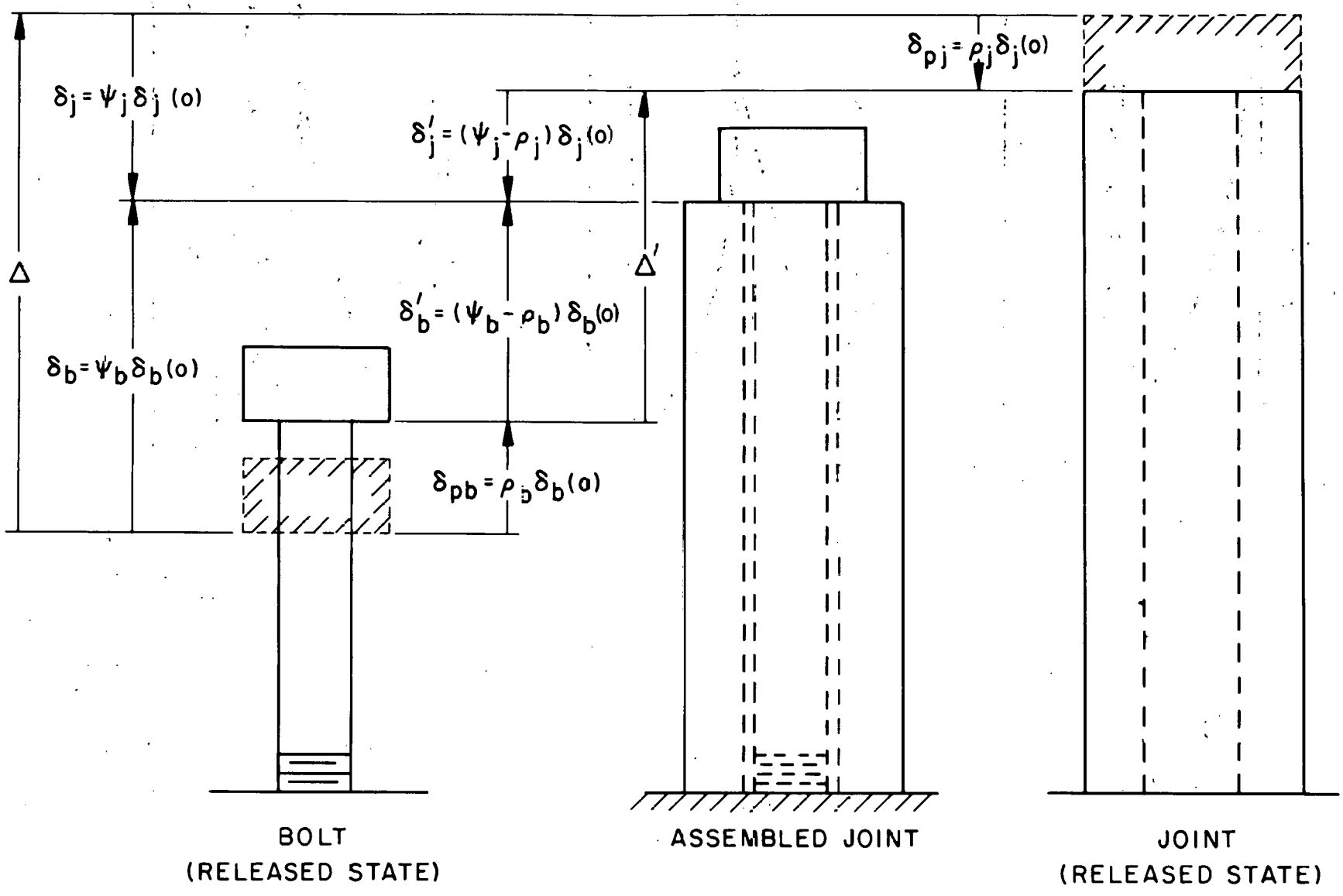

Figure E.2. Mismatches and Displacements (Total and Elastic Residual)

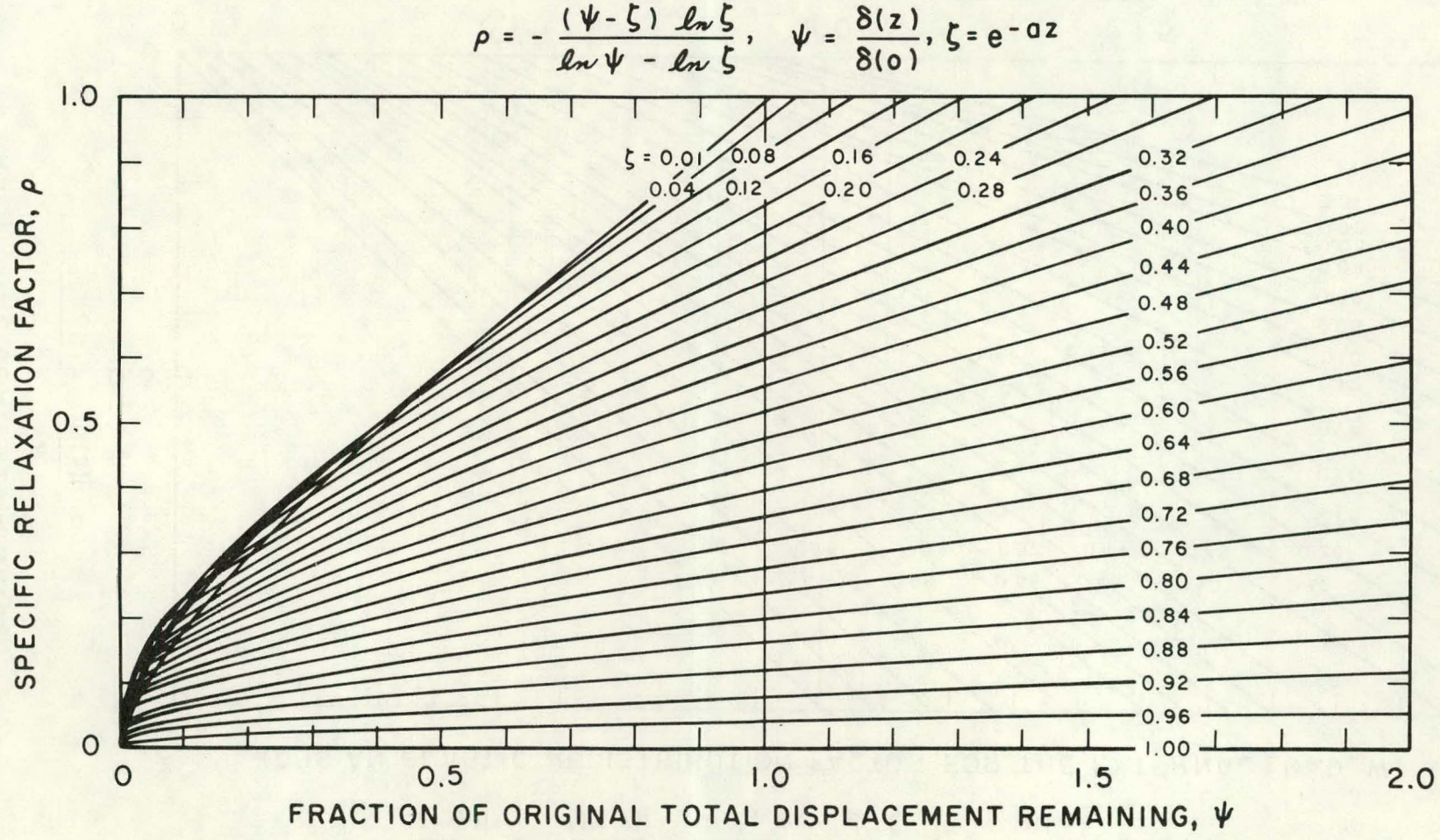

Figure E.3. Influence of ψ and ζ on Specific Relaxation Factor

$$\frac{P'}{|F(o)|} - C\frac{W}{|F(o)|} = \frac{\psi \ln \psi - \zeta \ln \zeta}{\ln \psi - \ln \zeta}, \quad \psi = \frac{\delta(z)}{\delta(o)}, \quad \zeta = e^{-az}$$

(C IS AN ELASTIC REDISTRIBUTION FACTOR FOR THE EXTERNAL LOAD, W)

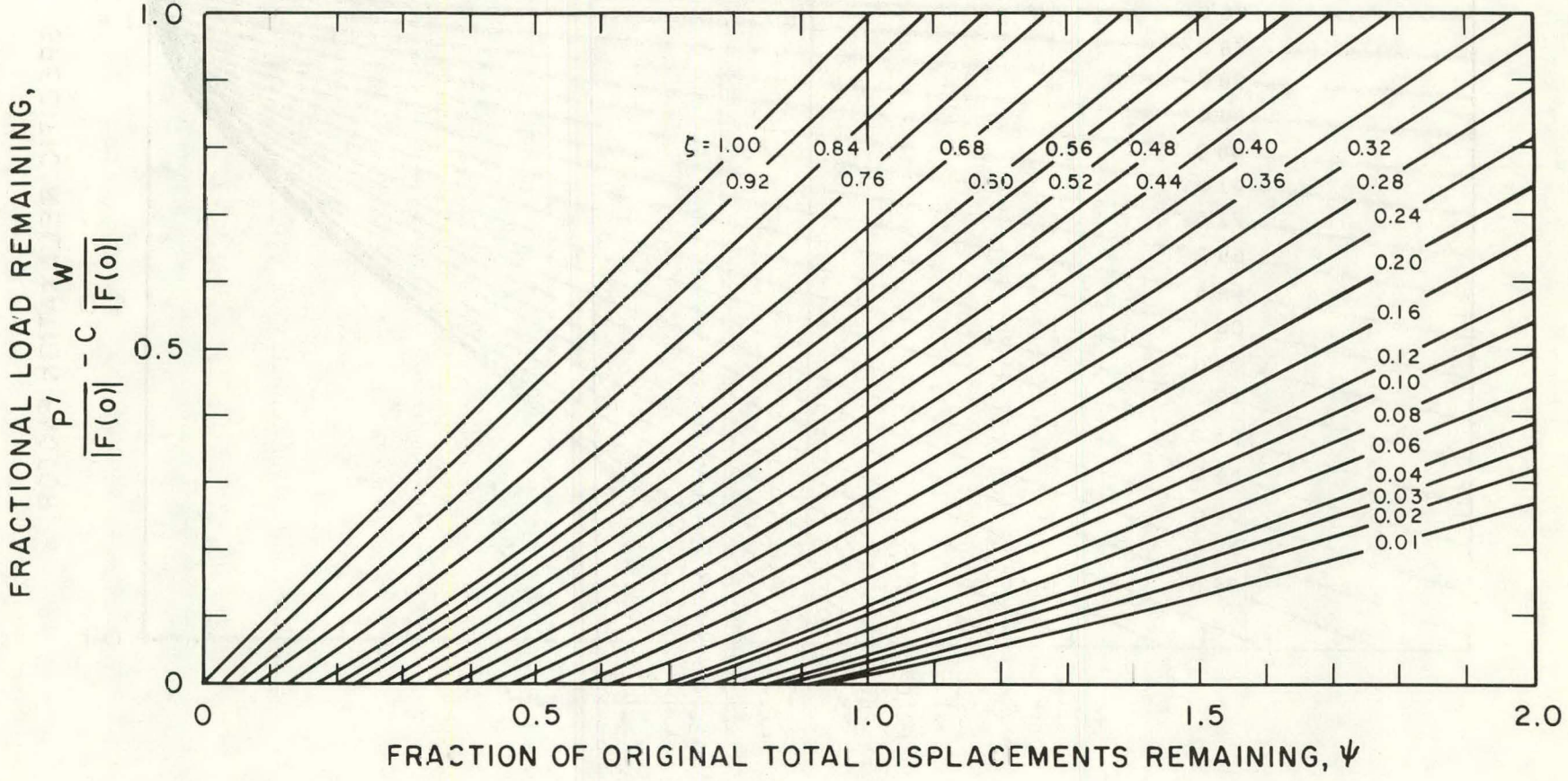

Figure E.4. Influence of ψ and ζ on Fractional Load Remaining

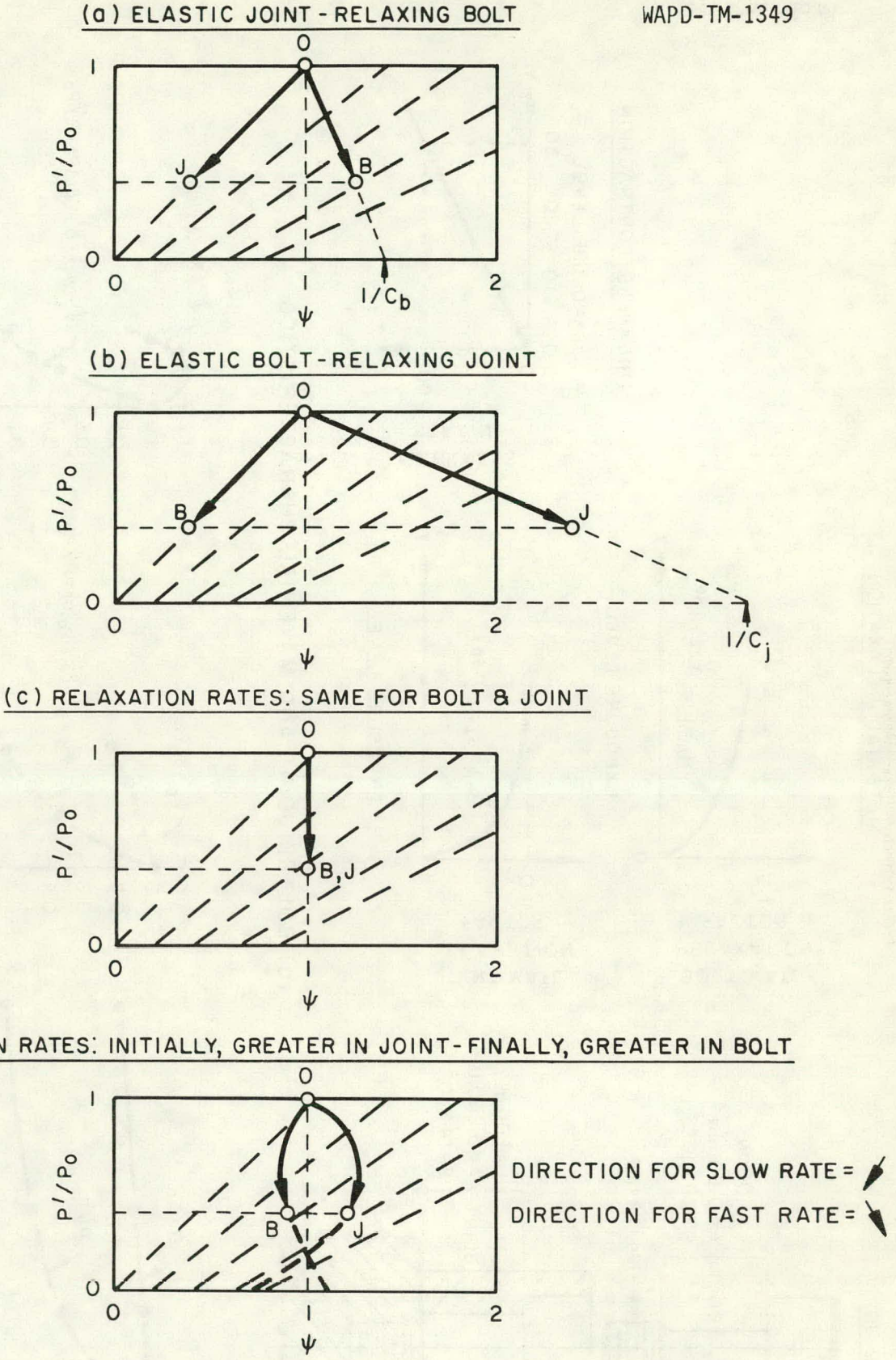

Figure E.5. Effect of Variations in Relaxation Rates Between Bolt and Joint in a Simple Two-Region Connection

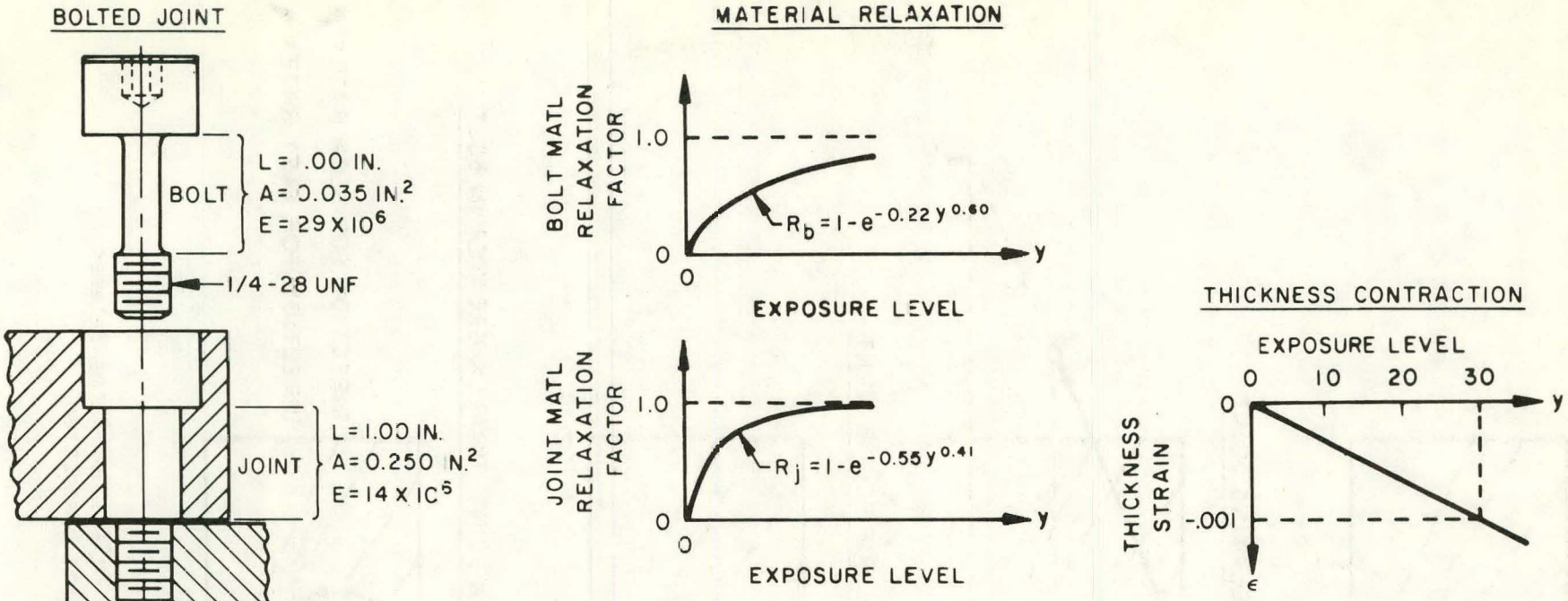

(a) BOLTED JOINT AND MATERIAL CHARACTERISTICS

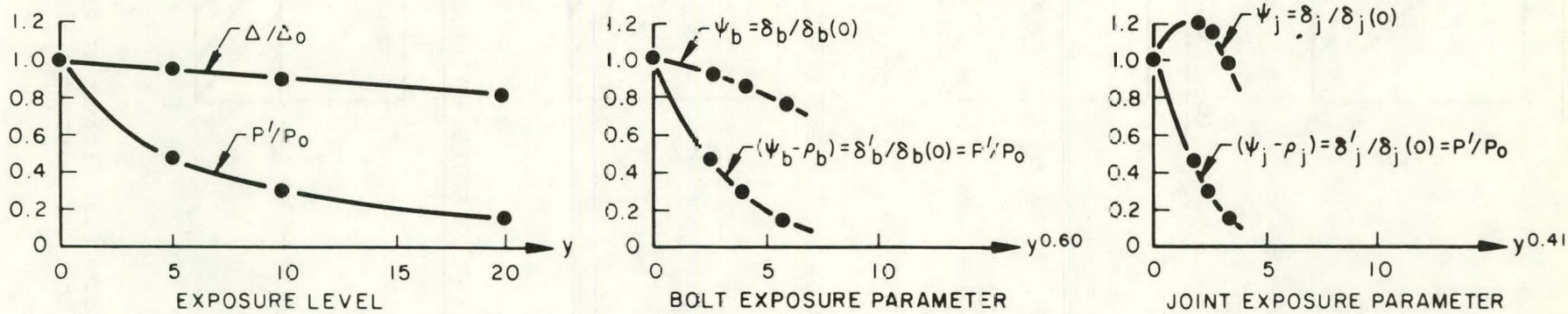

(b) VARIATION OF MISMATCH, PRELOAD, AND DISPLACEMENT FRACTIONS

Figure E.6. Example Problem for Assessment of Relaxation Factor when Total Displacements are not Constant

Table E2. Calculated Results for Example Problem (Figure E.6)

	ITEM	SYMBOL/RELATION	CALCULATED RESULTS			
	Torque	T (lb-in)	120.			
	Assembly Coef.	C	0.165			
	Nom. Thd. Dia.	D	0.250			
	Init. Preload	$P_o = T/CD$, (lb)	2910.			
	Bolt Flexibility	$1/K_b$, (in/lb)	9.85×10^{-7}			
	Joint Flexibility	$1/K_j$, (in/lb)	2.86×10^{-7}			
	Composite Flex.	$[1/K_b + 1/K_j]$, (in/lb)	1.27×10^{-6}			
	Mismatch	$\Delta_o = [1/K_b + 1/K_j] P_o$, (in)	3.69×10^{-3}			
	Bolt Elast. Fract.	$C_b = (1/K_b)/[1/K_b + 1/K_j]$	0.78			
	Joint Elast. Fract.	$C_j = (1/K_j)/[1/K_b + 1/K_j]$	0.22			
Type of Calculation Performed ↓	Exposure Level	y	0.00	5.00	10.00	20.00
	Bolt Param.	$Z_b = y^{0.60}$ *	0.00	2.63	3.98	6.03
	Joint Param.	$Z_j = y^{0.41}$ *	0.00	1.93	2.57	3.42
Const. Tot. Mismatch: Conventional Calculation (See Eq. 28, Sec. II.A.3)	Total Mismatch	Δ	3.69×10^{-3}	3.69×10^{-3}	3.69×10^{-3}	3.69×10^{-3}
	Mismatch Fract.	Δ/Δ_o	1.00	1.00	1.00	1.00
	Bolt Relax. Param.	$(1-R_b) = e^{-A_b Z_b} = \zeta_b$	1.00	0.56	0.42	0.27
	Joint Relax. Param.	$(1-R_j) = e^{-A_j Z_j} = \zeta_j$	1.00	0.35	0.24	0.15
	Preload Fract. Relax.	$(P'/P_o) = (1-R_b) C_b + (1-R_j) C_j$	1.00	0.51	0.38	0.244
Const. Tot. Mismatch: Realistic Calculation (Per Appendix E, using Fig. E.4)	Total Mismatch	Δ	3.69×10^{-3}	3.69×10^{-3}	3.69×10^{-3}	3.69×10^{-3}
	Mismatch Fract.	Δ/Δ_o ←	1.00	1.00	1.00	1.00
	Preload Fract. Relax.	P'/P_o (GUESS)	1.00	0.51	0.38	0.237
	Bolt Relax. Param.	$e^{-A_b Z_b} = \zeta_b$	1.00	0.56	0.42	0.27
	Bolt Tot. Disp. Param.	ψ_b	1.00	0.93	0.93	0.94
	Joint Relax. Param.	$e^{-A_j Z_j} = \zeta_j$	1.00	0.35	0.24	0.15
	Joint Tot. Disp. Param.	ψ_j	1.00	1.25	1.25	1.19
	Calc. Mismatch Param.	$(\Delta/\Delta_o) = \psi_b C_b + \psi_j C_j$ (COMPUTATION) (ITERATION CHECK)	1.00	1.000	1.000	0.995

Table E2. (Cont)

	ITEM	SYMBOL/RELATION	CALCULATED RESULTS			
Linear Varying Totl. Mismatch: Realistic Calc. (per Appendix E, using Fig. E.4)	Total Mismatch	Δ	3.69×10^{-3}	3.52×10^{-3}	3.36×10^{-3}	3.02×10^{-3}
	Mismatch Fract.	Δ/Δ_o ←	1.00	0.954	0.911	0.818
	Preload Fract. Relax.	P'/P_o (GUESS)	1.00	0.48	0.32	0.14
	Bolt Relax. Param.	$e^{-A_b Z_b} = \zeta_b$	1.00	0.56	0.42	0.27
	Bolt Tot. Disp. Param.	ψ_b	1.00	0.89	0.84	0.77
	Joint Relax. Param.	$e^{-A_j Z_j} = \zeta_j$	1.00	0.35	0.24	0.15
	Joint Tot. Disp. Param.	ψ_j	1.00	1.20	1.14	0.99
	Calc. Mismatch Param.	$(\Delta/\Delta_o) = \psi_b C_b + \psi_j C_j$ ↓ (COMPUTATION) (ITERATION CHECK)	1.00	0.958	0.906	0.818

*Using $R = 1 - e^{-Ay^B}$ to fit standard relaxation test, let $A_b = 0.22$ and $B_b = 0.60$ for bolt, and let $A_j = 0.55$ and $B_j = 0.41$ for joint.

Table E3. Calculated Bolt and Joint Displacements for Example Problem
(Displacements expressed in mils)

Constant Mismatch - Constant Total Displacements - Conventional Calculation

Exposure Level, y	Total		Elastic		Plastic	
	δ_b	δ_j	δ'_b	δ'_j	δ_{pb}	δ_{pj}
0	2.88	-0.81	2.88	-0.81	0.00	0.00
5	2.88	-0.81	1.47	-0.41	1.41	-0.40
10	2.88	-0.81	1.09	-0.31	1.79	-0.50
20	2.88	-0.81	0.70	-0.20	2.18	-0.61

Constant Mismatch - Variable Total Displacements - Appendix E Calculation

Exposure Level, y	Total		Elastic		Plastic	
	δ_b	δ_j	δ'_b	δ'_j	δ_{pb}	δ_{pj}
0	2.88	-0.81	2.88	-0.81	0.00	0.00
5	2.68	-1.01	1.47	-0.41	1.21	-0.60
10	2.68	-1.01	1.09	-0.31	1.59	-0.70
20	2.71	-0.96	0.68	-0.19	2.03	-0.94

Table E3. (Cont)

Variable Mismatch - Variable Total Displacement - Appendix E Calculation

Exposure Level, y	Total		Elastic		Plastic	
	δ_b	δ_j	δ'_b	δ'_j	δ_{pb}	δ_{pj}
0	2.88	-0.81	2.88	-0.81	0.00	0.00
5	2.56	-0.97	1.38	-0.39	1.18	-0.58
10	2.42	-0.92	0.92	-0.26	1.50	-0.66
20	2.22	-0.80	0.40	-0.11	1.82	-0.69

NOTE: Displacements were computed as follows: total disp., $\delta_i = \psi_i \delta_i(o)$; elastic disp., $\delta'_i = (P'/P_o)\ \delta_i(o)$; plastic disp., $\delta_{pi} = \delta_i - \delta'_i$; where i = "b" for bolt or "j" for joint.

REFERENCES

(a) G. R. Sharp, "Determination of Stiffness and Loading in Bolted Joints Having Circular Geometry," WAPD-TM-1105, Department of Energy Report, November 1975.

(b) R. E. Little, "Bolted Joints: How Much Give?" Machine Design, Vol. 39 No. 26, November 9, 1967.

(c) M. F. Spotts, "Design of Machine Elements," Fourth Edition, Prentice-Hall, Inc., Engelwood Cliffs, NJ.

(d) D. R. Connors, et al., "Design of the Shippingport Light Water Breeder Reactor" WAPD-TM-1208, Department of Energy Report, January 1979.

(e) R. J. Roark and W. C. Young, Formulas for Stress and Strain, Fifth Edition, McGraw-Hill, New York, 197, p. 290.

(f) Appendix A5, "Screw Thread Standards for Federal Services," National Bureau of Standards Handbook H28, 1969, Part 1: U.S. Department of Commerce.

ACKNOWLEDGEMENTS

The authors express their grateful appreciation to the many people at Bettis Laboratory who generously offered their knowledge and experience on analysis and testing of bolted joints. In particular the authors acknowledge the personal support and guidance received from Dr. A. H. Pacella and Mr. J. J. Brennan in the course of developing analytical methods and obtaining test data during final assembly of the LWBR core. Further, the help of Mr. M. J. Schneider, Dr. G. R. Sharp, and Mr. R. A. Frederickson is also acknowledged for their painstaking reading of the manuscript for this report, and the many improvements and suggestions they proposed. Since much of the test results presented were not obtained by the authors, the following credits are in order: Mr. M. S. Stiegel and Mr. E. H. Schwer for the M208 preload test data, Mr. R. D. Mallozzi and Mr. H. E. Himes for the SCC test joint data, and Mr. W. R. Bish for the bearing load deformation test data.

JOINT NAME:_____ STIFFNESS CALCULATIONS

1.	Material					
2.	A (A_{min}, A_{max})					
3.	(D_{hole}, D_{nut})					
4.	(D_h / D_n)					
5.	L (L/D_h or $2L/D_h$)					
6.	($\beta°$, cone angle)					
7.	(ρ, TM-1105 p20)					
8.	A/L					
9.	T_1					
10.	E_1					
11.	$K_1 = E_1 A/L (= E, D_h \rho)$					
12.	$1/K_1$					
13.	$\bar{\alpha}_1$					
14.	$\bar{\alpha}_1 L$					
15.	T_2					
16.	E_2					
17.	$K_2 = E_2 A/L (= E_2 D_h \rho)$					
18.	$1/K_2$					
19.	$\bar{\alpha}_2$					
20.	$\bar{\alpha}_2 L$					
21.	R_{th} (therm relax)					
22.	R_{irr} (irrad relax)					
23.	$R = 1-(1-R_{th})(1-R_{ir})$					
24.	$(1-R)/K_2$					

$\frac{1}{K_b} =$

$\frac{1}{K_j} = \sum_i \frac{1}{K_{ji}} =$

$\left[\frac{1}{K_b} + \frac{1}{K_j}\right] =$

$\frac{1}{K_b} =$

$\frac{1}{K_j} = \sum_i \frac{1}{K_{ij}} =$

$\left[\frac{1}{K_b} + \frac{1}{K_j}\right] =$

$R^* = \frac{\sum \frac{1-R_i}{K_i}}{\sum \frac{1}{K_i}} =$

* Include bolt in R

Model Work Sheet for Stiffness Calculation

JOINT NAME: _____ **CALCULATED PRELOADS AND STRESSES**

$$P_{cold} = \begin{cases} \frac{1}{CD_{th}} T \\ P_o + m\theta \end{cases}, \qquad P_{hot} = \frac{\Delta_{hot}}{\left[\frac{1}{K_b} + \frac{1}{K_j}\right]_{hot}}$$

$$\Delta_{cold} = \left[\frac{1}{K_b} + \frac{1}{K_j}\right]_{cold} P_{cold}, \qquad \Delta_{hot} = \Delta_{cold} + \left[\delta_{thj} - \delta_{thb}\right] (\Delta T°)$$

1.	T (lb-in) or P_o (lb)					
2.	C or m					
3.	D_{th} or $\theta°$					
4.	Amin (for lines 14,16,18)					
5.	P_{cold} (T= °)					
6.	$\sigma = P_{cold}/A_{min}$					
7.	Reduced P_{cold} (Pl. Def.)					
8.	$\left[\frac{1}{K_b} + \frac{1}{K_j}\right]_{cold}$					
9.	Δ_{cold}					
10.	$\delta_{thj} = \Sigma \bar{\alpha}_{ji} L_{ji}$					
11.	$\delta_{thb} = \bar{\alpha}_b L_b$					
12.	$\left[\frac{1}{K_b} + \frac{1}{K_j}\right]_{hot}$					
13.	P_{hot} (T= °)					
14.	$\sigma = P_{hot}/A_{min}$					
15.	Reduced P_{hot} (Pl. Def.)*					
16.	$\sigma = P_{hot}/A_{min}$					
17.	Ext. Load, W					
18.	$\sigma = W/A_{min}$					
19.	Max Bolt Load, F_b					
20.	Resid. Torque (hot), T_r					
21.	Ave Stress Intens, $\bar{S}$					
22.	Overall Relax. Factor					
23.	Reduced P_{hot} (Relax)					
24.	Separation Load, W_{sep}					

* IF APPLICABLE, ADDITIONAL REDUCTION TO PRELOAD FROM TIME-INDEPENDENT PLASTICITY EFFECTS (APPENDIX D)

Model Work Sheet for Calculated Preloads and Stresses

•U.S. GOVERNMENT PRINTING OFFICE: 1981/703-014/363